Probing a strongly interacting Fermi gas

by

John Stewart

B.S. Physics and B.S. Mathematics, Texas A&M University, 2004

A thesis submitted to the
Faculty of the Graduate School of the
University of Colorado in partial fulfillment
of the requirements for the degree of
Doctor of Philosophy
Department of Physics
2009

This thesis entitled:
Probing a strongly interacting Fermi gas
written by John Stewart
has been approved for the Department of Physics

Dr. Deborah S. Jin

Dr. Eric A. Cornell

Date

The final copy of this thesis has been examined by the signatories, and we find that both the content and the form meet acceptable presentation standards of scholarly work in the above mentioned discipline.

Stewart, John (Ph.D., Physics)

Probing a strongly interacting Fermi gas

Thesis directed by Professor Dr. Deborah S. Jin

This thesis presents experimental work probing a strongly interacting Fermi gas of atoms. The work presented here contributed to the demonstration that strongly interacting Fermi gas systems are accessing universal physics. The universality of these systems means that we can use an atomic Fermi gas to gain an understanding of strongly interacting Fermions occurring elsewhere in nature, such as nuclear and neutron matter, high transition temperature superconductors, and the quark-gluon plasma. Once the universality of these systems was verified, experiments were performed to extract the microscopic quantities of an atomic Fermi gas. These experiments employ a technique akin to photoemission spectroscopy for electrons found in condensed matter physics. The photoemission spectroscopy experiments presented here directly reveal the spectral function which contains many valuable microscopic quantities such as the energy dispersion and quasi-particle lifetime. These experiments provide stringent tests of many-body theories.

Acknowledgements

It is hard to know where to begin when acknowledging everyone that has led me to the path I'm on. So, I will begin at the beginning. Firstly, and most importantly, I would like to thank all of my wonderful family. My family has been incredibly supportive and encouraging in my schooling ever since I was young. Somehow, they had complete faith that I could achieve anything I set my mind to and keeping their faith has been my driving force when the classes got hard and the hours got long. Through my parents, I grew up believing I could literally do anything that I set my mind to. Their acceptance of my choices and desire for my happiness has made my life such a joy. My siblings have always been there for me and I trust they always will. My brothers have been a constant for me in these last years of college and grad school. Even though we've been thousands of miles apart, hearing from them every week has made me still feel very close to them and I consider them my very best friends.

My high school years were an important time for me. I think I was one of those nerds that loved learning. My many great teachers: Mrs. Comstock, Mrs. Anderson, Mr. Ladley, and Mrs. Vice, to name a few, really opened my mind to the world of math, science, and critical thinking. I would especially like to thank Mrs. Comstock for her wonderful teaching of this weird class of "physics" which just blew me away. Physics, to me, was so bizarre and counter-intuitive, and hard, that I just had to get my mind around it. I would also like to thank all

of my friends from high school who all loved learning and really made school fun. I would especially like to thank Justin McAllister who has been a true friend over the years.

During my college years at Texas A&M I developed into the person I am today. While there I learned that my future is in the laboratory. It really is like a playground where we get to explore the secrets of the universe with expensive toys. I have to thank Dr. Thomas Walther for that first opportunity to work in the lab. I knocked on his office door my first week at A&M and he graciously accepted my offer and taught me the joys of experimental physics. I'd also like to thank him for recommending me to come to Boulder. It was also during college that I learned that the field of physics was more expansive then I could ever imagined. I would like to thank Dr. Agnolet, in particular, for being a fantastic teacher and giving me a deep appreciation for quantum mechanics and thermodynamics. Perhaps most importantly, in college I met my best two friends Marcus Teague and Michael Hatridge. College certainly would not have been the experience it was without them. We somehow meshed countless hours of homework sessions with ample amounts of video games, queso, and margaritas. I'd like to thank Mike for teaching me how to screen-look and Marcus for teaching me how to appreciate quality b-class sci-fi.

My graduate studies have been so much better then I could ever have hoped for. My advisor, Deborah Jin, is one of the great scientific minds of our time. If I have picked up even a fraction of her problem solving skills, intuition, and excitement for cool physics, I will consider myself fortunate. I have always appreciated that she gave us so much experimental freedom and the possibility to steer the direction of the experiment. JILA as a whole has been just fantastic. The infrastructure is designed to succeed: from the administrative staff and the electronics and machine shops, to the overall collaborative mind set of the Fel-

lows and students. In particular, I'd like to thank Eric Cornell and the tri-group. Preparing some recent data for a tri-group meeting or talk has taught me how to organize and motivate my research. If you can give your talk in front of the tri-group and field their questions, you can give a talk with confidence anywhere in the world. I would also like to thank Krista Beck, she has been a huge help throughout my graduate career and while I was a JILA graduate representative. I have to thank John Bohn of teaching me the secrets of the tasty home brew.

During graduate school I have been blessed with some really great friends. John Gaebler showed up ready to go on day one and everything in this thesis, and much more that is not, was done in equal participation with him. I have come to value John's opinion on anything from physics, economics, to politics. He generally has a unique and compelling argument that contradicts the convenient or status-quo. Juan Pino and I have shared many a trip up to the mountains, many a concussion trying some stupid trick, and many a conversation about life. I will always value his opinion as real and challenging. There are many JILAns that I have the pleasure to call friends in a variety of different settings including: snowboarding, climbing, hiking, climbing, homework sessions, video games, tri-group challenges, and just talking physics. For this reason I'd like to thank: Russ Stutz, Aaron Leanhardt, Giacomo Lamporesi, Laura Sinclair, Galen O'Neil, Amy Bloom, Shihkuang Tung, Rob Wild, Huanqian Loh, Ty Cumby, John Perrault, and Kang Kuen Ni, to name a few. I'd also like to thank Ian Schenck for all his help, knowledge and friendship.

To my wife, Kara Renee Nelson-Stewart, I am forever indebted. She picked up and left her family and friends so that we could be together here in Colorado. She has been the most supportive and encouraging partner, way beyond anything I could have hoped for. Many nights it was only at her insistence that I stayed late to finish some experiment or analysis. I am continually amazed by her selflessness.

She has been the glue that held us together for the last five years. It is to Kara that I dedicate this thesis.

Contents

Chapter

Chapter 1

Introduction

1.1 Strongly interacting Fermi systems

Strongly interacting Fermi systems (sometimes called strongly correlated Fermi systems) present some of the most intriguing and unsolved problems in modern physics [1]. This is quite remarkable considering many of these strongly interacting systems have been studied for many decades. Perhaps the reason these systems have stayed at the forefront of physics for so long is that a complete theory built from the ground up is computationally impractical in reasonable timescales. In addition, experimental progress can be difficult (experiments may require extremely low temperatures, high densities, very high magnetic fields, extremely clean samples, etc.). Ultimately, I suspect it is the varied and counterintuitive properties of strongly interacting systems that keeps the human mind so baffled and intrigued. From a practical point of view, strongly correlated systems can have useful properties for device applications, giving further motivation to understand these systems.

Of course, there are many systems that do not require a many-body understanding to explain observed phenomena. For example, the properties of simple metals can be explained rather accurately by simply assuming the electron is a non-interacting particle [2]. Non-interacting in this sense means assuming the electron (fermion) does not interact with the other electrons in the system, it is

a free particle. The atomic gas analog here would be the ideal Fermi gas. When allowing for interactions between the fermions, amazingly, many phenomena can be described by again assuming that the electrons are free particles but that the effect of interactions is to simply renormalize the system, for example the fermion mass as in Fermi liquid theory. Despite the success of these simple theories, there exist interesting phenomena in interacting Fermi systems that cannot be described within the free-particle framework.

The special types of interacting Fermi systems I refer to exhibit strong pairing interactions between pairs of spin-up and spin-down fermions. These strongly interacting Fermi systems can be found in superconductors, neutron and nuclear matter [3, 4, 5, 6], the quark-gluon plasma [7], and now include the atomic Fermi gases we study in this thesis. An important feature for these systems is that they exhibit universality [5, 8, 9, 10]. Universality here means that for these strongly interacting Fermi systems, the details of the microscopic interaction are not important and at zero temperature the interparticle spacing becomes the only length scale. This is a most important feature because it means we can study any one of the systems to learn about the others. This is quite remarkable when you consider that the atomic Fermi gas system stands apart from its counterpart systems by many orders of magnitude in density and temperature.

Intrinsic to this special class of strongly interacting Fermi systems is fermionic superfluidity. The existence a well defined Fermi surface and attractive interactions between spin-up and spin-down fermions can lead to superconductivity in metals or, more generally, fermionic superfluidity [11, 12, 13]. Superconductors exhibit zero resistance, or persistent current, while superfluids exhibit persistent flow and vortices [14, 15]. Throughout this thesis I will mostly refer to superfluidity because we will be working with neutral atoms. Regardless, many of the properties of the atomic Fermi gas we study in this thesis such as high transition

temperature, small pair size, and pseudogap, are relevant for charged superconductors [16, 17].

At this point there is a fairly natural question: why study strongly interacting Fermi systems using ultra-cold atoms if they are already so thoroughly studied? Firstly, some of the other strongly interacting Fermi systems examples are hard or even impossible to achieve in the laboratory (such as degenerate neutron matter) and therefore are hard to study thoroughly. Even condensed matter experiments, which can be achieved in the laboratory setting, are subject to impurities, lattices, grain boundaries, etc., which can easily complicate what is already complicated physics. The atom gas, in contrast, is impeccably pure and simple. Secondly, atomic systems introduce a degree of control not easily found in the other strongly interacting Fermi systems. For example, one cannot easily change the density of a neutron star, or change its temperature. Or, in electron systems, one cannot typically change the interaction strength between fermions, something easily tuned in atomic systems. Using our simple, pure, tunable atomic Fermi gas, we can help to understand unexplained phenomena found in these other systems at a very basic level. Additionally, we can easily use our tunability to enter into new and interesting regimes that may have not even been realized previously.

1.2 Ultra-cold atomic Fermi systems

Atomic systems provide an opportunity to study many-body problems in a system that is relatively free of complexity and very well understood at the few-body level [18]. In particular, atomic Fermi gases are very valuable in testing many-body theories because they are simple, pure, tunable samples with smooth density profiles. Then, as the underlying physics becomes known, one can then introduce lattices [19], impurities [20], disorder [21, 22], etc., to the atomic system to simulate real material properties with a ground-up understanding.

Before addressing the interesting physics we can study with our atomic Fermi gas, I think it is worth appreciating all the recent and rapid progress in atomic physics that allowed us to get to this point. Considering Bose-Einstein condensation (BEC) was achieved experimentally only 14 years ago [23, 24], it is quite remarkable that we can already use our atomic Fermi gas to gain new understanding of such a wide variety of strongly interacting Fermi systems. The major breakthroughs in atomic physics that led to BEC, namely laser cooling and evaporative cooling, were applied to cool fermions. Because the quantum statistics of the particles does not manifest until very cold temperatures, a gas of fermions can be initially cooled using the same techniques as bosons. However, below a temperature of order 20 μK, the atoms are cold enough that they collide only via s-wave scattering, where the orbital angular momentum of the colliding particles is zero [25]. However, since identical fermions cannot collide via s-wave scattering (the two-particle wave function must be anti-symmetric upon exchange of the particles), the cooling of fermions requires at least two distinguishable particles. The first experiments to overcome this obstacle and create a quantum degenerate gas of fermionic atoms occurred here at JILA, in 1999, on the same machine as the experiments in this thesis [26].

Although the creation of a quantum degenerate gas of fermions was already a remarkable achievement, it was not the ultimate goal of the experiment. As it turns out, when one creates a degenerate non-interacting Fermi gas it does not undergo a phase transition as in the case of bosons. Instead the fermions simply fill every available energy level up to the Fermi energy, forming the so-called Fermi sea [26, 2]. The next natural step was to tune the interactions in the system. In fact, it had been proposed that if one could increase interactions to be suitably strong, by using a scattering resonance known as a Fano-Feshbach resonance, then the transition temperature to the superfluid state could be within reach for

experimenters [27, 28, 29]. The requirements for achieving superfluidity: a colder and more strongly interacting gas, were non-trivial and pursued here at JILA with the culmination of fermionic superfluidity [30, 31]. Obviously, JILA was not the only place where experimenters were creating these exciting new Fermi gases. The creation of other degenerate interacting Fermi gases, including ^{40}K [32], ^{6}Li [33, 34, 35, 36, 37] and now ^{176}Yb [38], as well as some I've certainly forgotten, are being pursued all over the world.

The ability to tune interactions is one of the unique features of the atomic gas. The Fano-Feshbach resonance allows one to access attractive or repulsive interactions at arbitrary strength. On one side of the Fano-Feshbach resonance, there exists attractive interactions and one can in principle study BCS-like superfluidity. On the other side of the resonance, there exists a two-body bound state and pairs of fermions, which are composite bosons, can Bose condense. In between these two limiting cases is the so-called BCS-BEC crossover. This crossover from BCS physics to BEC physics was proposed [39, 40, 41] well before atomic gas experiments had achieved quantum degeneracy. However, the ability to tune interactions in atomic gases makes them well suited for realizing this crossover. Indeed, the next step in the evolution of atomic Fermi gases was to control interactions for just this purpose [42, 43, 44, 45, 35].

A particularly exciting regime within the BCS-BEC crossover occurs for very strong attractive interactions in which a pseudogap exists. The concept of a pseudogap will be discussed later in more detail in this thesis but for now it serves as another connection to work done in condensed matter physics. The pseudogap has been discussed in relation to high-Tc superconductors [46] and is a feature of virtually every BCS-BEC crossover theory. Finally, for a review of the early works on the BCS-BEC crossover I recommend the theses of C. A. Regal [47], M. W. Zwierlein [48], and G. B. Partridge [49].

1.3 The work presented here

In the previous sections I attempted to set the stage for the work done in this thesis. I was handed a new shiny toy and told to play with it. The hard work of many groups throughout the world had effectively opened a new field of physics: ultracold strongly interacting atomic Fermi gas physics. To help set the stage for this thesis, I would recommend the thesis of my two predecessors who were instrumental in opening this new area of physics: Brian DeMarco [50] and Cindy Regal [47]. I began my thesis work in the Summer of 2004. At my disposal was an ultracold Fermi gas with tunable interactions. Temperatures on order of half the superfluid transition temperature were already achievable. The phase diagram throughout the BCS-BEC crossover had been mapped out [30] (see Fig. 1.1), collective excitations [51, 52] and momentum distributions [53] had been studied, and vortices had been observed [54].

By the time I began my thesis work, superfluidity in atomic Fermi gas systems was so thoroughly established that we were really in a position to ask: what can this experiment teach us about strongly interacting systems? As we have argued, atomic Fermi gases are simple, pure, tunable systems well poised to test many-body theories. Therefore, a natural way to proceed in answering the above question is to design experiments that can provide stringent tests of (and differentiate between) various many-body theories. In this thesis, I will describe two experiments that we performed towards answering the question of just how much atomic Fermi gases have to offer.

The first experiment I will describe brings us back to the topic of universality. In order to use our Fermi gas experiment to shed light on the general class of problems dealing with strongly interacting Fermi systems, we first had to prove that our system was universal. In a very clear way we were able to prove this by

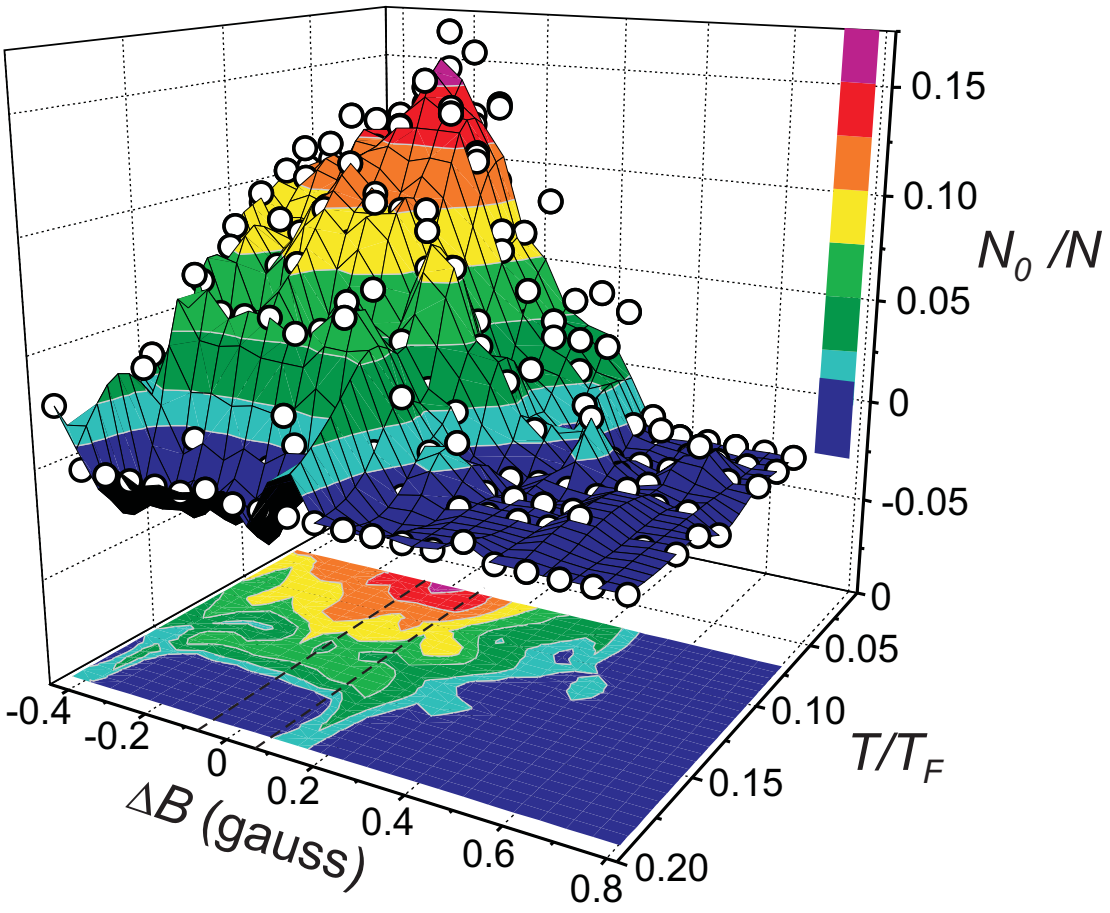

Figure 1.1: Phase diagram of condensate fraction across the BCS-BEC crossover. Figure taken from Ref. [30] showing condensate fraction as a function of temperature and magnetic field. Positive magnetic field tends toward the BCS side and negative magnetic field tends toward the BEC side. Measurements such as this established superfluidity in the strongly interacting Fermi gases.

measuring the potential energy of the Fermi gas a function of interaction strength [55]. Measuring the potential energy allowed us to extract a universal parameter, β, that was actually first proposed in nuclear theory and later applied to atomic Fermi gases [5]. The value of β we measured agreed well with previous results using a different atom, ^{6}Li [43, 56, 45, 35, 57, 58, 59], as well as many different theoretical approaches [6, 60, 61, 62, 63, 64, 65, 66, 67]. This agreement showed that although the microscopics of two atomic Fermi gases may be quite different they are indeed probing the same universal physics. More importantly, it means that we can invoke universality to apply our results to a wide class of problems.

The measurement of β, as well as every other previous experiment in atomic Fermi gases, was a probe of the Fermi gas as a whole. Indeed, many of the early experiments on Fermi gases were probing macroscopic quantities of the system. On one hand, macroscopic quantities are already very interesting. For example, a precise measurement of β or collective oscillations allows the delineation between different many-body theories. On the other hand, if one could measure microscopic quantities of the system then one could have a much more stringent test of many-body theories. This goal was the driving motivation for the second experiment I will describe.

Let us take for example measurements in condensed matter systems. In condensed matter systems, if one can make a large variety of bulk measurements on a material (thermal and electrical conductivity, transition temperature, heat capacity, and many others) then there are enough constraints to say something meaningful about the system. However, in condensed matter physics, there also exists a measurement that has greatly improved the understanding of the microscopic quantities. Using angle resolved photoemission spectroscopy (ARPES) [68], experimenters have been able to map out the spectral function for many interesting strongly interacting systems and determine quantities such as the dispersion,

quasi-particle lifetime, energy gaps, etc. This technique is particularly powerful because once the spectral function is known these microscopic quantities can be directly compared to theory at a very fundamental level. Additionally, one can in turn determine many useful macroscopic quantities.

Using the condensed matter paradigm, it was natural to consider designing an ARPES type experiment for our atomic Fermi gas. In the second experiment I will discuss, we have implemented an ARPES technique for our Fermi gas and indeed we have uncovered valuable microscopic information about our system [69]. At the time of the writing of this thesis, the ARPES result we published is less than one year old. However, the microscopic information we obtained has already generated substantial theoretical interest and our data is being used to validate theories and point out possible discrepancies [70]. Also, due to the broad applicability of our new technique it will be exciting to see it implemented into other atomic gas experiments, including interacting bosons, optical lattices, spin-imbalanced systems, rotating systems, lower dimensional systems, etc. If we again look to the condensed matter experiments, ARPES can be used to study dynamics as well. Therefore, I suspect the ARPES technique described in this thesis will be a very valuable tool for many years to come.

1.4 Thesis Outline

The two main topics that I will discuss in this thesis (universality in Fermi gases and photoemission spectroscopy for Fermi gases) were described in Ref. [55] and Ref. [69], respectively. I will begin, in Chapter 2, by briefly describing the experiment techniques and the atomic physics used to create an ultra cold Fermi gas with strong interactions. In Chapter 3, I will discuss significant changes in the apparatus that have occurred during my tenure. Chapter 4 will describe universality in Fermi gases and our measurement of the parameter β. The rest of the

thesis will cover radio frequency (RF) spectroscopy and ARPES for Fermi gases. In Chapter 5, I will give a historical review of radio-frequency (RF) spectroscopy and the lessons learned. Chapter 6 will describe ARPES and our experiments on atomic Fermi gases. Finally, in Chapter 7, I will conclude and remark about future prospects.

Chapter 2

Creating an ultra cold Fermi gas with strong interactions

In this chapter I will discuss both the machinery needed to create a cold gas as well as the atomic physics used to create an interacting sample. For a more complete account of the cooling machinery I recommend the thesis of Brian DeMarco [50]. For a more complete account of the physics of Fano-Feshbach resonances and BCS-BEC crossover physics I recommend the thesis of Cindy Regal [47]. My goal here is simply to cover the basics needed for creating a cold interacting sample and to cover aspects of the experiment I think are particularly interesting or relevant for the rest of this thesis. Significant changes to the experimental apparatus are discussed in Chapter 3.

2.1 Creating a cold sample

Briefly, the procedure for creating a cold interacting Fermi gas in our experiment begins by collecting atoms in magneto optical traps (MOTs). From here, the atoms are loaded into a magnetic trap for a first stage of evaporative cooling. Finally, the atoms are transferred into an optical trap for a final stage of evaporative cooling. Once we have conducted an experiment, we extract information from the system by letting the gas expand from the optical trap and destructively imaging the atoms. I will now go into more detail to give a brief account of the trip an atom takes during one of our two minute experiment cycles.

2.1.1 MOTs and magnetic trap evaporation

As I mentioned earlier, many of the cooling techniques used in this experiment are re-creations of the techniques used to make the original BEC here at JILA. The double-MOT setup for this experiment is no exception [71]. The double-MOT takes advantage of two different vacuum chambers that are connected by a transfer tube. One vacuum chamber, the collection chamber, has a higher pressure due to the atomic sources that allow for high atom number capture. Then, the trapped atoms are transferred into a second chamber through the transfer tube. In the new chamber, the science chamber, the pressure is much lower allowing for trapped atom lifetimes on the order of 100 seconds. It is in this new chamber that the rest of the experiment takes place.

Atoms from the science chamber MOT are then transferred into a magnetic trap after using optical pumping to ensure that the atoms are in magnetically trappable spin states. Evaporative cooling is performed on the mixture of two spin states by removing the most energetic atoms via microwave spin-flip transitions to magnetically untrapped states. As the cloud rethermalizes to a lower temperature, the microwave frequency is reduced to continue removing the most energetic atoms. This process continues until we have a near quantum degenerate gas. At the end of this stage of the experiment, which takes on order 60 seconds, we have approximately ten million atoms at 5-7 μK. The degeneracy of the cloud, expressed as a ratio of the temperature to the Fermi temperature ($T_F = E_F/k_b$, where k_b is Boltzmann's constant) is around $T/T_F = 3$.

2.1.2 Optical trap evaporation

Once we have achieved these conditions in the magnetic trap we transfer the atoms into a far-off-resonance optical dipole trap. The motivation behind

this is three-fold. Firstly, the Fano-Feshbach resonance requires the atoms to be in particular Zeeman states. The exact states depend on the particular Fano-Feshbach resonance and atoms in these states are not necessarily magnetically trappable. Also, manipulating the atom-atom interactions near the Fano-Feshbach resonance requires one to tune the magnetic field. This can be complicated if one is trying to simultaneously trap the atoms using spatially inhomogeneous magnetic fields. More ideal is to optically trap the atoms and then apply a simple uniform magnetic field. Lastly, we have found that lower temperatures can be achieved if we finish the evaporation using optical trap evaporation as compared to magnetic trap evaporation. The most obvious reason is that the heating rate in the optical trap is very low, around 5 nK/s [47].

We achieve evaporation in the optical trap by reducing the power in the optical trap beam. A nice explanation of optical traps can be found in Ref. [72]. Reducing the power lowers the depth of the trapping potential the atoms experience. In this way, a similar forced evaporation occurs as in the magnetic evaporation stage because the most energetic atoms spill over the top of the potential and leave the trap. Evaporation in the optical trap is also much quicker due to the higher trapping frequencies. We evaporate the atoms transferred into the optical trap in about ten seconds and can typically produce a cloud of 10^5 atoms per spin state at a degeneracy of $T/T_F = 0.10(1)$.

We conduct evaporation in the optical trap with at mixture of atoms in two Zeeman states, the $|f, m_f\rangle = |9/2, -9/2\rangle$ state and the $|9/2, -7/2\rangle$ state, where f is the total atomic spin and m_f is the magnetic quantum number. These states are stable against spin-changing collisions and with them we reach our coldest temperatures. We conduct the majority of the optical trap evaporation at high magnetic field. Typically, we set the magnetic field at 205.7 G (on the atom side of the $|9/2, -9/2\rangle + |9/2, -7/2\rangle$ Fano-Feshbach resonance located at 202.1 G) where

the s-wave scattering length is approximately $a_s = -800a_0$, where a_0 is the Bohr radius. The large magnitude scattering length provides a large scattering cross section without a large inelastic loss rate (at our densities, which are typically between 10^{12} cm^{-3} and 10^{13} cm^{-3}). In addition, at this magnetic field we can then easily access the Fano-Feshbach resonance.

2.1.3 Absorption imaging and thermometry

Absorption imaging is the method by which we obtain nearly all the information we gather from the atoms. Once the final stage of evaporation in the optical trap has occurred and we have performed an experiment, we turn off the optical trap and let the gas ballistically expand for approximately ten milliseconds. We then apply a short resonant laser pulse to the atoms. Atoms in the cloud scatter photons and we capture the shadow of the atoms on a CCD camera. This type of imaging is referred to as time-of-flight absorption imaging.

Our imaging is done almost exclusively at magnetic fields near the Fano-Feshbach resonance, around 200 G, or "high-field imaging" as we call it. At these field strengths the transitions for imaging different Zeeman states are far enough separated that we can image spin-selectively. Typically, we are able to nearly simultaneously image atoms in the two spin states for each experiment. To achieve the highest signal-to-noise, we try to always image atoms in the $|9/2, -9/2\rangle$ state. Imaging atoms in the $|9/2, -9/2\rangle$ state gives the best signal-to-noise ratio because there is a closed cycling transition to the $|11/2, -11/2\rangle$ excited state.

Because we image the gas after ballistic expansion, we can obtain information about the atoms' momenta. In the simplest case of non-interacting atoms, an atom continues in the trajectory it had at the moment the trap was turned off (modified by gravity of course). Thus, for sufficiently long expansion times, the absorption image yields the momentum distribution. We then apply a least-squares

surface fit to the expected Fermi-Dirac momentum distribution to determine the number of atoms, their temperature and quantum degeneracy (T/T_F).

Ultracold Fermi gases have some intriguing behavior that make determining the temperature challenging. For example, for temperatures higher than about $0.5\,T_F$ the Fermi-Dirac distribution is well approximated by a classical distribution, and deviations from this classical distribution are small and hard to extract. Of course, in this limit, the temperature can be extracted from the width of the cloud. On the other hand, for temperatures lower than about $0.1\,T_F$, the momentum distribution has approached the zero temperature limit where the width of the distribution reflects only the Fermi energy. In this limit, any deviations from finite temperature occur right around the Fermi energy and are hard to detect in the 3D trapped distribution.

A substantial portion of my early lab work was set toward understanding temperature in these ultra-cold Fermi gases and trying to design new thermometers. I composed a simulation to understand the fundamental limits of our imaging and fitting routines. I also attempted to use condensate fraction as a thermometer with limited success. Finally, I attempted a clever technique mentioned in Cindy Regal's thesis, which was to use a third fermion as a thermometer. Again, this technique had limited success. Since I find this topic interesting and the results of my findings were not trivial (although not that applicable to the rest of this thesis) I include additional information in Appendix A where I discuss thermometry of ultracold Fermi gases.

2.2 Controlling interactions

In this section I will discuss how we manipulate the interactions between particles in our experiment. As I mentioned earlier, the use of Fano-Feshbach resonances was already a fairly standard technique by the time I began my thesis

work. As such, it will not be my goal here to give a complete overview of Fano-Feshbach resonances, but simply to outline their basic properties and how we use them in the experiment. This section will also be useful for understanding some of the terminology for the rest of the thesis. In particular, the way we characterize the interactions will be discussed. Finally, I will briefly explain how Fano-Feshbach resonances are used in the study of the BCS-BEC crossover.

2.2.1 Fano-Feshbach resonances

Fano-Feshbach resonances [73, 74, 75] are used to vary the interactions between particles in our system. As we learned in the previous section, these gases are in the ultracold regime and therefore are dominated by s-wave collisions. As such, the interactions can be understood in terms of the s-wave collision cross section, $\sigma = 4\pi a^2$, where a is the s-wave scattering length. To change the interactions we need to change a.

Away from a Fano-Feshbach resonance the background scattering length in ^{40}K is $a_{bg} = 174a_0$ [31], where a_0 is the Bohr radius. A Fermi gas at this interaction strength, for our typical temperatures and densities, is a very weakly interacting gas. Or, to put it another way, the mean-field energy, $\frac{2\hbar}{m}(na)$, for a gas at this interaction strength is on the order of 0.01 of the Fermi energy. Therefore, to create a strongly interacting Fermi gas we need a way to change the scattering length by orders of magnitude.

To give a feel for how a Fano-Feshbach resonance allows us to vary the interaction length in such a great way, we can solve a related problem we saw back in our quantum mechanics class (assuming you took Tom DeGrand's class). First, however, let us recall some important parameters regarding low energy scattering. A straight forward case is to imagine two atoms are interacting via a square well potential of height V_0, see Fig. 2.1. Recall, the wave function rises

linearly from zero and should be of the form $u(r) = \sin(kr + \delta)$, where δ is the the scattering phase shift. Then, in limit of low energy scattering ($k \to 0$), the scattering length a is related to the scattering phase shift and the effective range r_0 of the potential, via

$$k \cot \delta \approx -\frac{1}{a} + \frac{1}{2} r_0 k^2. \tag{2.1}$$

Consequently, we can now calculate the cross section, using the definition $\sigma = 4\pi \lim_{k\to 0} |k \cot \delta - ik|^{-2}$. To first order we arrive at the expected cross section $\sigma = 4\pi a^2$. If the potential V_0 is positive, then a linear extrapolation of the wave function at the barrier would reveal a positive scattering length a, Fig. 2.1a. If the potential is negative, then a can be either positive, negative, or divergent, depending on the depth of the potential, see Fig. 2.1b-c.

Returning now to our quantum mechanics example, a nice intuition for Fano-Feshbach resonances can be developed by solving the low energy scattering problem of a spherical square well with a bound state just below threshold. I will outline this problem here. Assume the potential has the form $V(r) = -V_0$ for $r < R$ and $V = 0$ otherwise. The incoming state is has positive energy, E_{scatt}, so the wave function is

$$u(r) = \begin{cases} \sin(Kr) & \text{if } r < R \\ \sin(kr + \delta) & \text{if } r > R \end{cases} \tag{2.2}$$

where $\frac{\hbar^2 K^2}{2m} = E_{scatt} + V_0$ and $\frac{\hbar^2 k^2}{2m} = E_{scatt}$. Now, if we go ahead and assume there is a bound state with energy E_b then its solution would be

$$u(r) = \begin{cases} sin(Gr) & \text{if } r < R \\ e^{-\lambda r} & \text{if } r > R \end{cases} \tag{2.3}$$

where $\frac{\hbar^2 \lambda^2}{2m} = |E_b|$ and $\frac{\hbar^2 G^2}{2m} = V_0 - |E_b|$. Using the usual matching of wave functions and their derivatives at the boundary conditions will allow the determination of these wave functions. However, the trick here is to recall that we are interested

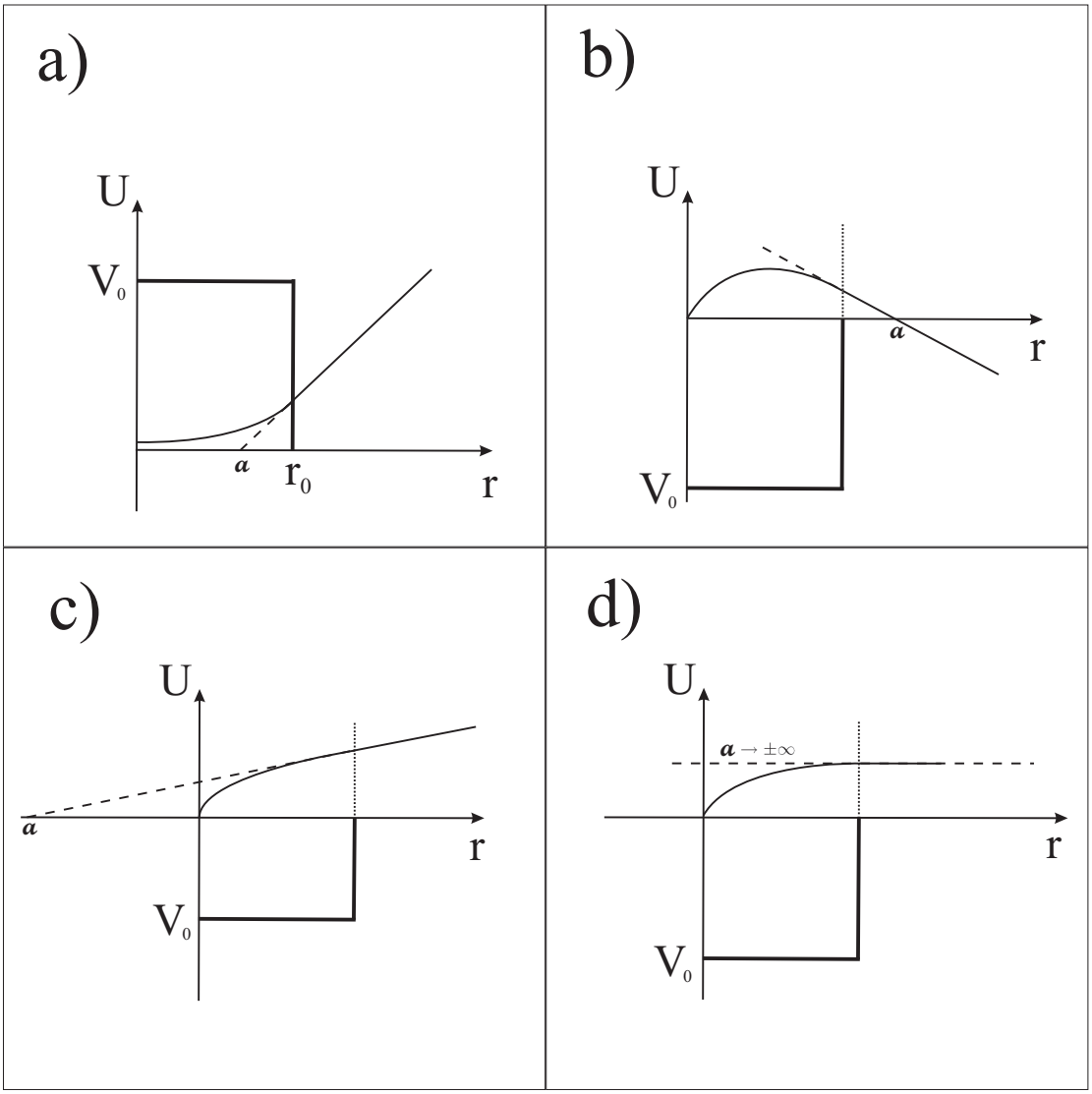

Figure 2.1: Schematic for understanding the scattering length, a. Consider the wave function of two atoms interacting via a simple square well potential (with range r_0) as a function of interparticle separation, r. a)Repulsive hard-core potential. V_0 suppresses the wave function under it and $a > 0$. b) An attractive potential can also give $a > 0$. c) A weaker attractive potential can give $a < 0$ as well. d) An intermediate attractive potential can give a divergent scattering length.

in the physics when a bound state is just coming through threshold. Therefore, we want to consider $|E_b| \to 0$ and since we are considering low energy scattering we also want $E_{scatt} \to 0$. Solving this boundary condition problem (using all the appropriate substitutions and Taylor expansions) we find $k \cot \delta = -\lambda + \frac{1}{2}(\lambda^2 + k^2)R$. We can now directly relate this result to Eqn. 2.1. In this way, we find the scattering length to be

$$\frac{1}{a} = \lambda - \frac{1}{2}R\lambda^2, \tag{2.4}$$

and R is just the effective range r_0. Now we see that as the bound state approaches threshold, $E_b \to 0$, and correspondingly $\lambda \to 0$, the scattering length diverges. Additionally, we find the scattering length is positive for a true bound state. Conversely, a is negative when the bound state is just "above" threshold. Therefore, assuming we can "tune" the height of the potential we have a technique for tuning the scattering length.

Although the physics of the Fano-Feshbach resonance is considerably more complicated, this simple example captures most of the essential features. It is important to note the main differences. First, a Fano-Feshbach resonance is a two-channel effect [76]. This means that a bound state is not coming through threshold as we describe above, but rather that a bound state in an energetically closed channel happens to coincide with the energy of two colliding atoms in the open channel. The second major difference is that we do not tune the height of the potential to move the bound state energy but rather change the energy difference between the thresholds of the two channels. This is possible because the magnetic moment of the closed channel bound state is different than the magnetic moment of the open channel state. Therefore, we can simply tune the relative energy difference by changing the magnetic field.

Fig. 2.2 b) shows how we can tune the scattering length with the magnetic

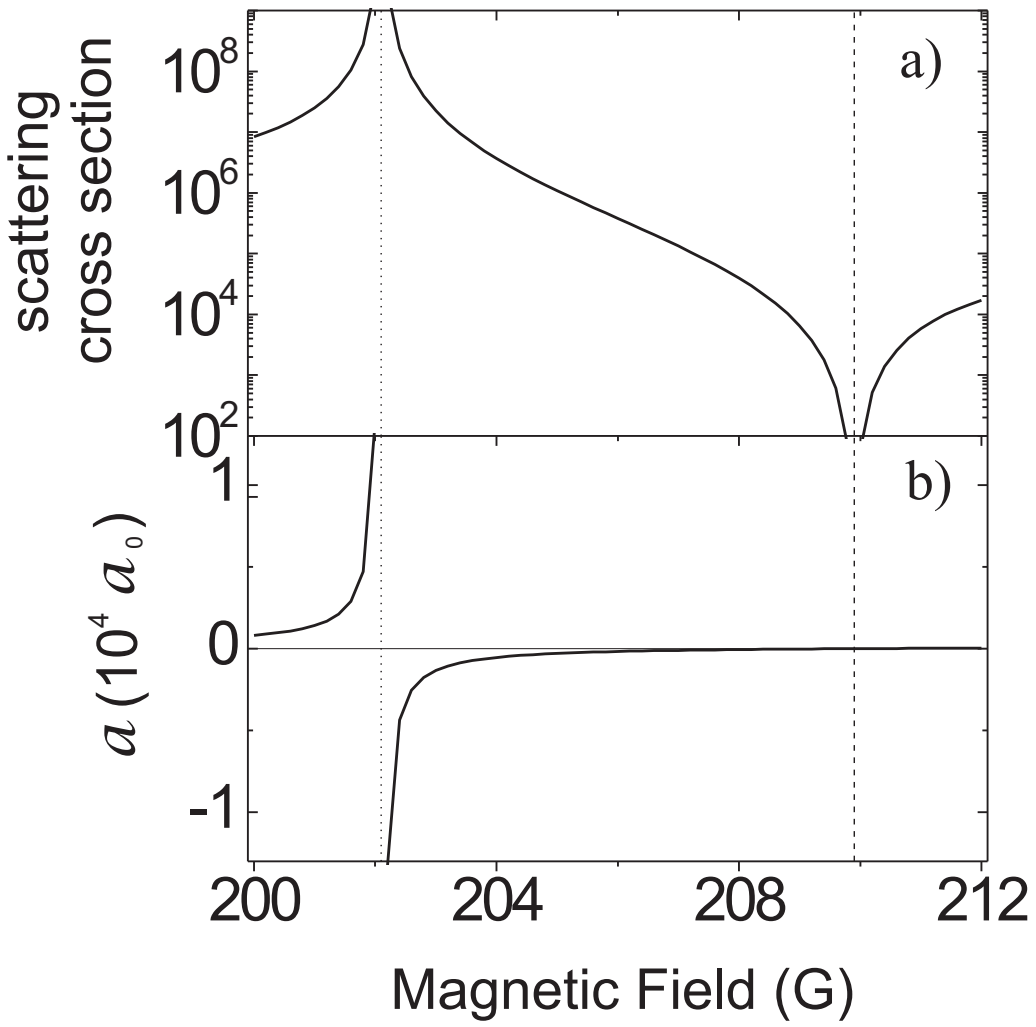

Figure 2.2: Calculated scattering length and cross-section near a Fano-Feshbach resonance. These are the parameters for the Fano-Feshbach resonance used throughout this thesis. The width is 7.8 G, the location of the resonance is 202.1 G (dotted vertical line), and the background scattering length is 174 a_0. The zero crossing of the scattering length occurs at 209.9 G (dashed vertical line). a) The scattering cross section ($4\pi a^2$) as a function of magnetic field. b) Scattering length a in units of the Bohr radius, a_0, as a function of magnetic field. We can tune the scattering length to arbitrary values using the magnetic field.

field near the Fano-Feshbach resonance [76]. The resonance shown here affects the scattering between ^{40}K atoms in the $|9/2, -9/2\rangle$ and $|9/2, -7/2\rangle$ states. This is the resonance used throughout this thesis work. The scattering length as a function of the magnetic field, B, is given by the following:

$$a(B) = a_{bg}\Big(1 - \frac{w}{B - B_0}\Big) \tag{2.5}$$

where $a_{bg} = 174a_0$ is the background scattering length introduced earlier, $w = 7.8$ G is the width of the resonance, and $B_0 = 202.1$ G is the location of the resonance [31]. It is important to note here that this is a broad Fano-Feshbach resonance [77, 47]. Broad in this sense means that the effective energy width (the range of collision energies for which there is resonant scattering) is much bigger than the Fermi energy of our sample. This is important because it means that when we approach the Fano-Feshbach resonance the entire sample is interacting resonantly and not just a portion of a cloud.

Fig. 2.2 a) shows the scattering cross section ($4\pi a^2$) over the same span of magnetic field. As expected, the cross section becomes very large near the Fano-Feshbach resonance (vertical dotted line). However, one of the unique properties of ^{40}K is that it has an easily accessible zero crossing of the Fano-Feshbach resonance (vertical dashed line), located at 209.9 G, see Eqn. 2.5. It is extremely useful to be able to systematically compare properties of a strongly interacting gas to a non-interacting gas. We will take advantage of this fact throughout this work and especially when we study universality in Chapter 4. In contrast, in ^{6}Li, there is no nearby zero crossing of the Fano-Feshbach resonance.

Fano-Feshbach resonances really opened the way to study new physics in Fermi gas systems. In addition to superfluidity, they allow the study of the BCS-BEC crossover, which we will discuss in the next section. However, Fano-Feshbach resonances have simultaneously found their way into the study of bosons, inter-

species mixtures, Bose-Fermi mixtures, atoms in optical lattices, etc. For now, they are *the* way to control interactions in atomic systems. There are also interesting Fano-Feshbach resonance physics on the horizon. To name one example, it may be possible to use external fields to modify the properties of some resonances, giving one the ability to tune the properties of the resonance [78, 79, 80].

2.2.2 BCS-BEC crossover

The goal of the work presented in this thesis is to use atomic Fermi gases to study the general problem of strongly interacting Fermi systems. That being said, these experiments inherently probe the physics of the BCS-BEC crossover and we often compare to BCS-BEC crossover theories. Further, many atomic Fermi gas experiments of the last few years studied BCS-BEC crossover physics, for example see the theses of C. A. Regal [47], M. W. Zwierlein [48], and G. B. Partridge [49]. As such, most of our terminology and intuition for the happenings of atoms and pairs near the Fano-Feshbach resonance is built upon the studies of BCS-BEC crossover physics. Therefore, in this section I will discuss the BCS-BEC crossover and its connection to Fano-Feshbach resonance physics. Without repeating too much that is already discussed in the theses listed above I will use this section to introduce how we have come to understand interactions and pairing in a strongly interacting Fermi gas.

We learned in the previous section that we have control of interactions through the use of a Fano-Feshbach resonance. To develop an intuition for BCS-BEC crossover physics we will follow a thought exercise similar to A. J. Leggett's 1980 paper [40]. Imagine we begin with a zero temperature Fermi gas at the zero crossing of the Fano-Feshbach resonance. This is the textbook Fermi gas with every state filled to form a perfect Fermi surface. Now, as we move to lower magnetic field we begin to turn on arbitrarily small attractive interactions (see Fig.

2.2 b).

Notice that these are the exact requirements for BCS theory. Recall BCS theory is the theory developed by Bardeen, Cooper and Schrieffer [11, 12, 13] that successfully explained superconductivity in electron systems. BCS theory is based on an observation made by Cooper that a spin-up electron and a spin-down electron in the presence of a well defined Fermi surface, and an attractive interaction, can pair up and lower their energy. These pairs of fermions (called Cooper pairs) behave as a composite boson that can Bose condense. One should note here that the pairing between fermions in BCS theory is in momentum space. Or, in other words, the pair size is much bigger than the interparticle spacing. Also, for completeness, the presence of the Fermi surface is required and this is truly a many-body effect (two fermions in vacuum will not form a bound state on their own).

Continuing on with our gedanken experiment, if we adiabatically decrease our magnetic field to well below the location of the Fano-Feshbach resonance then there exists a closed channel bound state. Here, our spin-up and spin-down fermions are paired as a bound molecule. Note that this effect is relevant for atoms and would not be possible for electrons. This composite boson will undergo Bose condensation. In contrast to BCS physics, this pairing mechanism is no longer a many-body effect (or rather, it is not density dependent) and this pair would exist even in vacuum. Also, in contrast to the BCS state, the pairing is in real space since the pair size is much smaller than interparticle spacing. Another useful way to understand the pairing is in terms of interaction strength. We know that as we decrease the magnetic field we increase the attractive interaction between the fermions. In essence, we have increased the attractive interaction between the two fermions so much that they have become paired.

Now, for our gedanken experiment, we want to know what happens in be-

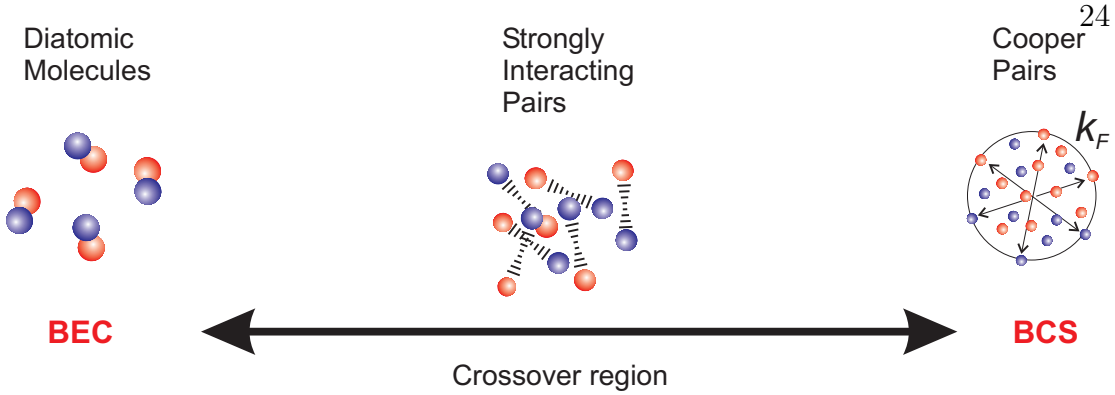

Figure 2.3: Cartoon drawing of pairing throughout the crossover region. In the BEC limit, fermions are tightly bound in molecules. In the BCS limit, pairing is a many-body effect occurring in momentum space. At the cusp of the crossover region, pairs have characteristics of both Cooper pairs and molecules, and pairing is a many-body effect.

tween these two limits. We know that at $T = 0$ on one side of the resonance we have a BCS superfluid, and on the other side of the resonance we have a BEC of bound pairs. The essence of the BSC-BEC crossover is that these two limits are very much linked and one does not pass through a phase transition to get from one to the other [39, 40, 41]. By increasing interactions one can smoothly and continuously move from a many-body pairing with a large pair size into a bound pair with a small pair size. The cusp of the BCS-BEC crossover occurs near the Fano-Feshbach resonance, where the binding energy of the two-body bound state goes to zero. This is a very interesting region. The pair size is very small as compared to Cooper pairs but very large as compared to molecules. The pair size is on the order of the interparticle spacing and the pairing would not be possible without the presence of the other fermions (it is a many-body effect). Using our understanding from the previous section, the cusp of the crossover occurs near the point where the scattering length diverges (i.e., the location of the Fano-Feshbach resonance). Our standard cartoon drawing of pairing in these three regions, the BCS, BEC, and cusp of the crossover, are shown in Fig. 2.3.

The crossover region occurs when interactions between two fermions are too strong to be described by BCS theory and yet too small to form tightly bound molecules that can be described by BEC theory. A convenient way to characterize the interaction strength in a Fermi gas is to compare the scattering length a to the Fermi wave vector $k_F = \sqrt{2mE_F}/\hbar$. Recall in a homogeneous Fermi gas that the Fermi energy is related to the density via $E_F = \frac{\hbar^2}{2m}(6\pi^2 n)^{2/3}$. Therefore, k_F is related to the inverse interparticle distance and $(k_F a)^{-1}$ is essentially a comparison of the scattering length to the interparticle distance. In addition, $(k_F a)^{-1}$ is the dimensionless quantity that characterizes interaction strength used in most BCS-BEC crossover theories [40, 41]. The BCS limit, where the interaction is weak and attractive, occurs for $(k_F a)^{-1} \ll -1$. Conversely, the BEC limit of tightly bound molecules occurs for $(k_F a)^{-1} \gg +1$. The crossover region occurs for interaction strengths not covered by either theory, and one finds significant deviations from either theory in the vicinity of $-1 < (k_F a)^{-1} < +1$ [16, 17]. To give a feel for the span of the BCS-BEC crossover in our experimental parameters, the crossover is approximately a 1 G region surrounding the Fano-Feshbach resonance position (see Fig. 2.2 b).

In this thesis I have not tried to give an exhaustive review of superfluidity. However, there is one important aspect of superfluidity that I will cover briefly, which is the gap parameter. The gap will become important later in the thesis when we discuss angle resolved photoemission spectroscopy (ARPES). BCS superfluids exhibit their "superness" because they require a minimum amount of energy to produce an excitation. This minimum energy required to produce an excitation, referred to as the gap energy, 2Δ, effectively protects the system against arbitrarily small excitations. For easy reference I repeat a figure from the thesis of Cindy Regal that qualitatively shows the gap Δ (and the chemical potential μ) as a function of $(k_F a)^{-1}$ [47], see Fig. 2.4. In the BCS limit, the gap falls

off exponentially with interaction strength, $\Delta = E_F\, e^{-\pi/k_F a}$. In the BEC limit, the energy needed to break apart a pair is the binding energy and Δ is half the binding energy. Again, the interesting regime is near the cusp of the crossover where many-body effects continue to play a role in the pairing and so we expect $\Delta \propto E_F$. As can be seen from Fig. 2.4, the gap in this regime is a large fraction of the Fermi energy. Recent Quantum Monte Carlo results put the zero temperature gap at $(0.45 \pm 0.05)E_F$ [81], and recent experiments also show the gap to be a large portion of the Fermi energy [69, 82]. This is a very large gap as compared to condensed matter superconductors where the gap is $\sim 10^{-4} E_F$.

There is one final topic I would like to cover regarding the BCS-BEC crossover physics, which is temperature. It was instructive in our gedanken experiment to assume a $T = 0$ gas. In reality, our Fermi gas is not at zero temperature, which means we cannot access the superfluid state for all interaction strengths. This can especially be seen in the BCS limit where the transition temperature, T_c, depends exponentially on the interaction strength, $T_c \propto T_F\, e^{-\pi/2k_F a}$ [83]. In fact, we cannot experimentally achieve temperatures much below $0.1\, T_F$ and therefore cannot observe a phase transition for values of $(k_F a)^{-1}$ less than about -1. In the BEC limit, we are simply condensing bosons and the transition temperature is density independent and can be determined from straight forward BEC theory. Again, throughout the crossover there is a smooth connection of the transition temperature from the BCS to BEC limits. For reference, in Fig. 2.5, I adapt a figure from Ref. [84] showing a sketch of the expected transition temperature.

While discussing temperature in the presence of strong interactions, there is yet another temperature scale which is referred to as the pairing temperature, T^*. In conventional superconductivity, pairing and superconductivity occur at the same temperature. In these strongly interacting systems, however, pairing and superfluidity can occur at different temperatures. This is because the very strong

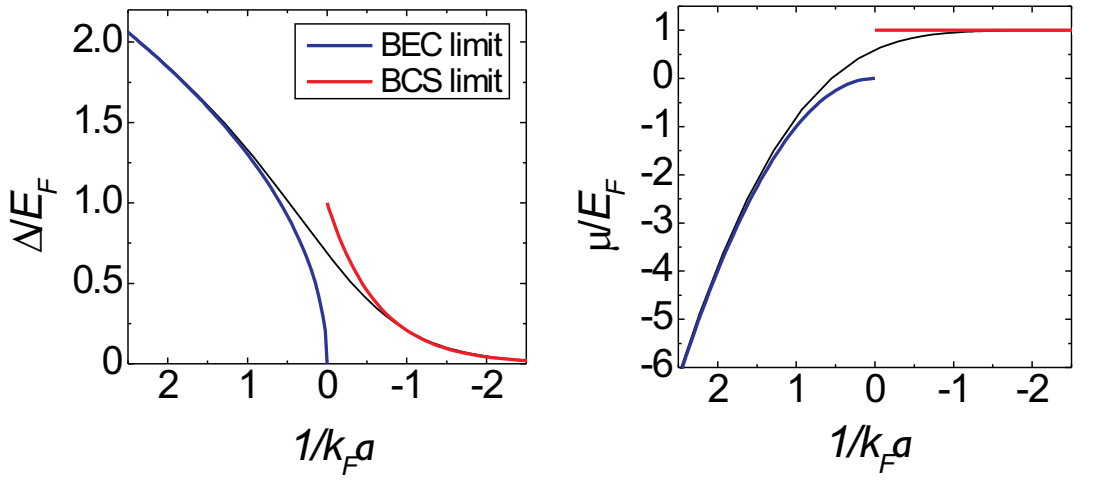

Figure 2.4: The gap Δ and chemical potential μ as predicted by NSR theory. On the BCS side the gap falls off exponentially with interaction strength. From comparison to the red and blue curves (BCS theory and BEC theory) we see that the crossover region indeed occurs from $-1 < (k_F a)^{-1} < 1$. Figure from Cindy Regal's thesis [47].

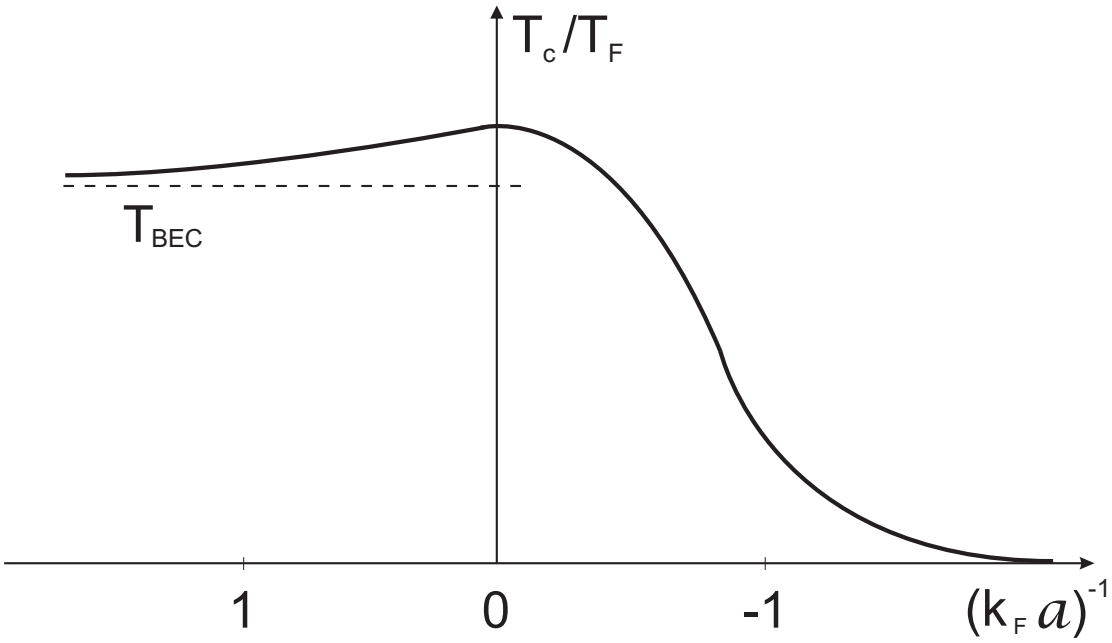

Figure 2.5: A sketch of the expected superfluid transition temperature as a function of $(k_F a)^{-1}$. On the BCS side the transition temperature falls of exponentially. Approaching the BEC limit the transition temperature approaches normal BEC transition temperature. The two limits are connected smoothly although the transition temperature is highest at the location of the Fano-Feshbach resonance.

interactions allow for incoherent pairing correlations at temperatures above the superfluid transition temperature [85, 86, 87, 88, 89, 90, 91, 92, 93]. The region between the pairing temperature and the superfluid transition temperature is referred to as the pseudogap phase. In the pseudogap phase the Fermi gas retains some of the characteristic superfluid signatures (such as a gap in the spectral function) and yet it is not a superfluid. We will study the pseudogap phase in Chapter 6.

Throughout this chapter we have noted that the region of $(k_F a)^{-1}$ near the Fano-Feshbach resonance holds some of the richest physics. A careful observer might question why the atomic cloud does not collapse or explode near the Fano-Feshbach resonance. After all, according to Fig. 2.4 b), the two-body scattering length is diverging near the resonance. Indeed, the Fermi gas does not implode or explode near this region but rather its density evolves smoothly from one side of the resonance to the other. In chapter 4 we explore why the Fermi gas is so well behaved in this regime, which will in turn help us to understand and introduce universality in strongly interacting Fermi systems.

Chapter 3

Apparatus

The apparatus needed to cool our sample of ^{40}K atoms to ultracold temperatures is a collection of lasers, hundreds of optics, vacuum equipment, atomic sources, magnetic fields, control computers, and more. Many of the core pieces, such as the vacuum equipment and magnetic coils, have remained untouched for over ten years. I bring this up because although servos have been modified and optical beam paths have changed many times, the core of this experiment was built extremely well and provides an awesome foundation to build upon. Beginning with a solid foundation (along with 10+ years of tweaking laser locks and evaporation trajectories) has led to an extremely robust experiment. Assuming the gremlins did not steal into the lab during the night and move some mirrors, we can regularly produce a degenerate Fermi gas within thirty minutes of turning on the experiment. It is not uncommon for the experiment to continue to operate well into the night, if needed, with minimal adjustment during the day.

The core components of this experiment are covered in detail in the theses of Brian DeMarco [50] and Cindy Regal [47]. In some ways, almost all of the changes to the experiment during my tenure were to simplify and modernize the experiment. These changes include, but are not limited to: upgrading to a new computer control system giving us better timing and voltage control, new RF delivery schemes, new and more powerful lasers, fancier and more robust locking

schemes, higher resolution imaging, etc. Here, I will highlight a few of the most significant changes including our implementation of a crossed dipole trap and new computer control. I will also discuss the vacuum pressure of our system, which has become a bit of an issue. My feeling leaving this experiment is that my changes have resulted in an experiment that is considerably simpler and less intimidating.

3.1 Crossed optical dipole trap

As discussed in Chapter 2, the final stage of evaporation in our system occurs in a far off resonant optical dipole trap. All of the work in this thesis was done in an optical trap potential slightly different from that described in Cindy Regal's thesis. In an effort to improve axial thermalization times we introduced another optical dipole trap beam in an orthogonal direction to the original trap beam. This is often called a crossed dipole trap. Our trap now consists of two focused beams with waists of approximately 30μm $\times$ 30μm along the horizontal direction and 200μm $\times$ 200μm along the vertical direction. This new vertical beam works to effectively cap-off the large Raleigh range of the main confining potential and reduce the aspect ratio. For typical conditions, the trap frequencies are $\omega_r/2\pi \approx 200$ Hz along the radial direction and $\omega_z/2\pi \approx 20$ Hz along the axial direction. This is approximately an order of magnitude reduction in the trap aspect ratio as compared to the previous setup.

Imperative to the implementation of our new optical trap setup was the careful designing of the new geometries and powers. In an atomic Fermi gas, there are many considerations for cooling such as density, trap frequencies, trap depth, single-photon scattering, etc. Of particular help has been a Mathematica notebook that was started by Cindy Regal and brought to its final form by me. In this notebook, we address many of the concerns for cooling a Fermi gas in order to design a great optical trap the first time. A 3D plot from our Mathematica

notebook for our new crossed dipole trap is shown in Fig. 3.1. As I understand it, this notebook has become a standard for optical trap design in JILA.

The laser light is provided by a 20W IPG fiber laser (which really appears to just be a fiber-amplified diode laser) which operates single-mode at 1064nm with an 100 kHz linewidth. (As a side note, while our laser has worked fine for years now, other IPG single-frequency lasers around JILA and other labs around the world have been notoriously unreliable and I would probably not recommend this laser.) The light is split into two beams and each beam is individually intensity controlled using acoustic optical modulators (AOMs). The AOMs are then used to ramp down the laser power for evaporation. Only when a significant portion of the optical trap evaporation has occurred is the vertical optical trap applied. This is because the vertical trap has a relatively weak intensity and only contributes significantly to the trap strength near the end of evaporation.

3.2 Computer control

Ultra cold atomic gas experiments are sufficiently complicated that they require computer control. Additionally, since every experiment effectively destroys the sample, we require the sort of reproducibility that only a computer can provide. The experiment, as it was handed to me, ran on an old computer that did not even boot into Windows. Instead, the control code was written in QBasic and ran from DOS. The two major faults with this setup were that because the computer was so old, replacement parts could only be found on eBay. And, because the equipment was so old, we were at capacity for its capabilities. Newer systems have better timing, more voltage control, and more channels. The downside of most newer systems is that they tend to be programmed in LabView, which can become very tedious and slow with such complicated experiments. The question was then: can we keep the low-level programming we like (Basic) while upgrading

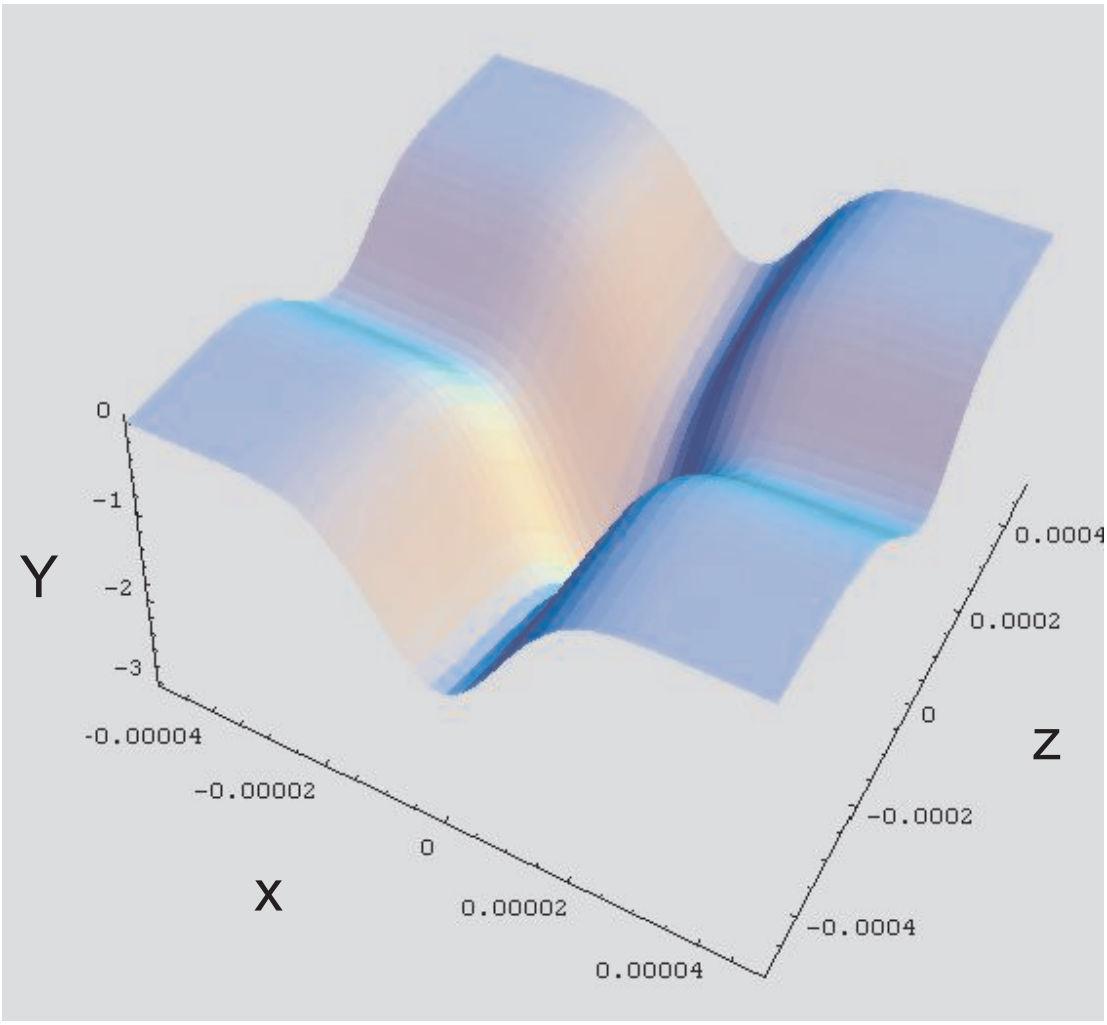

Figure 3.1: A 3D plot of our crossed optical dipole trap. The potential is in μK and the axes are in meters. The second optical trap (vertical) acts to cap off the large Raleigh range of the main confining trap (horizontal).

the hardware?

We decided to go with Visual Basic because the old QBasic syntax could be copy and pasted into the newer version. The main challenge was to modify the QBasic code to talk to the new digital (NI PXI DIO64) and analog boards (NI PXI 6733) in Visual Basic. This hard work was initiated by Travis Nicholson and finished by Tara Drake. We also decided to go with a PXI chassis (NI PXI-10420) from National Instruments, into which the analog and digital boards are inserted. In this way, the chassis is connected to the computer via a single board and it will be easy to replace a computer if it breaks or parts become outdated.

Fig. 3.2 is a picture of the control setup during the switch from old to new. The process was quite tedious but it paid off. With the new control computer setup we have approximately 50% more digital and analog lines. We have also gained about a factor of thirty in timing and voltage resolution. The new control computer has such better capabilities that we removed about six different commercial pulse generators (and the sub-routines to talk to them) and numerous JILA-made pulse-summers, inverters, and pulse generators. I was able to remove hundreds of meters of BNC cables, power cables and GPIB cables and correspondingly able to remove hundreds of lines of control code. All in all, the upgrade to a newer control system has been a great success and resulted in an experiment that is a lot less intimidating and much more transparent. Our experimental control computer and code is so reliable that we typically go months without restarting the code or the computer. I suspect that this system will also become a new standard for computer control in JILA.

3.3 Vacuum pressure

Over the last couple years we have been having problems with the vacuum pressure in the science cell. Because we do not have a vacuum gauge in our system,

Figure 3.2: A picture of our computer control setup while we were in the middle of switching to our new setup. Switching to a newer setup was a daunting task but thorough preparation resulted in less than one week of downtime.

we use the atoms to determine to the vacuum pressure. This is typically done by measuring the "lifetime" of atoms held in the magnetic trap, using either MOT recapture or the magnetic trap after evaporation. In atomic systems, the lifetime of the atoms is either long enough or not long enough. In other words, only when the lifetime of trapped atoms becomes comparable to evaporation timescales does it pose a problem.

In Fig. 3.3, I plot the atom lifetime as measured with MOT recapture (or magnetic trap) since the first measurement in the early months of 1998. In the early days, atom lifetimes on the order of a few hundred seconds were regularly measured. In fact, there are spans of many months in which a lifetime was never measured because it was always good enough. As time went on, there were downturns in the lifetime but these were usually promptly fixed by either switching to a new getter or firing the ti-sub pump and even turning off one of the ion pumps. However, there has been a steady decrease in the atom lifetime in the last few years, especially during my tenure. The horizontal dashed line indicates a typical evaporation timescale. As all previous measurements of the lifetime were above this line there was never much concern for the vacuum. However, as the most recent lifetime measurements are approaching this timescale we have trouble evaporating to quantum degeneracy and it becomes a problem we have address.

We have three pumps in our vacuum system: two ion pumps (a 40 L/s and a 20 L/s) and a titanium-sublimation (ti-sub) pump. As of a few years ago (before I came to the lab), the 20 L/s ion pump was turned off because it appeared to be hurting the atom lifetime. So, we are left with a single ion pump (which is continually on) and the ti-sub pump. Whereas in the theses of Brian DeMarco and Cindy Regal the ti-sub pump was fired less than once a year, we find ourselves firing every few months now, usually with mixed results. The options I see for improving the vacuum lifetime are either turning on the ion

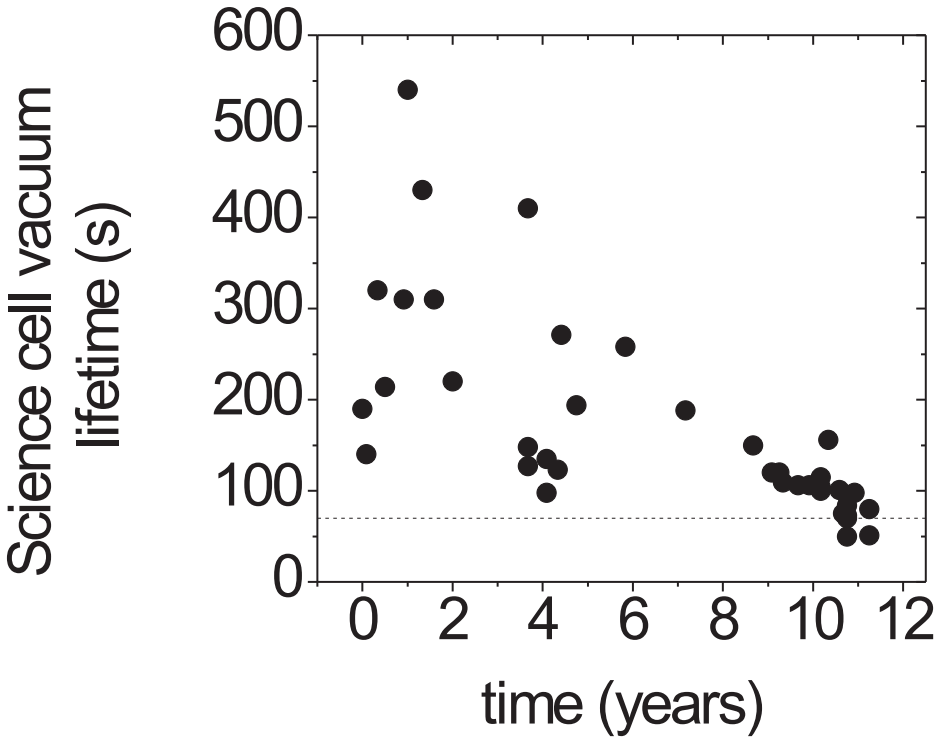

Figure 3.3: The atom lifetime in the science cell. Determined from a combination of measurements including MOT recapture and holding at the end of the magnetic trap. The vacuum was first pumped down and baked in the early months of 1998 [50]. Since then, the lifetime in the science cell has slowly drifted down. The dashed line indicates a typical evaporation timescale. If the lifetime dips below the dashed line we will have difficulty evaporating to quantum degeneracy.

pump which has been decommissioned, or doing a bake of the vacuum system. A bake is particularly challenging in our science chamber where the magnetic trap is basically a permanent fixture of the vacuum. Thus, a bake would need to be mild and probably of a long duration to be effective at removing contaminates from the cell walls. If the contaminates are primarily ^{40}K atoms then this type of bake could have some nice improvement to the atom lifetime since alkali atoms have weak bonding with the cell walls.

In conclusion, I cannot say enough good things about the experimental apparatus I have had the pleasure to work with. It is a robust experiment that has produced some amazing results over the years. I suspect this is due to the strong foundation and relative simplicity of the experiment (only one atomic species). Assuming that the getters continue to produce ^{40}K and the vacuum lifetime problems can be kept at bay, this experiment should continue to produce strongly interacting degenerate Fermi gases for some time to come.

Chapter 4

Universality in Fermi gases

Universal behavior in physics is often very powerful. In principle, by studying just one system, one can learn about every other system for which the universal behavior applies. Universal, as defined here, will refer to behavior that does not depend on the microscopic details of the interactions, and instead only depends on density and temperature. In this chapter, we will study universality that occurs in the limit of very strong interactions. In this limit, in which the length which characterizes the interaction between particles is much larger than the interparticle spacing, fermion systems display universal behavior and universal thermodynamics. This universal regime is related to nuclear and neutron matter and is also expected to be found in the quark-gluon plasma. Demonstrating universal behavior means showing that the physics we observe is not specific to our atomic species. The experiment shown here serves as a good example of how studying universal properties an atomic Fermi gas can inform us about an entire class of problems.

4.1 The only scale: E_F

Generically, as a gas of fermions is cooled from the classical regime to quantum degeneracy, the Pauli exclusion principle becomes manifest in the properties of the ultracold gas [26, 94]. This is evident in a confined zero-temperature ideal

Fermi gas as a finite energy and a finite size. The Pauli exclusion principle acts as "pressure," called the Fermi pressure, and is responsible for the stability of white dwarf and neutron stars. In this chapter, we investigate what happens if we begin with a quantum degenerate non-interacting Fermi gas and then adiabatically turn on attractive interactions.

We can characterize the interactions between two fermions using the two-body scattering length, a. It is instructive to imagine we can then tune a however we like, for example by using a Fano-Feshbach resonance. If we tune the scattering length to be negative, corresponding to attractive interactions, one would expect that the gas should be compressed due to attractive interactions and eventually pairing effects [95]. As the magnitude of the negative scattering length is increased, and the interactions become arbitrarily strong and attractive, one might expect the trapped gas to collapse to high density, or implode. In fact, the Pauli exclusion principle prevents the gas from imploding and the Fermi gas exhibits universal behavior [5, 3, 8].

We can gain some insight into the effect of diverging interactions by considering a simple mean-field approach. While this approach neglects pairing and therefore is not sufficient to fully describe the behavior, it provides a flavor of how the Fermi gas is affected by interactions. Following the argument outlined in Ref. [96], the equation of state for a confined zero-temperature Fermi gas is

$$\mu = \epsilon_F(\mathbf{x}) + U_{MF}(\mathbf{x}) + U_{trap}(\mathbf{x}), \tag{4.1}$$

where μ is the chemical potential, $\epsilon_F(\mathbf{x})$ is the local Fermi energy, $U_{MF}(\mathbf{x})$ is the mean-field contribution, and $U_{trap}(\mathbf{x})$ is the trapping potential. We can relate $\epsilon_F(\mathbf{x}) = \frac{\hbar^2}{2m}k_F^2(\mathbf{x})$ to the density $n(\mathbf{x}) = \frac{1}{6\pi^2}k_F^3(\mathbf{x})$ via $\epsilon_F(\mathbf{x}) = \frac{\hbar^2}{2m}[6\pi^2 n(\mathbf{x})]^{2/3}$. The interactions appear in the density dependent mean-field contribution, $U_{MF}(\mathbf{x}) = \frac{4\pi\hbar^2 a}{m}n(\mathbf{x})$.

For the case in which a diverges, the equation given above for $U_{MF}(\mathbf{x})$ becomes unphysical. As $a \to \pm\infty$, the only finite energy scale in the problem is the Fermi energy. To incorporate this we can approximate the scattering length by an effective scattering length set by the Fermi energy, $a_{eff} = -1/k_F$. Using this substitution into $U_{MF}(\mathbf{x})$ we see that the local mean-field energy is proportional to the Fermi energy, and one can define a constant of proportionality β given by $U_{MF}(\mathbf{x}) = \beta\epsilon_F(\mathbf{x})$ [97, 43]. Now, we arrive at the new equation of state for a strongly interacting Fermi gas:

$$\mu = (1 + \beta)\epsilon_F(\mathbf{x}) + U_{trap}(\mathbf{x}). \tag{4.2}$$

From this new equation of state it is particularly clear that the interactions have dropped out of the problem and we are left with a universal result that depends solely on the Fermi energy [5, 3, 8]. Notice that the new equation of state is simply a re-scaled version of the non-interacting equation of state ($\beta \to 0$ in the non-interacting case). Also note that only a zero temperature gas will depend solely on the Fermi energy. More generally, a strongly interacting Fermi gas will also depend on the relative temperature T/T_F.

In our simple mean-field estimate, we can make the substitutions to find $U_{MF}(\mathbf{x}) = -\frac{4}{3\pi}\epsilon_F(\mathbf{x})$, or $\beta_{MF} = -0.42$. The negative sign is not obvious from this approach, but a more sophisticated many-body approach shows the mean-field interaction should be attractive [5]. Theories and Quantum Monte Carlo (QMC) simulations that include the effects of pairing find β to be more negative, or rather, the ground-state energy is even lower than one would predict from the simple mean-field approach. Theoretical and QMC values for β all come in around $\beta = -0.6$ [6, 60, 61, 62, 63, 64, 65, 66, 67].

If one can measure a property of the gas that is related to the equation of state and compare measurements for a strongly interacting gas and a non-

interacting gas, then the universal parameter β can be determined. As we learned in Chapter 2, we have the ability to control the scattering length with a Fano-Feshbach resonance and we can study both the strongly interacting and non-interacting Fermi gases. In the next section, I discuss how we measure β, and for the first time its temperature dependence, using our atomic gas.

4.2 Measuring β in an atomic Fermi gas

We learned in the previous section that by studying the equation of state for a Fermi gas with and without strong interactions we can determine the universal parameter β. To see this more explicitly for the trapped atomic Fermi gas, we will first consider the ideal gas case. We can use the equation of state to express the number of atoms $N = \int_0^{x_F^0} n^0(x) d^3x$ in terms of the chemical potential μ^0. Here, x_F^0 is the Fermi radius and the superscript $(^0)$ refers to a quantity of a non-interacting Fermi gas. Using (4.1) with $U_{MF}(\mathbf{x}) = 0$ and expressing $\epsilon_F(\mathbf{x})$ in terms of $n(\mathbf{x})$, we can solve for the number

$$N^0 = \frac{1}{6\pi^2} 4\pi \int_0^{x_F^0} x^2 \left[(\mu^0 - \frac{1}{2} m\omega^2 x^2) \frac{2m}{\hbar^2} \right]^{3/2} dx \tag{4.3}$$

where $U_{trap}(\mathbf{x}) = \frac{1}{2} m\omega^2 x^2$ is the trapping potential and m is the mass of ^{40}K and ω is the angular trap frequency for a spherically symmetric trap. At the edge of the trap the density goes to zero ($n(x_F^0) = 0$ and $\mu^0 = \frac{1}{2} m\omega^2 (x_F^0)^2$) so evaluating (4.3) we find

$$N^0 = \frac{1}{6} \left(\frac{\mu^0}{\hbar\omega} \right)^3. \tag{4.4}$$

This analysis (determining the number of atoms in terms of the chemical potential) works similarly in the limit of strong interactions. Using the modified equation of state (4.2), we see that the only difference from the non-interacting case is that the Fermi energy is multiplied by $(1 + \beta)$. Thus, we find the atom

number at unitarity to be

$$N = \left(\frac{1}{1+\beta}\right)^{3/2} \frac{1}{6} \left(\frac{\mu}{\hbar\omega}\right)^3. \tag{4.5}$$

Equating the number in both cases,(4.4) and (4.5), we find

$$\frac{\mu}{\mu^0} = \sqrt{1+\beta}. \tag{4.6}$$

Now we have arrived at the relation between the chemical potential for the strongly interacting trapped Fermi gas and the universal parameter β.

The question is then, how can we relate the quantity μ/μ^0 to a measurable quantity in Fermi gases. In the non-interacting limit, we can relate the chemical potential μ_0 to the potential energy through the virial theorem. Recall that the virial theorem states that in a confining potential of the form $V(r) = \alpha r^2$, then the average total potential energy E_{pot} is related to the average total kinetic energy via $E_{kin} = E_{pot}$. Further, we know the average total energy is $\frac{3}{4}E_F$ for a trapped Fermi gas in a harmonic trap [50]. Thus, in the non-interacting limit, we can relate the potential energy to the chemical potential via $E^0_{pot} = \frac{3}{8}\mu^0$. As it turns out, the virial theorem also holds on resonance as first proposed by J. E. Thomas in Ref. [98]. More recently, a generalized virial theorem for all interaction strengths has been proposed [99], and on resonance the ideal gas virial theorem is recovered. Thus, by using the virial theorem for both a weakly and strongly interacting Fermi gas, we can directly relate the chemical potential to a measurable quantity: the potential energy.

By the time we began our experiments to determine β, there were several experiments reporting or inferring β in ^{6}Li [43, 97, 45, 35, 57, 58, 59]. For the ^{6}Li experiments, the values for β were all coming in around $\beta = -0.6$. While the ^{6}Li values were in good agreement with theory, we felt that a measurement using a different atomic species was essential to demonstrate the universality of

strongly interacting atomic Fermi gases. Since ^{40}K and ^{6}Li are different atomic species with different atomic interatomic potentials and different Fano-Feshbach resonance properties, agreement on β using these two difference species would be a clear demonstration of universality.

As a bit of a side note, a Fano-Feshbach resonance is not a sufficient requirement for realizing the universal regime. In fact, the resonance must be a broad Fano-Feshbach resonance in order for the gas properties to not depend on the details of the interatomic potential [100, 101, 77, 102]. In other words, good agreement between the two species would also put to rest some theoretical claims that the Fano-Feshbach resonance in ^{40}K is not a wide resonance [103, 104].

4.2.1 β from the potential energy

At the time we set out to measure β in ^{40}K, measuring the potential energy seemed the most obvious route since we could make a direct comparison with β obtained in similar measurements done in ^{6}Li. In addition, the potential energy can be obtained from a measurement of the Fermi gas in the trap and can be related directly to the chemical potential via the virial theorem. As it turns out, Cindy Regal had measured the momentum distribution throughout the BCS-BEC crossover and we were able to use her measurement to determine β as well. I will discuss how to extract β from the momentum distribution in 4.2.2. Regardless, our initial experiment was to measure β using the potential energy and I will cover that approach first.

Recall that we can extract β from the ratio of interacting to non-interacting potential energies. Therefore, to extract β, we must measure the potential energy after an adiabatic field sweep to the Fano-Feshbach resonance and the potential energy after an adiabatic field sweep to the zero crossing of the Fano-Feshbach resonance. Adiabaticity here requires that the time over which we make a significant

change to the scattering length is long compared to the axial trapping period. This means that ideally we want $\dot{a}/a \ll 2\pi/\omega_z$, where ω_z is the angular trap frequency in the axial direction. However, the magnetic field sweeps cannot be too slow, because we observe significant heating rates near the Fano-Feshbach resonance due to inelastic collisions. For this reason we had to add additional axial confinement to our optical trap setup, as discussed in Chapter 3. By increasing $\omega_z/2\pi$ from approximately 2 Hz to 20 Hz, the ramp duration required for adiabaticity was reduced to tens of milliseconds from hundreds of milliseconds. After each ramp the Fermi cloud was allowed to expand for a short time, 1.876 ms. During this short expansion time there is significant expansion in the radial direction, which helps to reduce the optical depth of the gas, but negligible expansion in the axial direction. Therefore, by imaging along one of the radial directions we can probe the density distribution of trapped gas in the axial direction.

For each absorption image we perform a 2D surface fit to a finite temperature Fermi-Dirac function

$$OD(y,z) = pk\, g_2\Big(-\zeta\, e^{-\frac{y^2}{2\sigma_y^2}-\frac{z^2}{2\sigma_z^2}}\Big)/g_2(-\zeta) \tag{4.7}$$

where ζ, σ_y, σ_z, and pk are independent fitting parameters and $g_n(x) = \sum_{k=1}^{\infty} \frac{x^k}{k^n}$ [50]. This is the expected optical depth (OD) distribution for a non-interacting cloud both in trap and after expansion. Empirically we find that this function also fits well in the strongly interacting regime. The potential energy of the trapped gas is obtained from the cloud profile in the axial direction. The potential energy per particle in the axial direction is given by

$$E_{pot} = \frac{1}{2} m \omega_z^2 \sigma_z^2 \frac{g_4(-\zeta)}{g_3(-\zeta)} \tag{4.8}$$

where m is the mass of ^{40}K and ω_z is the axial trapping frequency.

In previous experiments using ^{6}Li atoms, the measured cloud sizes and energies were normalized to a *calculated* value for the non-interacting gas. This can

introduce systematic errors because the calculation relies on the atom number and trap frequencies, which can have systematic errors. The reason that measuring the non-interacting size or energy is impractical in ^{6}Li is that the Fano-Feshbach resonance is extremely wide and one would have to move the magnetic field hundreds of Gauss to access the zero crossing. In ^{40}K, the zero crossing is roughly 10 G away and we can measure both E_{pot} and E^0_{pot} directly. Therefore, systematics in determining β are substantially reduced. Experiments accessing the zero crossing of the ^{6}Li have now been accomplished [105].

In Fig. 4.1, I show the measured potential energy ratio as a function of $1/k^0_F a$, where again a superscript naught indicates a measurement made in the non-interacting regime. As expected, the data show that as attractive interactions are increased there is a strong reduction in the potential energy due to a compression of the trapped gas. Strictly speaking, β is only defined at the location of the resonance, but the potential energy should behave universally as a function of $1/k^0_F a$ as well. The solid line is a mean-field calculation valid for the BCS-side of the resonance [53] and has good agreement for $1/k^0_F a < -1$. Notice, however, that it breaks down as interactions approach the BCS-BEC crossover regime. On the BEC side of the resonance one would expect that E_{pot} will depend on condensate fraction. For temperatures similar to these experiments we find a maximum condensate fraction of approximately 15% on resonance; this fraction decreases as detuning from the resonance is increased [30].

The error bars in Fig. 4.1 include statistical uncertainty in repeated measurements as well as an uncertainty due to heating during the magnetic-field ramps. The magnetic-field ramps must be sufficiently slow to be adiabatic; however, heating during the ramp can be a problem for slower ramps. For final magnetic fields around the resonance and especially on the BEC side of the resonance we would observe some heating which can alter the determination of E_{pot}.

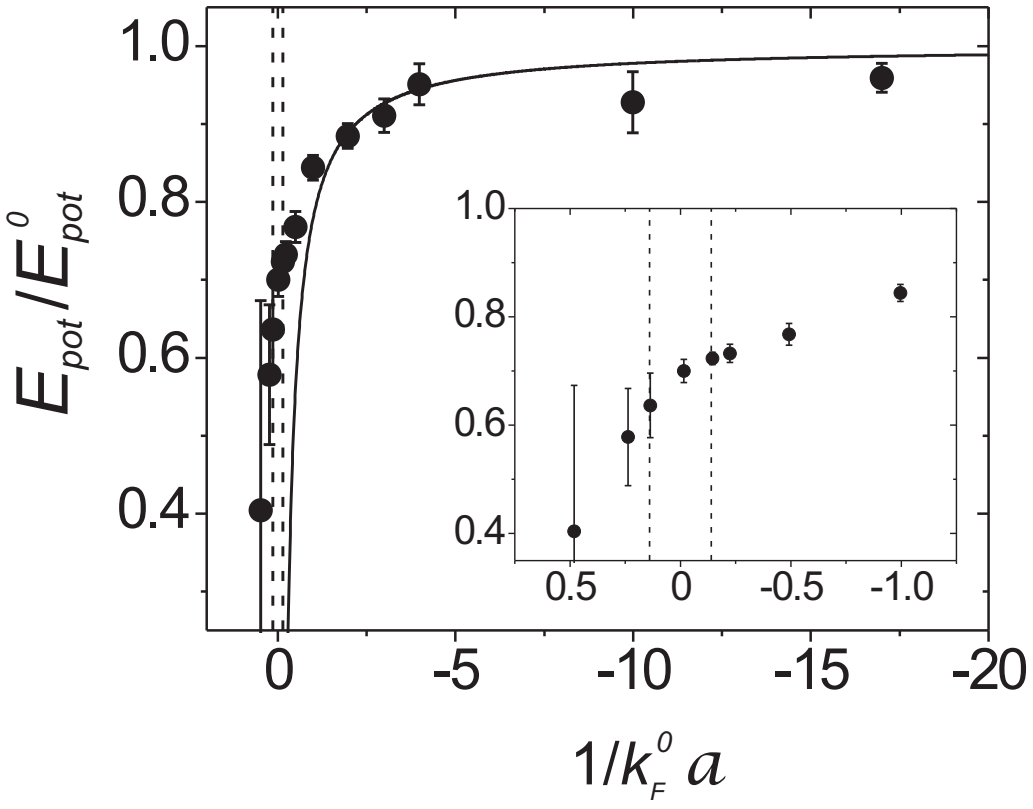

Figure 4.1: Measured potential energy, E_{pot}, normalized to the value measured in the non-interacting regime, E^0_{pot}, versus $1/k^0_F a$. Here (^{0}) denotes a quantity measured in the non-interacting regime, i.e., at the zero crossing of the Fano-Feshbach resonance. The resonance is located at 202.10 ± 0.07 G [30]; the dashed lines show the uncertainty in the resonance location. Data points toward the BCS limit show good agreement with a zero temperature mean-field calculation (solid line). The larger error bars on the BEC side of the resonance reflect uncertainties due to heating of the gas due to inelastic loss. In the strongly interacting region there exists ± 0.1 uncertainty in $1/k^0_F a$ due to uncertainty in the resonance position. (inset) Subset of the data focusing on the strongly interacting region near resonance.

We investigate the dependence of the measured potential energy by varying the duration of a linear ramp. An example of this is shown in Fig. 4.2 where the gas was ramped from the magnetic field used for evaporation to the resonance position.

To determine the optimum ramp rate, as well as the effect of heating on the potential energy measurement, we fit data such as that shown in Fig. 4.2 to an exponential decay (due to adiabaticity) plus linear (due to heating). From the fit we determine the final potential energy of the cloud if heating were not present. This introduces a correction that is applied to the data and error bars shown in Fig. 4.1. On the BCS side of the resonance we see little or no heating due to magnetic-field ramps, and the error bars are dominated by shot-to-shot statistical uncertainty.

From the data in Fig. 4.1, we find $E_{pot}/E^0_{pot} = 0.70 \pm 0.02$ on resonance, from which we can use Eq. (4.6) giving $\beta^* = -0.51 \pm 0.03$. Whereas β is normally only defined for $T = 0$, I introduce $(^*)$ to denote that the system is at a finite temperature $(T/T_F)^0 = 0.08 \pm 0.01$. Including uncertainty in the resonance position we find $\beta^* = -0.51^{+0.04}_{-0.12}$. Error bars include statistical error as well as the heating effects mentioned above.

At the time we made this measurement it was not clear to us that β^* at a temperature of $(T/T_F)^0 = 0.08 \pm 0.01$ should be the same as zero temperature β. In fact, this was a point seemingly ignored by all previous measurements. To determine the temperature dependence of β^* we measured the potential energy ratio at resonance for different starting temperatures. In Fig. 4.3, I show the ratio E_{pot}/E^0_{pot} as a function of initial temperature $(T/T_F)^0$. Clearly the universal many-body parameter β depends strongly on temperature.

To determine the initial temperature we prepare a gas as described previously and then ramp to the zero crossing of the Fano-Feshbach resonance and fit

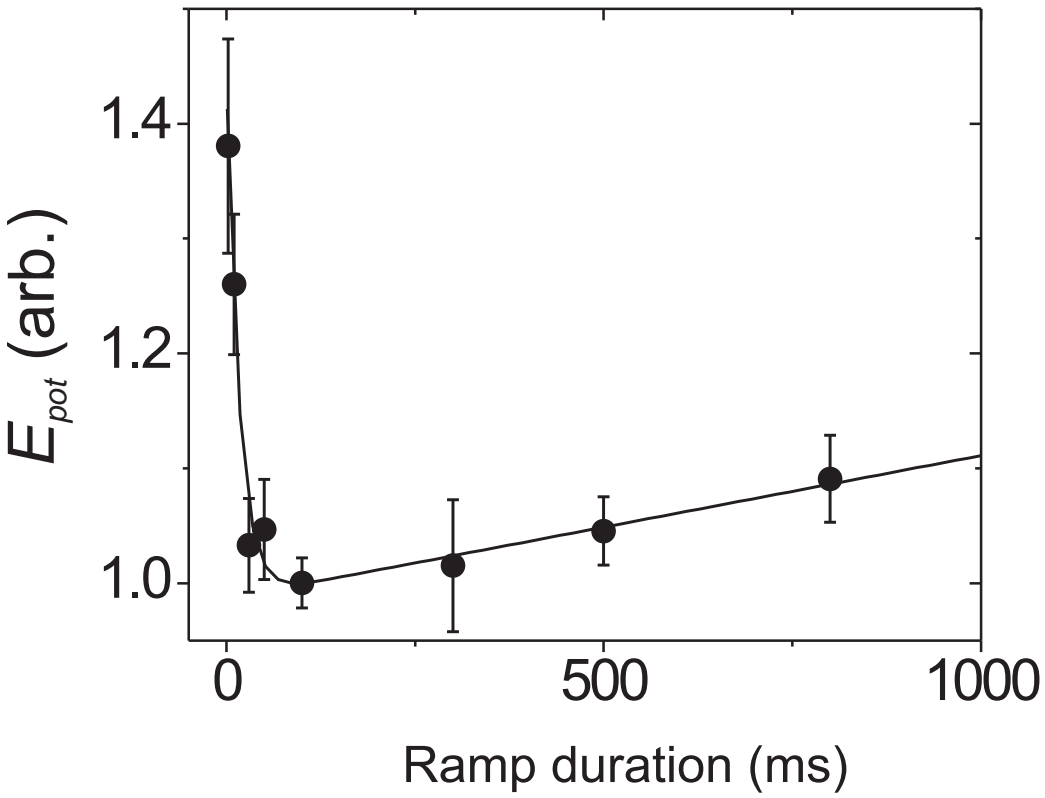

Figure 4.2: Measured potential energy at the Fano-Feshbach resonance versus magnetic-field ramp duration. For very fast ramps, we measure a higher energy because of nonadiabaticity. For very slow ramps, heating due to inelastic collisions increases the measured energy. We use a simple empirical fit to determine optimum ramp rate and E_{pot}.

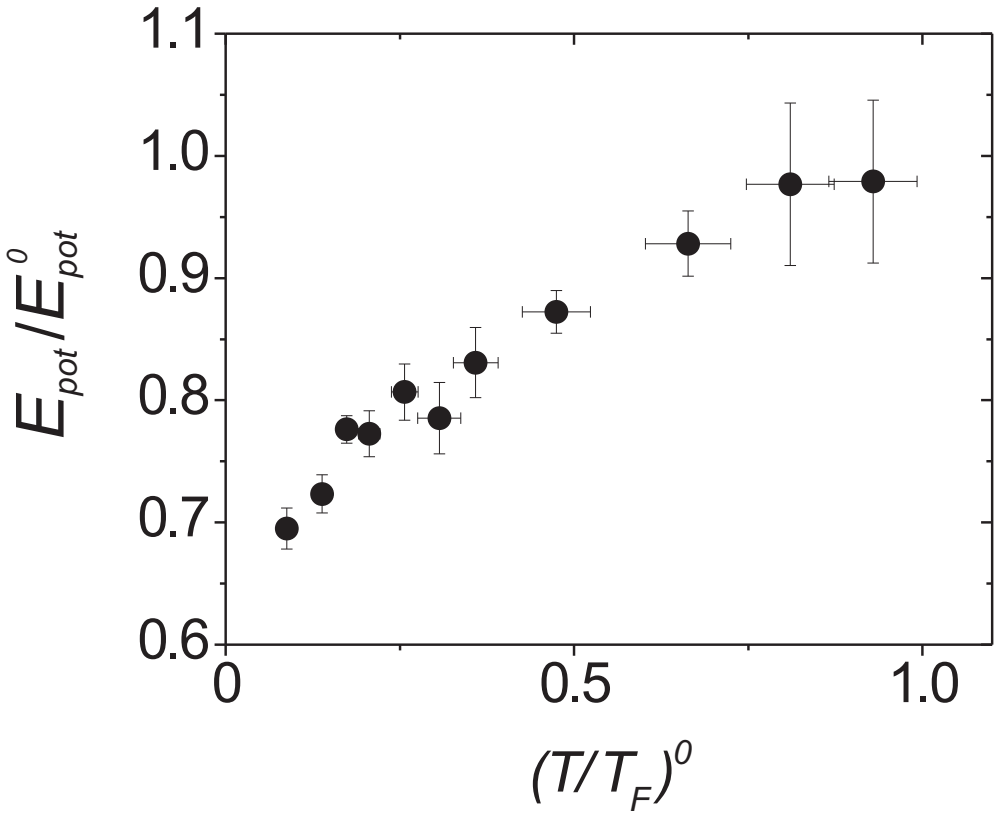

Figure 4.3: Potential energy E_{pot} normalized to the measured energy in the non-interacting regime E^0_{pot} verses the noninteracting gas temperature $(T/T_F)^0$. The cloud is heated by parametrically modulating the trapping potential. For these data the trapping frequencies in the radial direction vary from $\sim$ 180 to 450 Hz and in the axial direction from $\sim$ 18 to 21 Hz.

the expanded cloud to Eq. (4.7). We extract $(T/T_F)^0$ from the fugacity ζ using $g_2(-\zeta) = -(T/T_F)^{-3}/6$. We only measure the temperature for a non-interacting gas because interactions distort the expansion of a strongly interacting gas. However, because we know the temperature for our non-interacting gas and our field ramps are adiabatic, theory can be used to extract the new temperature [63, 106]. To vary the temperature we parametrically modulate the optical trap strength. To ensure harmonic confinement the trap strength is chosen to be substantially higher than the Fermi energy.

For the purpose of extracting a value for the zero temperature β we fit a quadratic function to the data points below $(T/T_F)^0 = 0.25$, from which we find $\beta = -0.54^{+0.05}_{-0.12}$. The error bars reflect the uncertainty in the extrapolation to $T = 0$ and the uncertainty in the resonance position. This value of the universal many-body parameter β, as well as the value at $(T/T_F)^0 = 0.08$, is in good agreement with the rough value of $\beta = -0.6$ found in theory and Monte Carlo calculations. These values are also in good agreement with multiple experimental reports in ^{6}Li: $\beta = -0.73^{+0.12}_{-0.09}$, -0.61 ± 0.15, -0.49, and -0.54 ± 0.05 in Refs. [107], [57], [59], and [58] respectively. In particular, I would like to note the most accurate measurement to date from the group of J. E. Thomas at Duke University, where they find $\beta = -0.60(2)$ and $-0.62(2)$ using two different techniques [105].

Our measurement of the universal many-body parameter β was the first of its kind in ^{40}K, and when added to the ^{6}Li measurements our result clearly demonstrated universality in atomic Fermi gases. We also made the first temperature dependent measurement of β and found that it can depend strongly on temperature, even at low temperatures. Also, the technique used here was expanded upon to determine the entropy and critical temperature in Ref. [108].

4.2.2 β from the kinetic energy

It was not until after we had made our measurement of β using the potential energy that we realized β could also be determined from a previous result by Cindy Regal *et al* [53]. In the previous measurement, the momentum distribution was mapped out throughout the BCS-BEC crossover and the kinetic energy on resonance was determined to be $E_{kin}/E^0_{kin} = 2.3(0.3)$ [53]. To see how β can be derived from the kinetic energy I will briefly sketch out the relation here.

The energy per particle of an ultracold Fermi gas in the universal regime scales as [109]

$$E(\mathbf{x}) = E_{kin}(\mathbf{x}) + E_{int}(\mathbf{x}) = \frac{3}{5}(1+\beta)E_F(\mathbf{x}) \tag{4.9}$$

where $E_{int}(\mathbf{x})$ refers to the interaction energy. Recall from the discussion in Section 4.1 that $E_{int}(\mathbf{x}) = U_{MF}(\mathbf{x}) = \beta\epsilon_F(\mathbf{x})$. Thus we have

$$E_{kin}(\mathbf{x}) = \Big(\frac{3}{5} - \frac{2}{5}\beta\Big)E_F(\mathbf{x}). \tag{4.10}$$

If we use the same procedure to determine the atom number as we did for Eqs. (4.4) and (4.5) and integrate Eq. (4.10) over the trapped gas, we find

$$E_{kin} = \frac{1}{8}\frac{3-2\beta}{1+\beta}\mu. \tag{4.11}$$

Recall that in a non-interacting Fermi gas the kinetic energy is $E^0_{kin} = \frac{3}{8}\mu^0$. Assuming we keep the atom number fixed for each case we have from Eq. (4.6) that $\mu/\mu^0 = \sqrt{1+\beta}$ and after simplification we can relate the kinetic energies

$$\frac{E_{kin}}{E^0_{kin}} = \frac{1-\frac{2}{3}\beta}{\sqrt{1+\beta}}. \tag{4.12}$$

Now we can clearly see that β can be determined by measuring the ratio of kinetic energies. If we use the mean-field estimate for $\beta = -0.42$ one finds that $E_{kin}/E^0_{kin} = 1.69$, which is substantially smaller than the experimental result. Again, this shows that more sophisticated theories that include the effects of

pairing are needed. The measured value of $E_{kin}/E^0_{kin} = 2.3(0.3)$ gives a value for β of $-0.62(7)$, which is in good agreement with theory and previous measurements.

As we have seen with the measurement of β, atomic Fermi gases can already provide constraints on theoretical models. In particular, we have seen a large discrepancy between a simple mean-field estimate for $\beta = -0.42$ and the more complicated theoretical and experimental works that put the value closer to $\beta = -0.6$. This example serves as a reminder that pairing in these systems cannot be ignored but in fact makes up a substantial portion of the physics. The rest of this thesis will study pairing using radio frequency spectroscopy, providing much more detailed microscopic information as well as stringent tests for many-body theories.

Chapter 5

RF spectroscopy: A historical perspective

Probing an atomic gas can require a fair amount of ingenuity. This is because classical probes such as thermometers or electrical leads are not applicable. All measurements are effectively "hands off." Basically, the only tools one has are E & M fields: light, electric fields and magnetic fields. One of the experimental tools that has had continued success probing atomic Fermi gases is radio-frequency (RF) spectroscopy, for example see Refs. [42, 110, 111, 44, 112, 113, 114, 115, 69, 82]. In Chapter 6, we discuss a new probing technique where an RF photon is used to "photo-emit" atoms into another Zeeman state in an experiment similar to photoemission spectroscopy (PES) experiments in condensed matter physics. Therefore, it is my goal in this chapter to introduce the role of RF in atomic systems and its role as a spectroscopic probe, which was already a powerful tool before we applied it to PES for atoms. I will present RF spectroscopy from a chronological point of view to better illustrate its evolution into a spectroscopic probe.

As we will review, RF spectroscopy has proven to be a very powerful probe of interactions in atomic gases. It was instrumental in determining the physics around Fano-Feshbach resonances. It can also be used to associate and disassociate molecules and is a microscopic probe of strongly interacting atomic gases. I will begin by outlining the simple theory regarding the coupling of states using

RF and then move on to its use as a spectroscopic probe.

Our chronological tour of RF spectroscopy as powerful probe will eventually come to a "bump in the road." This is because RF spectroscopy is only valid when a particular set of conditions are met. If these conditions are not met, such as can easily be the case in ^{6}Li, then they can lead to results that are misleading and can be misinterpreted. I will try to highlight the pitfalls of RF as a spectroscopic probe, the lessons learned, and how the field eventually got back on the right track.

5.1 RF basics

Typically, we use RF in the lab for internal spin-state manipulation. Examples include removing high energy atoms during magnetic trap evaporation, achieving correct spin states for optical trap evaporation, or for spectroscopy. For RF spectroscopy, atoms are transferred between different Zeeman states, see Fig. 5.1 a). The RF frequency is typically in the 10-100 MHz range. Hence, the wavelength of the RF radiation is very long, on order of 3-30 m, and the momentum transferred to the atom is completely negligible. Therefore, we can think of RF spectroscopy as only changing the internal state of the atom and leaving its kinetic energy and momentum unchanged.

It is useful to remind ourselves how one can drive a transition between two internal states of an atom. Due to the long lifetime of the internal states we are dealing with we can assume a two-level system: the state we are starting out in $|g\rangle$ and the state we wish to couple to $|e\rangle$, where the energy difference is $E_g - E_e = \hbar\omega_0$. For the coupling field we will assume the RF is monochromatic and "strong" so we can treat it classically. Then, the coupling field can be written as $E = E_0 \cos(\omega_L t)$, where E_0 is the electric field strength and ω_L is the frequency of the RF. Then, we can write down our Hamiltonian as $H = H_{atom} + V_{atom-light}$,

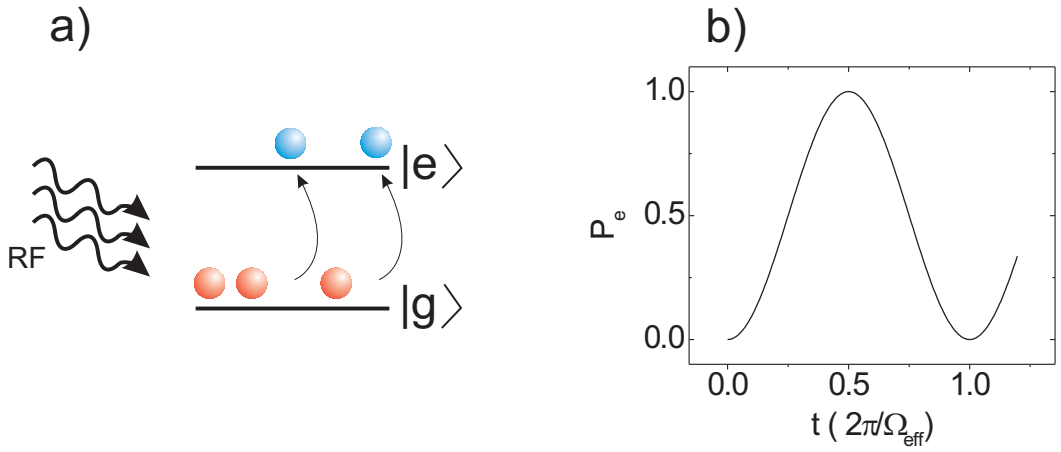

Figure 5.1: RF basics. a) We apply radio frequency to transfer atoms between two internal Zeeman states. b) Population in state $|e\rangle$ as a function of RF duration assuming resonant RF.

where in matrix form:

$$H_{atom} = \begin{pmatrix} 0 & 0 \\ 0 & \hbar\omega_0 \end{pmatrix}, \; V_{atom-light} = \begin{pmatrix} 0 & dE \\ dE & 0 \end{pmatrix}, \tag{5.1}$$

where d is the dipole matrix element $d = \langle e|e\,\hat{\pi}\cdot\vec{r}|g\rangle$. We want to know what happens to the states of the atom as a function of the strength, duration and frequency of applied RF. To do so we need to solve the time dependent Schrodinger equation $i\hbar\frac{\partial\psi}{\partial t} = H\psi$ with our wave function $\psi = c_1(t)|g\rangle + c_2(t)|e\rangle e^{i\omega_0 t}$, where c_1 and c_2 are the probability amplitudes. Using the rotating wave approximation (i.e., assume the RF frequency is near resonance) we end up with the set of equations

$$i\frac{d}{dt}\begin{pmatrix} c_1 \\ c_2 \end{pmatrix} = \begin{pmatrix} 0 & \Omega e^{-i\delta t} \\ \Omega e^{-i\delta t} & 0 \end{pmatrix}\begin{pmatrix} c_1 \\ c_2 \end{pmatrix}, \tag{5.2}$$

where $\Omega = dE_0/\hbar$ is the Rabi frequency and $\delta = \omega_L - \omega_0$ is the detuning of the applied RF. Solving these coupled equations with the boundary condition that all atoms begin in state $|g\rangle$ at $t = 0$ we find the probability to find an atom in state $|e\rangle$ is

$$P_e(t) = \frac{\Omega}{\delta^2 + \Omega^2}\sin^2\Big(\frac{\sqrt{\delta^2+\Omega^2}}{2}t\Big). \tag{5.3}$$

$P_e(t)$ is plotted in Fig. 5.1 b). To fully transfer all of the atoms into the $|e\rangle$ state one should apply resonant RF ($\delta = 0$) for $t = \pi/\Omega$; this is referred to as a $\pi-$pulse.

The energies for our atomic Zeeman states in a magnetic field can be calculated exactly using the Breit-Rabi formula. Therefore, we can choose ω_L to be exactly resonant and transfer atoms between Zeeman states by applying RF through an RF antenna [47]. An example of such a spin-state transfer is shown in Fig. 5.2. We deliver the RF in a gaussian envelope pulse to minimize unwanted frequencies. The RF lineshape, for a non-interacting gas, has a linewidth limited

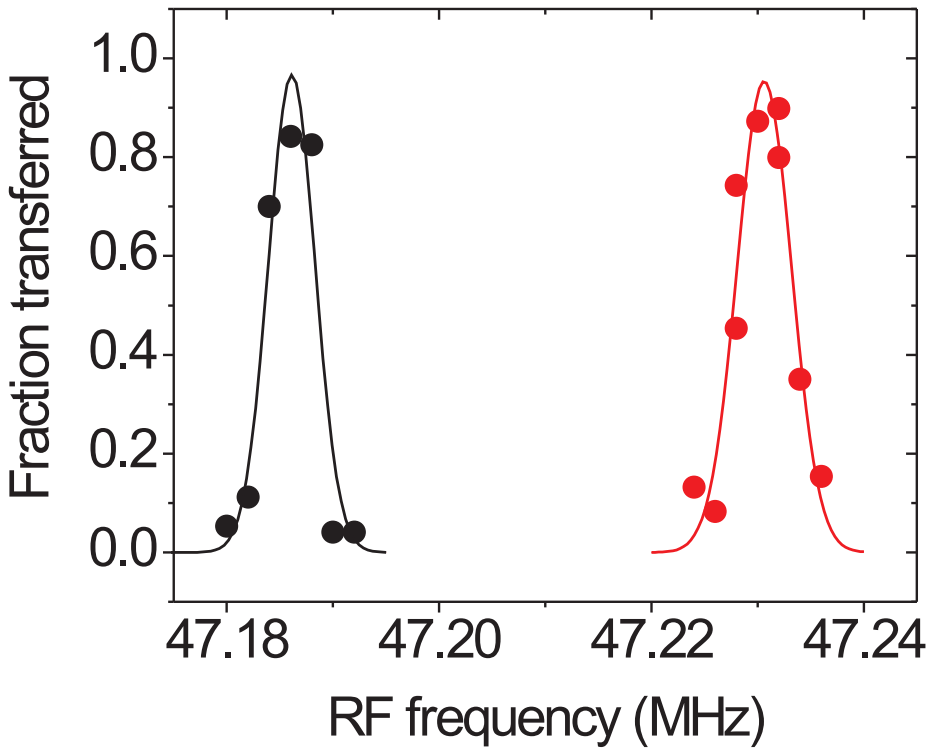

Figure 5.2: RF can be used to spectroscopically determine the magnetic field. On the vertical axis is the fraction of atoms transferred to a new internal Zeeman state. The horizontal axis shows the RF frequency. The red and black lineshapes are taken at two different magnetic fields approximately 100 mG apart.

by the inverse pulse duration. Our linewidths are ultimately limited by noise in the magnetic field. Typically, we can measure linewidths to 1 kHz or less, consistent with magnetic field stability on the order of a few mG. Good frequency sensitivity and magnetic field stability are imperative for using RF as a spectroscopic probe.

Using RF to determine the magnetic field and its stability is already a great example of RF as a spectroscopic probe. By varying ω_L one can take a lineshape to determine ω_0, see Fig. 5.2. Then, the Breit-Rabi formula can be used to determine the magnetic field. We use this technique quite often in the laboratory to calibrate the magnetic field as a function of current through the magnetic-field coils.

5.2 RF spectroscopy and interactions

One of the most illustrative examples of how RF can be used as a spectroscopic probe is also one of the earliest experiments that used RF to study interactions [111, 44]. In particular, RF spectroscopy can be used to determine the mean-field energy, $U_{MF} \propto na$, where n is the density and a is the s-wave scattering length. Near a Fano-Feshbach resonance a can be either positive or negative and therefore so can the mean-field energy. By taking RF lineshapes as the scattering length a is varied, one can determine how the resonant frequency is shifted by the mean-field energy.

When discussing RF spectroscopy in context of measuring interactions I will generally be discussing an experiment that involves three spin states. I will try to be consistent and refer to the two interacting states as $|\uparrow\rangle$ and $|\downarrow\rangle$, and a third state $|3\rangle$, which I will call the probe state. Typically, RF spectroscopy will refer to the transfer of atoms in the $|\downarrow\rangle$ state into the $|3\rangle$ state. For example, the Fano-Feshbach resonance in ^{40}K at 202.1 G affects the interactions between atoms in the $|9/2, -9/2\rangle$ and $|9/2, -7/2\rangle$ states ($|\uparrow\rangle$ and $|\downarrow\rangle$) and the probe state would

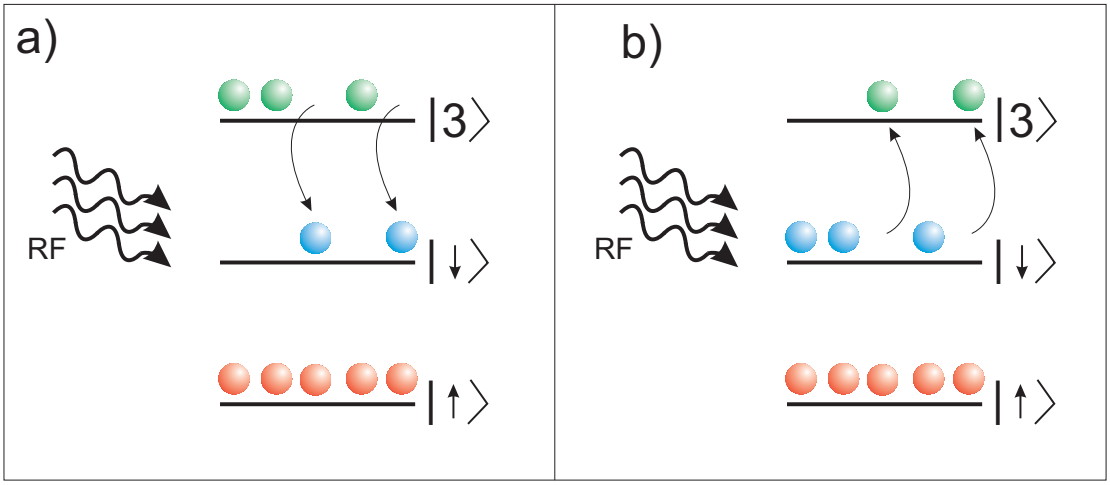

Figure 5.3: RF spectroscopy (when interactions are involved) will typically involve three internal states. RF spectroscopy can be used to probe the interactions between $|\uparrow\rangle$ and $|\downarrow\rangle$ in two complimentary ways. a) Sending some atoms from the non-interacting state $|3\rangle$ to the interacting state $|\downarrow\rangle$, will be sensitive to mean-field energy shifts. b) Alternatively, energy shifts can be probed by sending some atoms from the interacting state $|\downarrow\rangle$ into the non-interacting state $|3\rangle$.

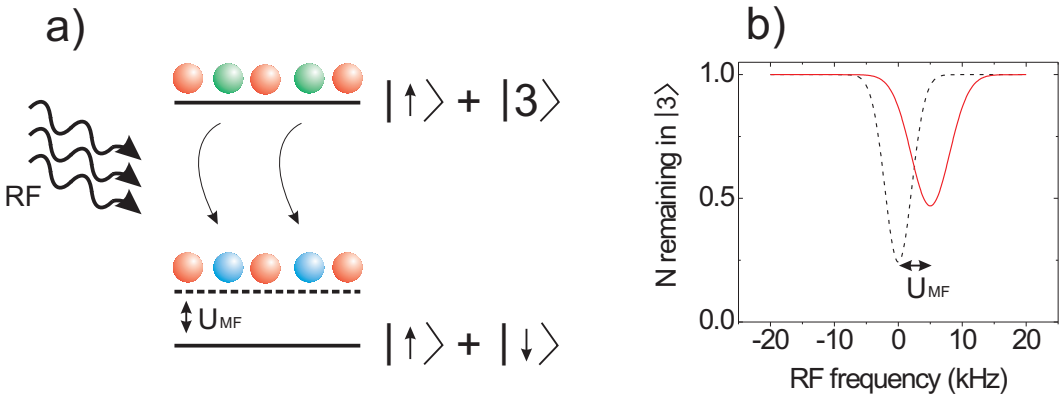

Figure 5.4: Measuring the mean-field energy using RF spectroscopy. a) Atoms from state $|3\rangle$ are transferred into state $|\downarrow\rangle$. The mean-field energy shifts the required RF frequency with respect to the single-atom resonance. b) Number of atoms remaining in state $|3\rangle$ as a function of the applied RF frequency. The interacting lineshape (red solid line) is shifted and broadened as compared to the non-interacting lineshape (black dashed line). $U_{MF} \propto na$ and therefore the interacting lineshape can be at higher or lower frequency than the non-interacting lineshape, depending on the sign of a.

then be the $|9/2, -5/2\rangle$ state ($|3\rangle$). One can determine the mean-field energy via RF spectroscopy by preparing a sample of $|\uparrow\rangle$ and $|3\rangle$ states and then applying an RF pulse to send some of the atoms from $|3\rangle$ state into state $|\downarrow\rangle$, see Fig. 5.3 a). Conversely, one can prepare a mixture of $|\uparrow\rangle$ and $|\downarrow\rangle$ states and then apply an RF pulse to send $|\downarrow\rangle$ to $|3\rangle$, see 5.3 b).

To measure the mean-field energy, experimenters measured the frequency shift needed to transfer atoms from the $|3\rangle$ state to the $|\downarrow\rangle$ state [111], see Fig. 5.4 a). The frequency is shifted because of the mean-field energy, given by

$$\Delta\nu = \frac{2\hbar}{m} n_{\uparrow}(a_{\uparrow,\downarrow} - a_{\downarrow,3}), \tag{5.4}$$

where $n_{\uparrow}$ is the density of atoms in state $|\uparrow\rangle$, $a_{\uparrow,\downarrow}$ is the scattering length between states $|\uparrow\rangle$ and $|\downarrow\rangle$, and $a_{3,\uparrow}$ is the scattering length between states $|\uparrow\rangle$ and $|3\rangle$. In fact, this technique was not only used to measure the mean-field shift $\Delta\nu$ but it was also used to determine $a_{\downarrow,\uparrow}$ [111]. Notice the frequency shift, Eq. (5.4), can be both positive or negative. In the experiment, this is determined from a raising or lowering of the resonant frequency required for transfer, see Fig. 5.4 b). This mean-field shift in energy is referred to as the "clock shift" in atomic clock experiments, as it is one of the dominant sources of systematic error [116].

I will now review for which cases we would expect to see a mean-field energy shift. This material is covered thoroughly in Ref. [36] and only outlined here; it will illuminate why fermions require the use of three spin states to measure energy shifts. As we established earlier, the mean-field energy between two states $|\uparrow\rangle$ and $|\downarrow\rangle$ is $\propto n a_{\uparrow,\downarrow}$. Suppose we begin with a spin-polarized sample in state $|\uparrow\rangle$ and apply RF to transfer to state $|\downarrow\rangle$. One might suspect that the RF transition should already begin to be shifted by U_{MF} as atoms are transferred into the new state; however, this is not the case because we are dealing with fermions and the transfer is coherent. The RF is coherent in that it creates a superposition of $|\uparrow\rangle$

and $|\downarrow\rangle$ simultaneously for all the atoms. Or rather, they are still polarized in their new superposition state and since they are fermions, s-wave collisions are forbidden and there is no mean-field shift. Note, if there was a frequency shift we would not be able to use one-state RF spectroscopy to determine the magnetic field strength as described above.

Imagine now that we have a mixture of two spin states, $|\uparrow\rangle$ and $|\downarrow\rangle$. While the atoms' energies are shifted by the mean-field energy, an RF pulse to flip atoms between $|\uparrow\rangle$ and $|\downarrow\rangle$ is not shifted. The argument follows similarly to the spin polarized case. Atoms originally in $|\uparrow\rangle$ are transferred coherently into a superposition of $|\uparrow\rangle$ and $|\downarrow\rangle$, while atoms originally in $|\downarrow\rangle$ are transferred coherently into the orthogonal superposition. The RF transition is not modified by the mean-field energy and RF transfer between two interacting spin states cannot be used to probe their interactions.

To probe interactions, one needs to use three spin states. If we now create a mixture of $|\uparrow\rangle$ and $|\downarrow\rangle$ states and apply RF to couple the transition from $|\downarrow\rangle$ to $|3\rangle$ we are sensitive to the interactions between $|\uparrow\rangle$ and $|\downarrow\rangle$. This is because while the transition between $|\downarrow\rangle$ to $|3\rangle$ does not see a mean-field shift, due to the arguments above, the energy of state $|\downarrow\rangle$ is indeed modified by state $|\uparrow\rangle$. Ideally, for RF spectroscopy to be an effective probe, state $|3\rangle$ should be unoccupied and weakly-interacting with either $|\uparrow\rangle$ or $|\downarrow\rangle$. Of course, mean-field energy is not the only way the atoms' energy can be shifted. For example, far on the BEC side of the Fano-Feshbach resonance, atoms can pair and acquire a binding energy which is not density dependent. At JILA, RF spectroscopy was again employed to study this new state [110].

5.3 Using RF to measure energy gaps

RF spectroscopy similar to that used to measure mean-field energies can also be used to probe molecular binding energy. This was demonstrated in an atomic Fermi gas when RF spectroscopy was used to measure the binding energy of Fano-Feshbach molecules [110]. In this experiment, atoms were prepared in a mixture of $|\uparrow\rangle$ and $|\downarrow\rangle$ states and adiabatically ramped through the Fano-Feshbach resonance to create two-body bound pairs. Then, RF was applied to transfer atoms from the $|\downarrow\rangle$ state into the $|3\rangle$ state. In order to dissociate the molecule, the RF frequency must be large enough to incorporate both the Zeeman energy as well as the binding energy of the molecule. An example of such a spectra is shown in Fig. 5.5 a). The RF spectra has the characteristic "double-peak" structure expected when probing an energy gap. There exists a narrow peak at the location of the free atom transition due to unpaired atoms in the sample and a separated second asymmetric broad peak that arises from dissociating bound molecules. The free atom feature is narrow because it is a two level transition between different long-lived internal states of the atom. The molecule feature is wide and asymmetric because the RF photon can drive a transition from the molecule to a continuum of scattering states of two atoms. These scattering states can have different relative momentum, depending on the RF photon energy, see Fig 5.5 b). The lineshape then depends on the overlap of the molecule wave function and free atom wave function [110, 117].

The separation between the peaks results from the energy gap in the system, which in this case comes from the binding energy of the molecules [110, 117]. RF spectroscopy is useful for probing energy gaps because the probe (a spin-flip of one of the $|\downarrow\rangle$ atoms) is inherently a *single*-particle measurement [70]. For example, in the dissociation of a molecule, the RF photon results in a single-particle excitation,

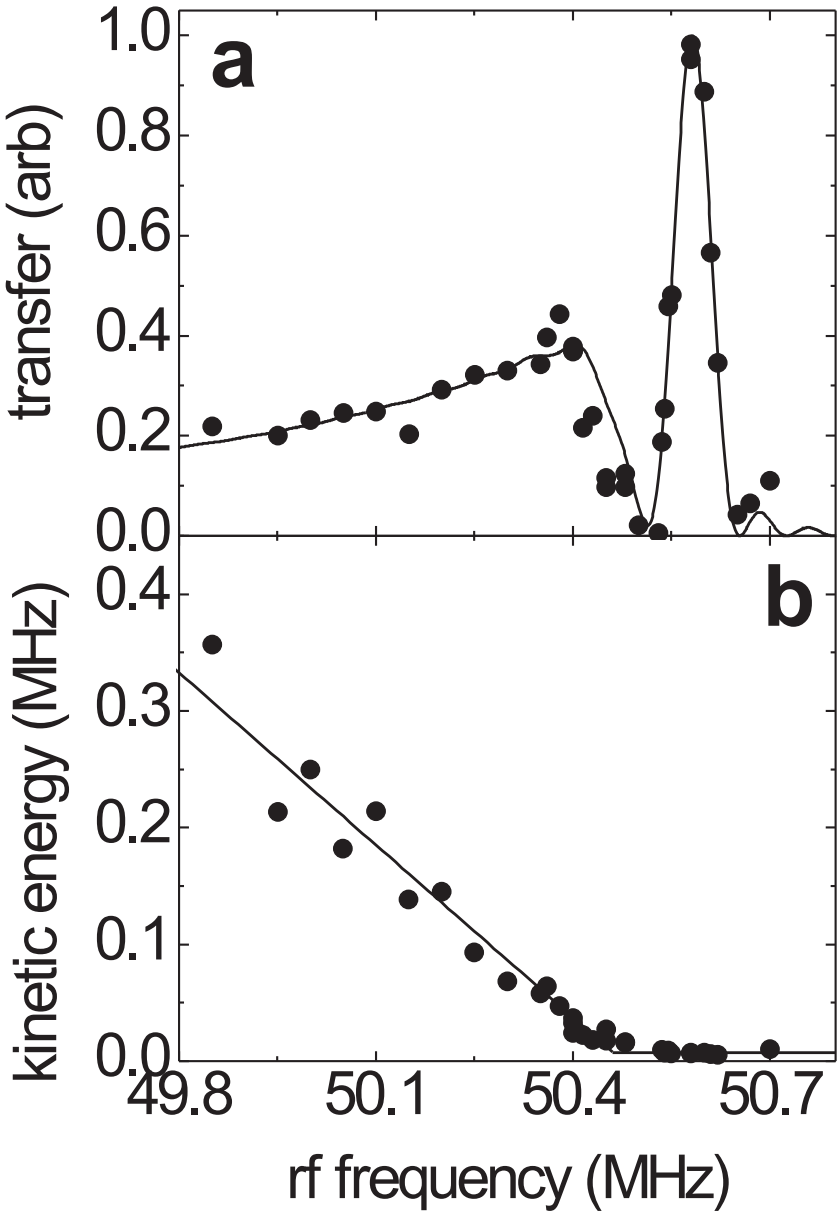

Figure 5.5: RF spectra of weakly bound Fano-Feshbach molecules. a) Fraction of atoms transferred into the probe state as a function of RF frequency. The narrow feature comes from unpaired atoms. The broad asymmetric feature results from the dissociation of molecules. b) Atoms from the dissociated molecules can carry away excess RF energy in the form of kinetic energy. Energy and momentum are conserved because the constituent atoms fly apart with equal and opposite momentum. Figure taken from Ref. [47].

namely removing an atom in the $|\downarrow\rangle$ state. An RF pulse with a frequency less than the binding energy will not be absorbed by the molecule. Only when the RF photon has sufficient energy to dissociate the molecule can it be absorbed. Or, in other words, RF spectroscopy as we have described it is not a probe of two-particle excitations. We will review this concept in our discussion of momentum-resolved RF spectroscopy next chapter.

Following the success of RF spectroscopy in probing energy gaps for weakly bound molecules, it was extended to probe the rest of the BCS-BEC crossover region by the group of R. Grimm in Innsbruck in 2004 [118]. The RF spectra observed by the Innsbruck group using ^{6}Li atoms exhibited "double-peak" structure throughout the crossover region and was attributed to a paring gap. Recall from our discussion of the BCS-BEC crossover that in the regime of $(k_F a)^{-1} \leq 0$, superfluidity is a many-body effect and the gap (or superfluid order parameter) is an important parameter for describing the superfluid. Therefore, the work of the Grimm group as the first measurement of the superfluid gap throughout the crossover region was initially very well received. Giving the experimental work additional scientific weight was a "back-to-back" theoretical article published by the group of P. Torma, which confirmed the gapped spectra observed by the Innsbruck group as evidence for a superfluid gap [119].

In the months and years that followed, however, a number of theoretical works were published calling into question the simple interpretation of double-peak spectra as evidence for an energy gap. While the interpretation worked fine for density-independent energy gaps, such as the weakly bound molecules studied at JILA, several theoretical papers questioned the effect of interactions on atoms transferred into state $|3\rangle$. These effects are often referred to as "final-state effects." In addition, it is important to appreciate the role that the density inhomogeneity for atoms in a trap plays in RF spectra. In the ^{6}Li data, these effects are not at

all negligible. We will discuss the importance of these effects in the next section.

5.4 Final-state effects and trap inhomogeneity

As I began my thesis work it was understood that the superfluid gap had already been measured throughout the BCS-BEC crossover. The determination of the superfluid gap came from the interpretation of double-peak structure as an energy gap [118], seen in an RF experiment by Grimm and co-workers. I schematically recreate their findings in Fig. 5.6 as inferred from Figs. 1 and 3 in Ref. [118]. Here, I have re-scaled the RF frequency in terms of the Fermi energy. They observed a single peak at the free atom Zeeman resonance for temperatures well above the pairing temperature, Fig. 5.6 a). As the temperature was reduced, a second peak was observed to appear at higher frequencies. This was attributed to paired atoms Fig. 5.6 b). As the temperature was reduced further, the free atom peak finally disappeared completely and only the peak attributed to paired atoms remained Fig. 5.6 c).

At the time, the interpretation of double-peak structure as evidence of a pairing gap seemed like a logical conclusion because of the success of the previous experiment here at JILA on weakly-bound two-body molecules [110]. The JILA experiment, as described in the previous section, correctly determined the binding energy of $density-independent$ weakly-bound molecules from the observation of two well-separated peaks in the RF spectra. Extending this simple experiment into the strongly interacting region near a Fano-Feshbach resonance, however, must be done carefully, especially when pairing is a many-body effect. Since the Innsbruck experiment and initial theoretical description [118, 119], numerous theoretical works have made it clear that the interpretation of RF spectroscopy near a Fano-Feshbach resonance must be handled with care [117, 121, 122, 123, 124, 125, 126, 89, 127, 128, 129, 15, 130, 131, 132, 133]. In par-

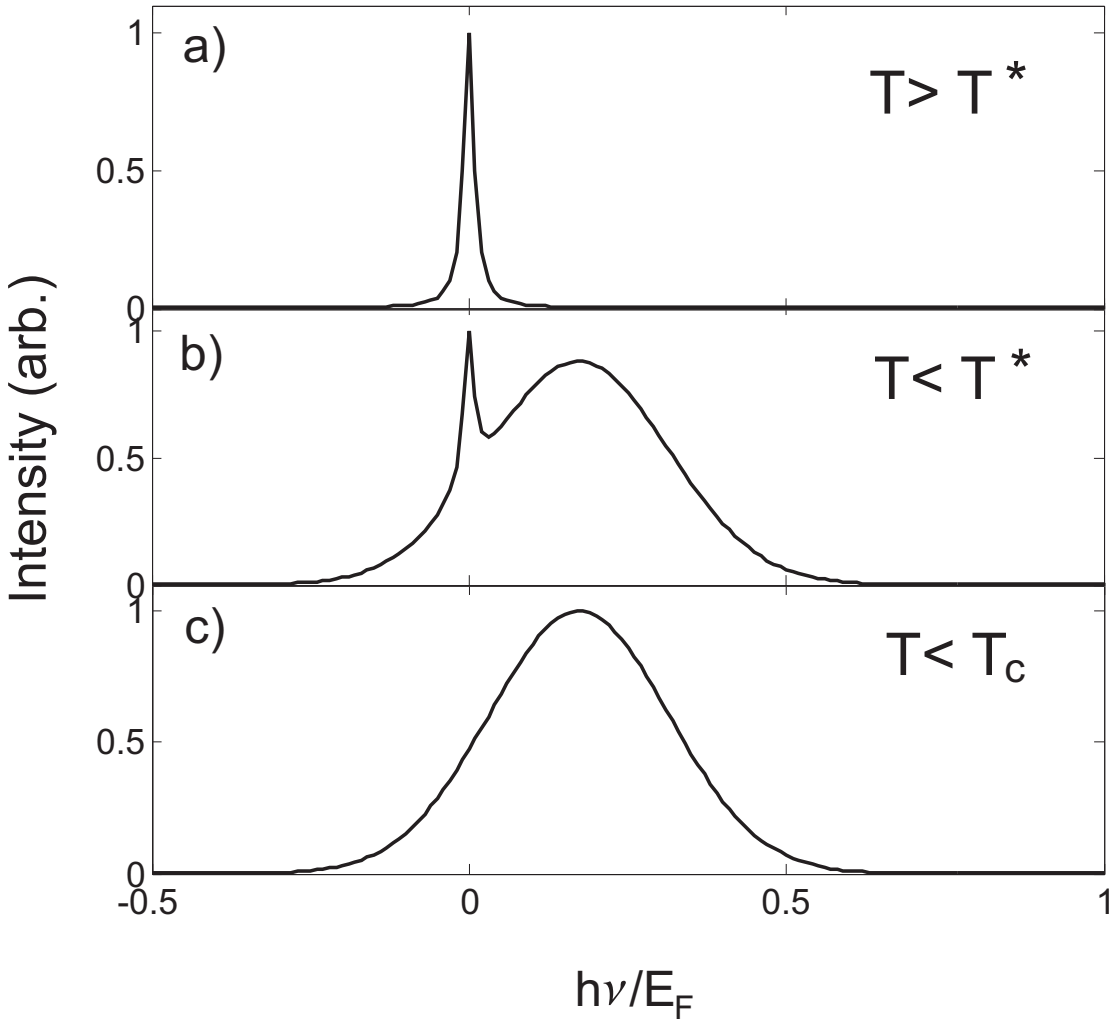

Figure 5.6: A schematic diagram showing RF spectra with double-peak structure such as observed for ^{6}Li by the Innsbruck group and later by the MIT group (see Figs. 3 and 4 in Ref. [118] and Fig. 2 in Ref. [120]). Here, the x-axis is the RF frequency in units of the Fermi energy. For reference, compare these spectra to the expected pair dissociation spectra, solid line in Fig. 5.7. It is clear that the RF spectra are strongly modified by final-state effects.

ticular, it became evident that double-peak structure could arise very generically and was not necessarily an indication of an energetically gapped state. Theories for double-peak structures tend to fall into one of two categories. The first considers the effect that interactions with the third spin state, or the probe spin state, can have on the RF spectra (as it turns out this is quite negligible for ^{40}K but is a huge effect for ^{6}Li). The second considers the density dependent mean-field energy shift and how one can observe double-peak structure in a harmonic trap. Although a complete theory should contain both effects, either one can give a double-peak structure even when the system does not have an energy gap.

5.4.1 Final-state effects

Recall from section 5.2 that one can probe interactions between the $|\uparrow\rangle$ and $|\downarrow\rangle$ states by using an RF pulse to transfer atoms to or from the $|3\rangle$ state. There, we assumed that state $|3\rangle$ was an ideal probe state, meaning that it had a small interaction strength with atoms in the $|\uparrow\rangle$ or $|\downarrow\rangle$ states. In ^{40}K, this is almost always the case, and the scattering length between the probe state and the strongly interacting states is less than a couple hundred Bohr radii. In ^{6}Li, however, there exist extremely wide Fano-Feshbach resonances (on the order of hundreds of Gauss wide) between all three spin states in close proximity to each other [82]. Thus, in ^{6}Li, when studying the Fano-Feshbach resonance between $|\uparrow\rangle$ and $|\downarrow\rangle$, the close proximity of wide resonances between $|\uparrow\rangle$ - $|3\rangle$ and $|\downarrow\rangle$ - $|3\rangle$ means state $|3\rangle$ is almost never an ideal probe [132].

A complete review of how interactions between the final state and the initial state affect the RF spectra is beyond the scope of this thesis. Indeed, there are now many theoretical papers discussing final-state effects on RF spectra for a variety of situations including weakly bound molecules, BCS-type pairing, BCS-BEC crossover, spin polarized, finite temperature, etc. As an illustrative example

of how final-state effects can distort the RF spectra, I will follow the argument of C. Chin and P. S. Julienne for weakly bound molecules found in Ref. [117]. In this paper, the authors calculate bound-to-free transitions as well as bound-to-bound transitions from weakly bound molecules. Normally, one would not need to consider bound-to-bound transitions if the final state was an ideal probe state. However, as we established, in the case of ^{6}Li the final state may also be near a Fano-Feshbach resonance so that the scattering length can be of arbitrary size and sign. To calculate the bound-free RF spectra one needs to use Fermi's golden rule:

$$\Gamma_{bf}(E) = \frac{2\pi}{\hbar}|\langle E|V|i\rangle|^2, \tag{5.5}$$

where i is the initial state, E is the final state, V is the RF coupling that we can write as $\hbar\Omega/2$ where Ω is the Rabi frequency. Note that energy conservation requires $E = \hbar^2k^2/2\mu = E_{RF} - E_0 - E_b$ where E_{RF} is the photon energy, E_0 is the continuum threshold, and E_b is the binding energy. Because we are considering weakly bound molecules we can write down the initial wave function:

$$|i\rangle = \phi_m(r) = \sqrt{\frac{2}{a}}e^{-r/a} \tag{5.6}$$

where a is the s-wave scattering length. We can write the outgoing final state wave function as

$$|E\rangle = \psi_E(r) = \sqrt{\frac{2\mu}{\pi\hbar^2 k}}\sin(kr + \delta') \tag{5.7}$$

where $(')$ indicates a parameter in the outgoing channel. Calculating the expectation value, squaring, and using the low energy expansion of the phase shift one eventually finds

$$\Gamma_{bf}(E) = \frac{\hbar^2\Omega^2}{\pi^2}\Big(1 - \frac{a'}{a}\Big)^2 \frac{1}{E_b^{3/2}} \frac{\sqrt{E}}{(1 + E/E_b)^2(1 + E/E_b')} \tag{5.8}$$

where $k^2a^2 = E/E_b$ and $k^2a'^2 = E/E_b'$ [117]. It can be useful here to make a translation $E \to E' - E_b$, so that the binding energy can be read directly from

the spectra as the difference from zero, such as is the case for the experiments. In the limit of no final-state interactions, this formula simplifies to the well known pair-dissociation formula which falls off as $E^{-3/2}$ for large E, see solid line in Fig. 5.7. However, as interactions in the final state are increased, the lineshape becomes substantially modified, see dashed line in Fig. 5.7. In this example, I have set $E_b = E_F$ and $a' = a/\sqrt{10}$, for which one finds the bound-to-free integrated spectra for the interacting case only contains 25% of the spectral weight of the non-interacting case. Where has the rest of the spectral weight gone? In this example, the remaining 75% of the spectral weight has gone into the bound-to-bound transition. This concept is covered explicitly for the case of ^{6}Li in Ref. [132]. Essentially, a bound pair made up of $|\uparrow\rangle$ and $|\downarrow\rangle$ states makes a two-body transition to a different bound pair made up of $|\uparrow\rangle$ and $|3\rangle$ states. Additionally, the high energy tail falls off with the wrong power, $E^{-5/2}$. Even from our relatively straightforward example it is already clear that final-state effects can severely affect RF spectroscopy.

The technique outlined here to determine RF spectra can be applied throughout the BCS-BEC crossover and into the BCS limit as long as one knows the appropriate wave function. In the absence of final-state interactions, the onset of the RF spectra is determined by the binding energy E_b in the BEC limit [117] and the superfluid gap $\Delta^2/2E_F$ in the BCS limit [122]. In the BCS-BEC crossover, with the presence final-state interactions, calculating the RF spectra is theoretically challenging and work is still ongoing [124]. However, more recent data for ^{6}Li from an experiment that included an effort to reduce final-state effects shows that the RF spectra evolve smoothly from the BEC-side to the BCS-side of the Fano-Feshbach resonance [115], and in all cases the spectra retain the pair-dissociation lineshape shown in Fig. 5.7. Unfortunately, even in this best case scenario for ^{6}Li, it is calculated that the bound-to-bound transition may still contain up to 59%

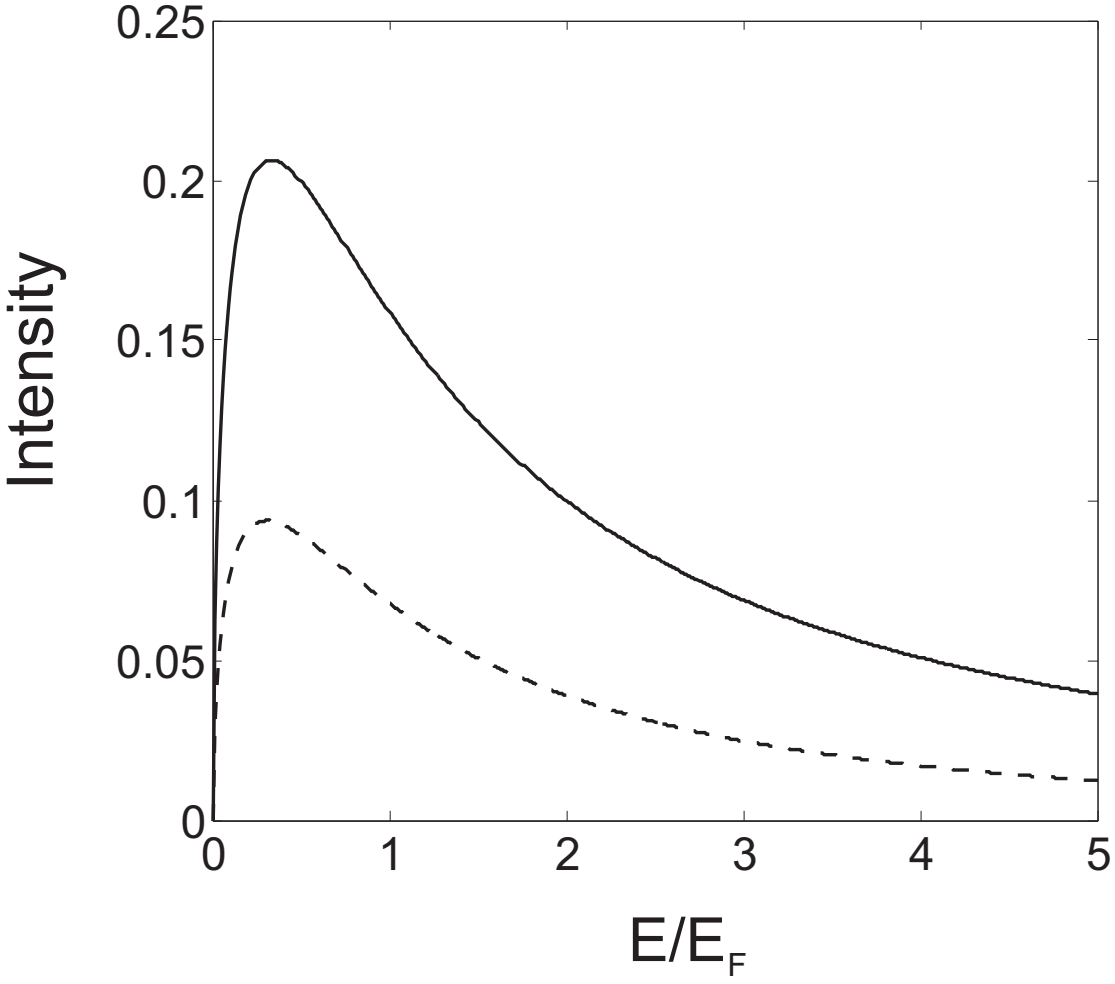

Figure 5.7: Theoretical RF spectra for weakly bound molecules (bound-to-free transition). The solid line is the RF spectrum for the case of no final-state effects for the parameters described in the text. The dashed line is for the case of final-state interactions that are $\sqrt{10}$ weaker than the interactions between the original two spin states. For the parameters given in the text, the interacting lineshape only contains 25% of the total spectral weight. The rest is in the bound-to-bound transition.

of the total spectral weight [132], suggesting the lineshape may still suffer from final-state effects.

Perhaps one of the most striking features of the RF spectra of Grimm and co-workers is that the feature does not have the pair-dissociation look to it, see Fig. 5.6. Rather, as the authors mention, they fit the their data to a Lorentzian plus a gaussian, which does not have the characteristic $E^{-3/2}$ tail. Also striking is that the entire lineshape occurs within a frequency span of about $E_F/2$. We can understand this in the case of ^{6}Li due to the close proximity of nearby Fano-Feshbach resonances. As a' approaches a, the bound-to-free transition vanishes (see Eq. 5.8) and only a bound-to-bound transition is left. Also, as one approaches $a' \to \infty$ the RF spectra again approaches a bound-to-bound delta function even though a bound state does not exist in the outgoing channel [117]. Presumably, the close proximity of the Fano-Feshbach resonance in the outgoing channel resulted in the entire RF spectra looking much more bound-to-bound than than one might have naively expected.

Here, I have only covered one theoretical explanation for double peak spectra due to the presence of final-state effects. However, there are numerous alternative and complementary explanations, see for example Refs. [122, 123, 124, 125, 126, 89, 127, 128, 129, 15, 131, 132, 133]. The universal conclusion is that double-peak structure in the RF spectra of a strongly interacting Fermi gas subject to final-state effects is complicated and is not convincing evidence for observing a pairing gap. In the next section, we see how density inhomogeneity due to the trapping potential can also produce double-peak structure.

5.4.2 Trap inhomogeneity

Typically, most atomic Fermi gases are confined using a far off resonant optical dipole trap. One or more focused laser beams intersect at the location

of the atoms to provide a trapping potential. The potential, while gaussian, can be well approximated as harmonic near the bottom of the trap. Because the trapping potential is spatially inhomogeneous, the cloud density varies as a function of distance from the trap center. The gas density is highest at the trap center and falls off as one approaches the trap edge. Consequently, shifts in the RF spectra due to density (mean-field shift, for example) will effectively depend on which part of the cloud is being probed. Naively, one might expect that since the density varies monotonically that any RF spectra would simply be broadened. As it turns out, this is not always the case. In fact, the density inhomogeneity can produce double-peak spectra even in the absence of final-state effects [121, 89, 130]. Indeed, as we will see, one does not even require pairing, much less superfluidity, to observe double-peak structure.

The most general theories explaining double-peak structure arising from density inhomogeneity were actually in response to a paper by the MIT group [120]. In short, the MIT group observed double-peaked spectra almost identical to the Innsbruck spectra (Fig. 5.6) in a system known to not be superfluid. Regardless, the theoretical results are general because they show that even when a system has no pairing, double-peak RF structure can arise from density inhomogeneity. If one were to take an RF lineshape at the center of the trap, we would expect it to be shifted with respect to the free atom transition due to density-dependent effects such as pairing and mean-field energy. Then, as one moves towards the edge of the trap, where the density goes to zero, we expect to recover the free atom RF spectra. At issue, however, is that the total RF spectra is the sum of these individual spectra, where signal coming from atoms at a distance r from the center of the trap is weighted by $r^2 n(r)$, where $n(r)$ is the density at r. The resulting total RF can show two peaks. One peak, due to a significant portion of the atoms near the center of the trap, is shifted with respect to the

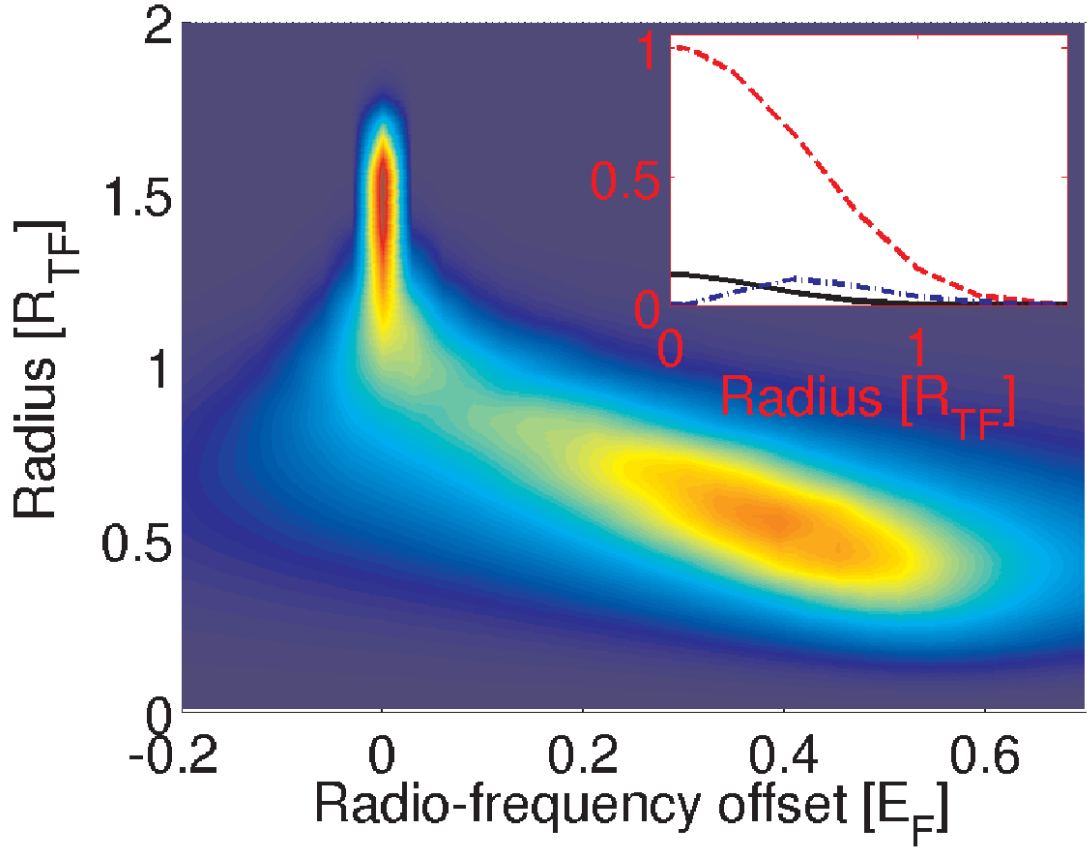

Figure 5.8: Figure from Stoof *et al.* in Ref. [89]. The figure is an intensity plot showing transition intensity as a function of radius in the cloud and RF frequency. This figure shows how double-peak structure can arise from density inhomogeneity. Note, at any given radius the RF spectrum only shows one peak. However, integrating over all radii give a total RF spectrum that has two separated peaks.

free atom transition. The other peak, due to a significant number of atoms at low density (because of the r^2 weighting) is centered at the free atom transition. I include a figure from Ref. [89] which shows this effect quite nicely, see Fig. 5.8. Notice, at any given radius there is only one peak in the RF spectra; however, integrating over all radii it is clear that double-peak spectra would be present. In 2007, in-situ tomographic techniques were used by the MIT group to observe single-peaked RF spectra as a function of position in the cloud [114].

5.4.3 Conclusion

In this chapter, we have seen how RF spectroscopy can be a very powerful probe, with applications ranging from measuring magnetic fields to probing interactions and pairing. However, we have also learned some important lessons regarding the interpretation and application of RF spectroscopy. Namely, we have to carefully consider final-state effects and density inhomogeneity in RF spectroscopy, especially when the signatures we are looking for are density dependent. Previous experiments claiming to measure a superfluid gap using RF spectroscopy [118, 120] were grossly affected by these effects. In the next chapter, we will once again turn to RF spectroscopy for studying energy gaps, but this time in an entirely new way.

Chapter 6

Photoemission spectroscopy

Throughout this thesis I have argued that the simplicity, purity, tunability, and universality of atomic Fermi gases make these gases model systems in which to test condensed matter theories. A challenge for experimenters is to find ways to probe these atom gases that relate directly to condensed matter ideas and enable sensitive searches for new phenomena that can advance our understanding of strongly correlated systems. For the most part, up until now, studies have measured macroscopic properties of the Fermi gas, such as: condensate fraction and its phase diagram, collective mode oscillations, vortices, RF spectra, potential energy, kinetic energy, etc. However, one would ideally like to probe the microscopic behavior directly and determine important microscopic quantities such as the dispersion, energy gaps and quasi-particle lifetimes.

In condensed matter physics, photoemission spectroscopy (PES) has proven to be a very powerful probe of the single-particle spectral function [134, 68]. I will begin this chapter by reviewing PES for electronic systems and its connection to the spectral function and many-body theory. Then, I will move on to our new technique, photoemission spectroscopy for atoms using momentum-resolved RF spectroscopy (in contrast to the momentum-integrated RF spectroscopy of the last chapter). With PES, we study new microscopic quantities such as the energy dispersion, energy gaps, and quasi-particle lifetimes as well as macroscopic

quantities such as the momentum distribution and density of states. Many of these quantities were probed for the first time in atomic Fermi gases with our new technique. This new ability to probe the microscopic quantities of a strongly interacting Fermi gas will allow detailed comparison to many-body theories. Also, we can study the pseudogap, which can have implications in both AMO and condensed matter communities.

6.1 Photoemission spectroscopy and many-body theory

At a very basic level, the effect of interactions is a modification of the single-particle states. As the strength of interaction is increased, the single-particle eigenstates of the non-interacting case become quasi-particles and phase transitions manifest themselves as qualitative changes in the excitation spectrum, such as the appearance of energy gaps. The single-particle excitation spectrum can be predicted by many-body theory and is a fundamental property of any interacting system.

For electronic systems, photoemission spectroscopy provides a powerful technique to probe the occupied single-particle states. In a typical photoemission spectroscopy experiment, see Fig. 6.1, electrons are ejected from a material through the photoelectric effect. The photoelectrons are collected, energy- and momentum-resolved, and counted to give a spectrum of intensity as a function of the measured kinetic energy, $\epsilon_k = \hbar k^2/2m$, where $\hbar = h/2\pi$, where h is Plancks constant, and m is the particle mass. By conservation of energy, the energy of the original single-particle state, E_s, is

$$E_s(k) = \epsilon_k + \phi + h\nu. \tag{6.1}$$

where $h\nu$ is the photon energy, ϕ is the work function of the surface and the quantity $(E_F - E_S)$ is often referred to as the binding energy [68]. As we will see,

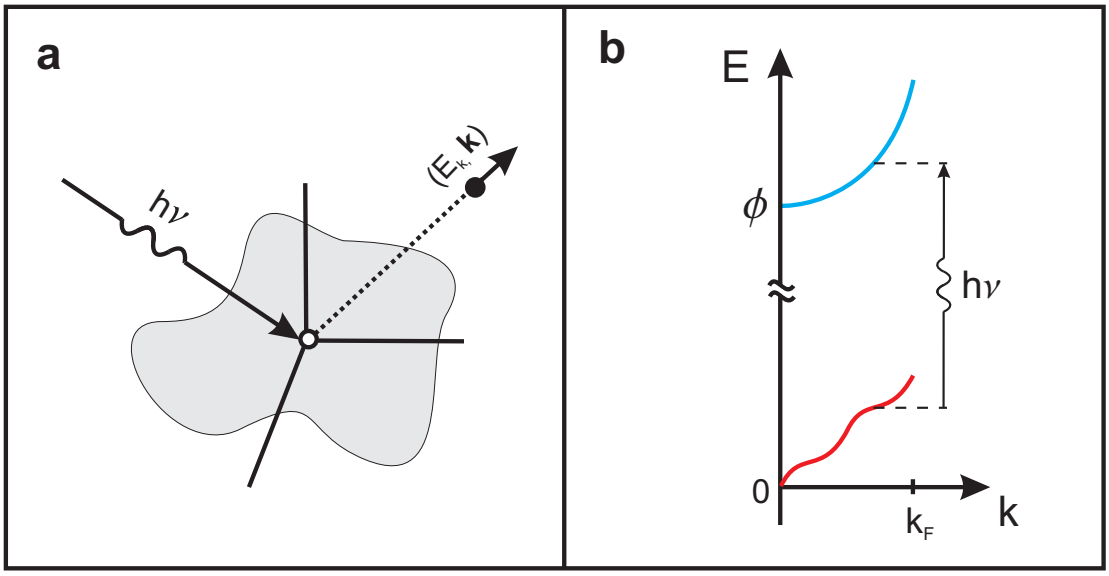

Figure 6.1: Photoemission spectroscopy for ultracold atom gases. a) In electron photoemission spectroscopy, the energy of electrons emitted from solids, liquids or gases is measured using the photoelectric effect. Using energy conservation, the original energy of the electrons in the substance can be determined. Similarly, in photoemission spectroscopy for atoms, a radio frequency photon with energy $h\nu$ transfers atoms into a weakly interacting spin state. b) The radio-frequency photon drives a vertical transition where the momentum k is essentially unchanged. By measuring the energy and momentum of the outcoupled atoms (upper curve) we can determine the quasi-particle excitations and their dispersion relation (lower curve). Here ϕ is the Zeeman energy difference between the two different spin states of the atom.

$E_s(k)$ directly gives the dispersion of the system, and its width in energy gives the quasi-particle lifetime.

Photoemission spectroscopy probes the single-particle spectral function which is directly related to the single-particle Greens function predicted by many-body theories. I will also frequently refer to ARPES, which is angle resolved photoemission spectroscopy. ARPES allows one to measure the spectral function with respect to energy and momentum. The intensity of photoelectrons emitted is given (assuming the sudden approximation) by

$$I_{ARPES}(\mathbf{k},\omega) = M_0(\mathbf{k},\omega) f(\omega) A(\mathbf{k},\omega) \tag{6.2}$$

where $M_0(\mathbf{k},\omega)$ is a matrix element which contains relevant selection rules [68, 70]. For our atom gas application, this matrix element will be unity. Now, we see that the ARPES intensity is determined solely by the Fermi function $f(\omega) = (e^{\hbar w/k_B T}+1)^{-1}$ and the single-particle spectral function $A(\mathbf{k},\omega)$. In this way, ARPES directly measures the occupied part of the spectral function.

I will now very briefly highlight how the spectral function is connected to the "interesting" physics that we care to probe. For a more complete consideration there exists much literature [1, 134, 68, 70]. The occupied single-particle spectral function is related to the Green's function via

$$A(\mathbf{k},\omega) = -\frac{1}{\pi}\mathrm{Im}[G(\mathbf{k},\omega)]. \tag{6.3}$$

For the case of interacting fermions, the Green's function is given by

$$G(\mathbf{k},\omega) = \frac{1}{\omega - \epsilon_k - \Sigma(\mathbf{k},\omega)}, \tag{6.4}$$

where $\Sigma(\mathbf{k},\omega)$ is called the self energy. The self energy contains all the interesting particle-particle correlations for the many-body system. The self energy can be written in terms of its real and imaginary parts as $\Sigma(\mathbf{k},\omega) = \Sigma'(\mathbf{k},\omega) + i\Sigma''(\mathbf{k},\omega)$,

where the real term contains all the information on the energy renormalization (in Fermi liquid theory this would be the effective mass [135]) and the imaginary term contains all the information on the quasi-particle lifetime [136, 137]. Finally, we can write the spectral function in terms of the self energy to more clearly see how ARPES, by being directly proportional the spectral function, directly probes the "interesting" physics

$$A(\mathbf{k},\omega) = \frac{1}{\pi}\frac{\Sigma''(\mathbf{k},\omega)}{[\omega - \epsilon_k - \Sigma'(\mathbf{k},\omega)]^2 + [\Sigma''(\mathbf{k},\omega)]^2}. \tag{6.5}$$

Useful insight can be gained by working this out for the Fermi liquid case in which $\Sigma(\mathbf{k},\omega) = \alpha\omega + i\beta\omega^2$, where α gives the effective mass and β the quasi-particle lifetime.

6.2 Photoemission spectroscopy for atoms

As we learned in the previous chapter, radio-frequency spectroscopy has been used to probe a strongly interacting atomic Fermi gas. In a typical experiment, a radio-frequency pulse drives atoms into an unoccupied Zeeman spin state, where they are counted to yield a spectrum of counts versus frequency. Previously, the radio-frequency outcoupled atoms had not been energy- or momentum-resolved. However, in analogy to electron photoemission spectroscopy, the momentum of the radio-frequency photon is negligible in comparison with the typical momentum of the atoms, and the momenta of the outcoupled atoms are therefore characteristic of the original atom states. Eq. 6.1 applies to photoemission spectroscopy of atom gases, by means of momentum-resolved radio-frequency spectroscopy, if we simply replace the work function ϕ with the Zeeman energy splitting, see Fig. 6.1. The extension of photoemission spectroscopy from condensed matter to cold Fermi gases was discussed in [138].

There are two essential requirements for using momentum-resolved RF spec-

troscopy to determine the excitation spectrum. The first is that the interaction energy be small enough that $\epsilon_k = \hbar^2 k^2/2m$ holds and the data are not subject to the complicated final-state effects we discussed in the last chapter. The second requirement is that collisions do not scramble the energy and momentum information carried by the outcoupled atoms. In previous momentum-integrated RF spectroscopy measurements in ^{6}Li, these requirements were not both satisfied [44, 118, 120, 115, 82]. In our ^{40}K gas, however, both of these requirements can be satisfied. The interaction energy of the outcoupled atoms is approximately $h \cdot 640$ Hz, which is much smaller than E_F. Furthermore, the mean free path of the outcoupled atoms is much greater than the size of the gas: $1/\sigma n \approx 6R_F$, where σ is the collision cross-section, n is the average density and R_F is the Fermi radius of the non-interacting gas.

Resolving the kinetic energy ϵ_k of the radio-frequency outcoupled atoms also requires that we apply a radio-frequency pulse that is short in comparison with the trap period. This ensures that the momentum of the outcoupled atoms is not significantly changed. We then immediately turn off the trap, let the gas ballistically expand and measure the velocity distribution using state-selective time-of-flight absorption imaging, Fig. 6.2 a). We take the data by varying the RF frequency and observing the velocity distribution of the atoms that are outcoupled. For reference, in Fig. 6.3, I show an example of how the momentum varies as a function of the applied RF. In Fig. 6.3 a), we see the fraction of atoms transferred to the third spin state as a function of RF frequency. Shown in Fig. 6.3 b) is the gaussian size returned from a fit of the absorption image for the outcoupled atoms. From data such as this it is clear that RF at different frequencies couples to atoms at different momenta.

To extract the kinetic energy ϵ_k of the outcoupled atoms it is not sufficient to use the gaussian size as shown in Fig. 6.3 b). This is because we need the 3D

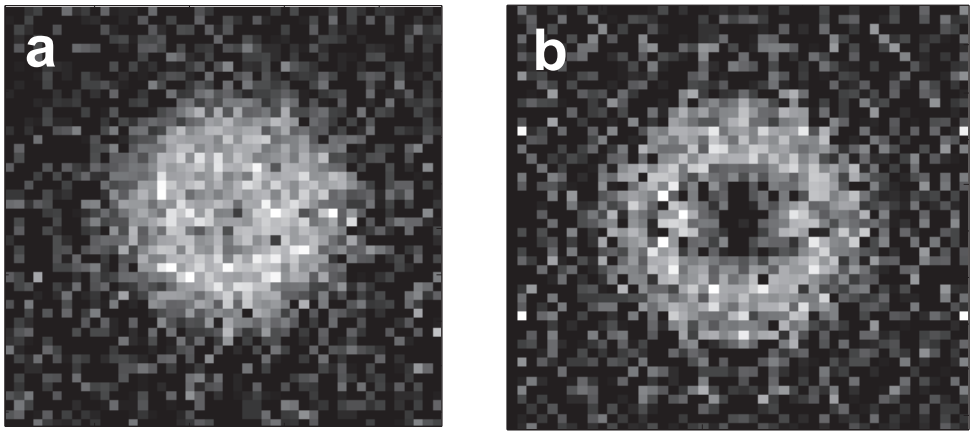

Figure 6.2: Extracting the three-dimensional momentum distribution. a) A time-of-flight absorption image (145 μ × 145 μm) of atoms that have been transferred into a third spin state is taken after applying a radio-frequency pulse to a Fermi gas on the BEC side of the Feshbach resonance. b) After performing quadrant averaging we use an inverse Abel transform to reconstruct the three-dimensional momentum distribution. In this example, a two-dimensional slice at the center reveals a shell-like structure for the momentum distribution of the outcoupled atoms.

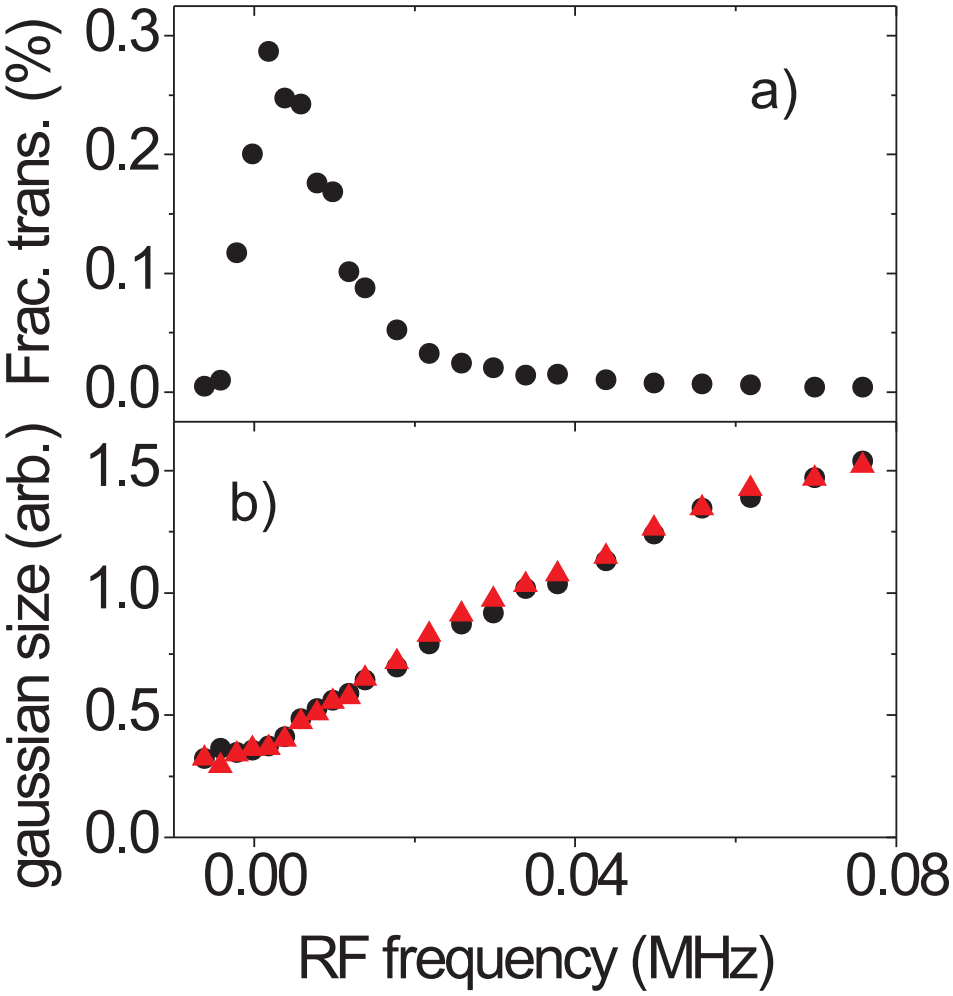

Figure 6.3: RF spectra for a strongly interacting degenerate Fermi gas. The Fermi energy is $h \cdot 8.2$ kHz, $(k_F a)^{-1} = 0.15$, and $T/T_F = 0.16(2)$. a) Integrated signal of outcoupled atoms as a function of RF frequency. The high-asymmetry and non-zero tail results from the strong interactions. (Note the similarity to a pair-dissociation lineshape as found in Fig. 5.7). b) Gaussian size (both radial directions) from a 2D fit to the outcoupled atoms' absorption image. At higher RF frequencies, we observe atoms with higher velocities. These high velocities occur when the two atoms are at high densities or close distances as within a pair.

momentum distribution to determine ϵ_k whereas the image we retrieve from the CCD camera is a 2D projection of the 3D momentum distribution. For example, a shell in 3D will look fairly gaussian when projected on to a 2D surface. Projecting a 3D object onto 2D space is referred to as an Abel transform. We extract the 3D distribution by performing an inverse Abel transform on the image which takes advantage of our cylindrical symmetry. An example of this is shown in Fig. 6.2b) where we have taken a slice through the center of the image after the inverse Abel transform revealing a shell-like structure. Clearly, even though the 2D projection can look fairly standard (Fig. 6.1a) the 3D momentum distribution may not be trivial.

Once we have determined the kinematics of the outcoupled atoms we can apply Eq. 6.1 to determine the single-particle energy E_s as a function of the momentum. To check that the photoemission spectroscopy is working as intended, we first apply it to a weakly interacting cold Fermi gas. To create a very weakly interacting gas, we adiabatically ramp the magnetic field to the zero crossing of the Feshbach resonance. In Fig. 6.4a, we plot the intensity, which is proportional to the number of atoms transferred into the third spin state, as a function of the original single-particle energy E_s and wavenumber k. Again, the data are obtained by varying the radio frequency and counting the outcoupled atoms as a function of their momenta. For the data here we define zero energy to be the energy of a noninteracting atom at rest in the initial spin state. This is in contrast to ARPES in electronic systems where zero is typically defined to be the Fermi energy. For a non-interacting Fermi gas we would expect the photoemission spectra to reveal delta function peaks at $E_s = \epsilon_k$, since ϵ_k is the expected quadratic dispersion for a non-interacting Fermi gas. To extract the dispersion we fit each energy distribution curve (EDC) to a single gaussian and mark the center as a white dot. EDCs are slices through the spectra at a given k. The dispersion (white dots)

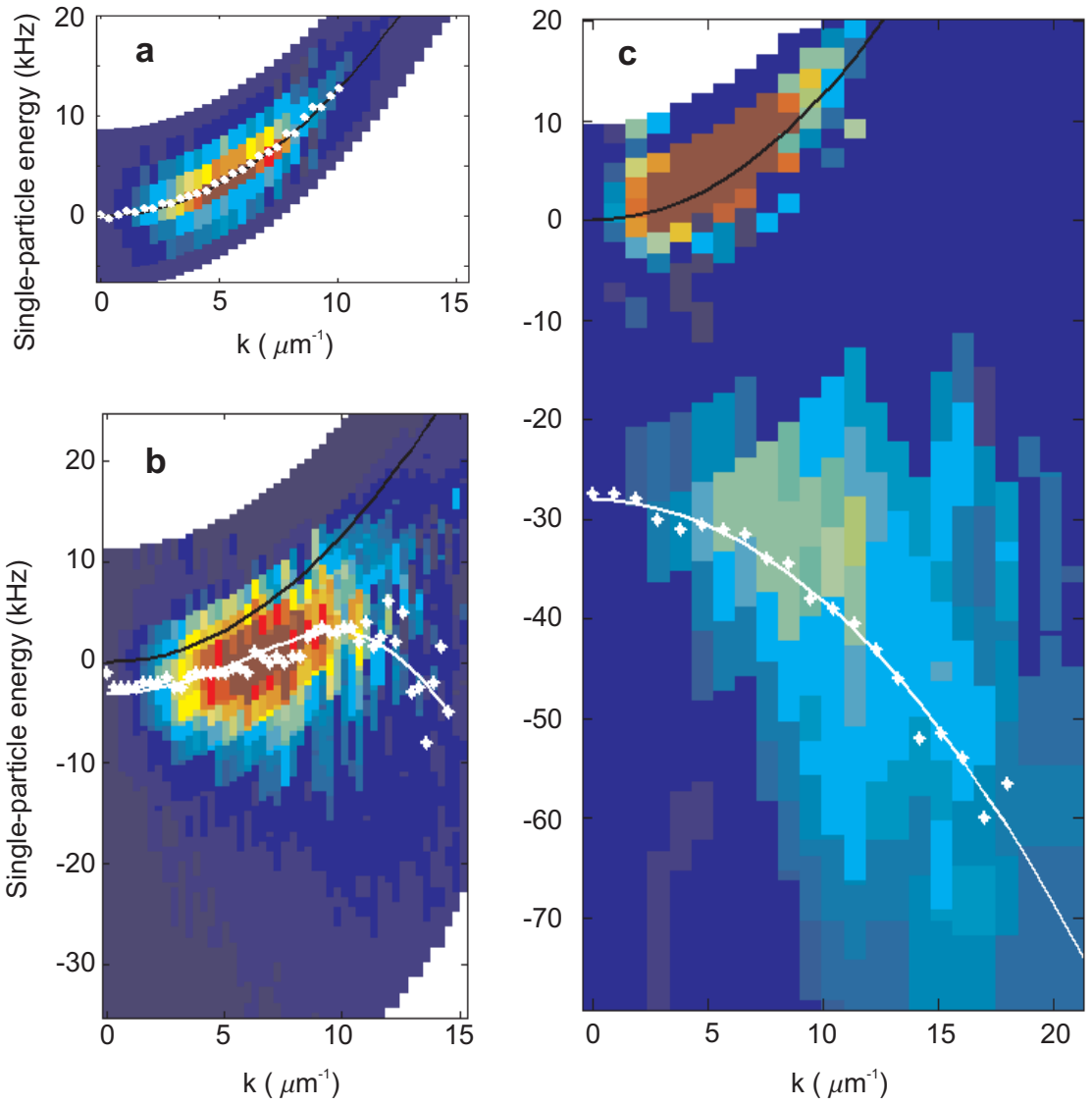

Figure 6.4: Single-particle excitation spectra obtained using photoemission spectroscopy of ultracold atoms. Plotted are intensity maps (independently scaled for each plot) of the number of atoms outcoupled to a weakly interacting spin state as a function of the single-particle energy E_s (expressed as frequency) and wavenumber k. Black lines show the expected dispersion curves for an ideal Fermi gas. White symbols mark the center of each fixed-k energy distribution curve. a) Data for a very weakly interacting Fermi gas. The Fermi wavevector k_F^0 is 8.6 ± 0.3 μm^{-1}. b) Data for a strongly interacting Fermi gas where $1/k_F^0 a = 0$ and $T \approx T_c$. The white line is a fit of the centers to a BCS-like dispersion. c) Data for a gas on the BEC side of the resonance where $1/k_F^0 a = 1$ and the measured two-body binding energy is $h \cdot (25 \pm 2$ kHz). We attribute the upper feature to unpaired atoms and the lower feature to molecules. The white line is a fit to the centers using a quadratic dispersion.

show good agreement with the expected free-particle dispersion (black curve). The root-mean-square width in E_s of the EDCs is $h \cdot 2.1$ kHz and is due to an energy resolution that derives from the radio-frequency pulse duration. In other words, at this level, our spectra is limited by measurement energy resolution and we observe no other deviation from the expected delta function peaks.

Now, we apply our photoemission spectroscopy technique to a strongly interacting Fermi gas. To create a strongly interacting Fermi gas, we adiabatically ramp the magnetic field to the location of the Feshbach resonance, where the s-wave scattering length a diverges and the dimensionless interaction parameter $1/k_F^0 a$ equals zero and k_F^0 corresponds to the peak density of the original, weakly interacting gas. Previous measurements have shown that after the ramp to $1/k_F^0 a = 0$, our Fermi gas initially with $T/T_F = 0.16$ will be very near but slightly below the superfluid transition temperature with $T = (0.9 \pm 0.1) \times T_c$ [30]. We extract the intensity map shown in Fig. 6.4b. The interactions lower the overall energy and flatten the dispersion curve. In addition, the energy width is broadened well beyond our energy resolution.

As we established in the previous chapter, the interpretation of previous radio-frequency spectroscopy measurements [118, 120] in terms of a pairing gap is a difficult problem that is still unsolved theoretically [15]. In contrast, the photoemission spectroscopy technique presented here directly measures the occupied single-particle states, and is therefore well suited to measuring pairing gaps [68]. The energy gap in BCS theory results directly from a gap in the spectral function as k approaches k_μ. Mapping out the location of the peak of the spectral function results in a BCS-like "back-bending" of the dispersion

$$E_s = \mu - \sqrt{(\epsilon - \mu)^2 + \Delta^2} \tag{6.6}$$

where μ is the chemical potential and Δ is the superfluid gap. I show a repre-

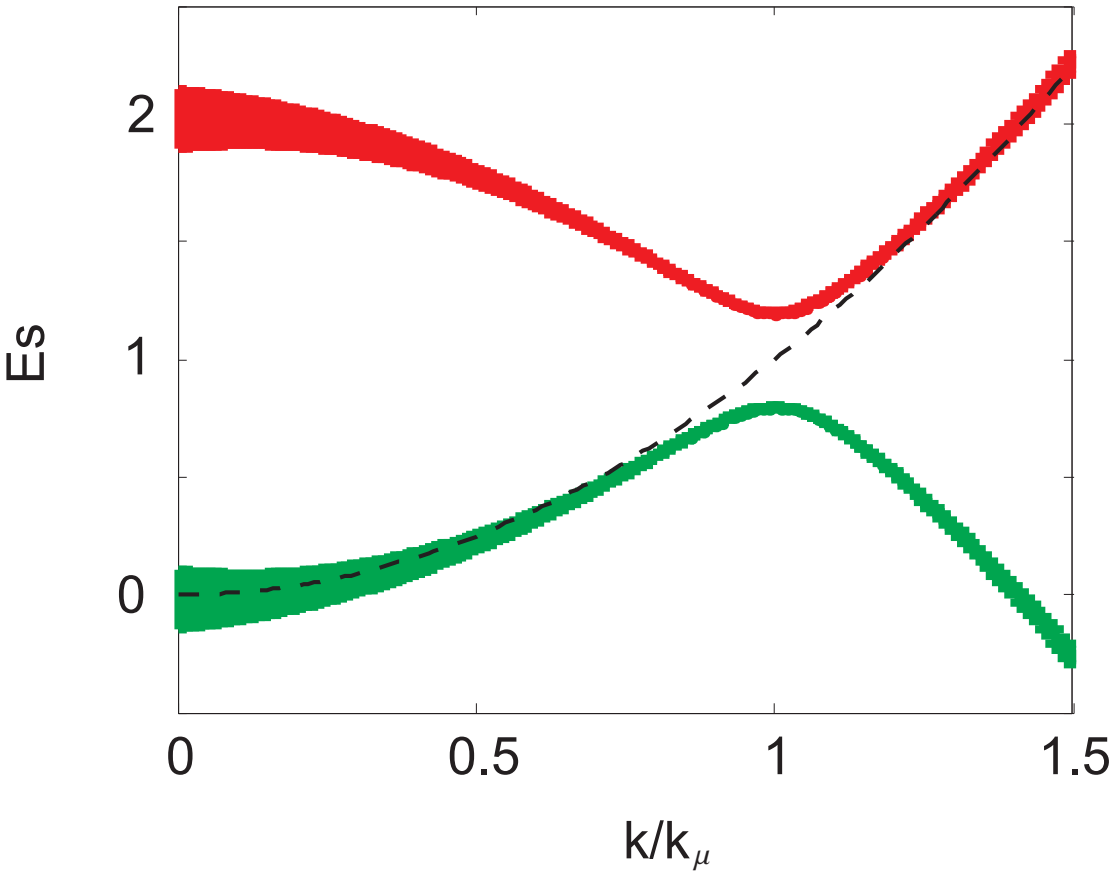

Figure 6.5: A sketch of BCS-like particle and hole dispersions. The occupied lower branch (green curve) increases similar to a free-particle dispersion (black dashed curve). However, near k_μ, the dispersion turns around and an energy gap forms in the excitation spectrum. The width of the lines loosely represents the quasi-particle lifetime.

sentative BCS-like dispersion curve in Fig. 6.5. Note that the dispersion loosely follows the free-particle dispersion until it eventually turns around near k_μ and then begins to decrease. The minimum energy required for an excitation is twice the superfluid gap, 2Δ, and occurs at $k = k_\mu$. The energy gap and back-bending dispersion are characteristic signatures of superconductivity in BCS-theory.

Recall that our data is taken at temperatures very near T_c. In BCS theory, the gap vanishes at T_c and so one might naively expect our spectrum to reveal a near-zero pairing gap. However, in the BCS−BEC crossover, a pseudogap due to preformed pairs is predicted to exist above T_c [85, 16, 86, 87, 88, 139, 90]. In the case of a pseudogap, the spectral function for a strongly interacting Fermi gas near T_c is predicted to retain its gap-like double-peak structure. In this sense, even though the system will not be superconducting (or superfluid), the spectral function peaks continue to follow a BCS-like back-bending dispersion curve where the BCS gap is replaced by the pseudogap [85, 16, 86, 87, 88, 139, 90]. As a first step in analyzing our data, we fit the centers of the intensity at each value of k (white dots) to Eqn. 6.6, where we replace the superfluid gap with the pseudogap. The best fit, shown as the white curve in Fig. 6.4b, gives $\mu = h \cdot (12.3 \pm 0.7 \text{ kHz})$ and $\Delta = h \cdot (9.5 \pm 0.6)$ kHz. Note that we have also performed photoemission spectroscopy on a gas well below the superfluid transition temperature and find the data to be qualitatively similar.

A fairly natural question is to what extent does density inhomogeneity play a role in this spectra? Recall from the last chapter that in all trapped gas experiments the density is inhomogeneous and that the pairing gap will depend on the density, or equivalently on the local Fermi energy. We can come to a qualitative understanding of how our spectra may look for a homogeneous gas by comparing our strongly-interacting spectra to our weakly-interacting spectra. Namely, we expect that atoms at the edge of the cloud are at low density and will therefore

follow the free-particle dispersion similar to Fig. 6.4a. While this may change slightly the best fit parameters, μ and Δ, it cannot cause the back-bending seen in the dispersion. In this way, our photoemission spectroscopy for ultracold atoms provides a robust signature for pairing.

Because the photoemission spectroscopy intensity plots contain vast amounts of information, one is left with the question of how to compare these new microscopic quantities to theory. In condensed matter ARPES experiments, the PES data is often presented in the form of energy distribution curves (EDCs). An EDC is a vertical slice through the photoemission spectra at a fixed k. Conversely, a momentum distribution curve (MDC) is a slice at fixed E_s. EDCs are especially useful because they can be directly related to the spectral function at a given k, such as we found in Eq. 6.5. Then, the peak position of the EDC indicates the dispersion at that k and the width of the feature indicates the lifetime of a single-particle excitation at that k. As expected, the very strong interactions in Fig. 6.4b result in a short lifetime for a particle in any given k and thus a very large width. In Fig. 6.6 we show energy distribution curves for Fig. 6.4b for select values of k. As k increases, the peak position of the EDCs approach the Fermi energy. However, as k approaches k_F, the peak positions turn around and then decrease for larger k. In this way, we clearly see the back-bending of the dispersion and we can directly compare to theoretical EDCs.

Continuing with our photoemission spectroscopy data, we now move to the BEC side of resonance. Far on the BEC side of the resonance, for $1/k_F^0 a \gg 1$, the pairing gap eventually becomes a two-body binding rather than a many-body effect that depends on the local Fermi energy. We measure the excitation spectrum of the Fermi gas at $1/k_F^0 a \approx 1$, where the molecule binding energy measured for a low density gas is $h \cdot (25 \pm 2$ kHz). We observe two prominent features (Fig. 6.4c). The first feature is narrow in energy, starts at zero energy and follows

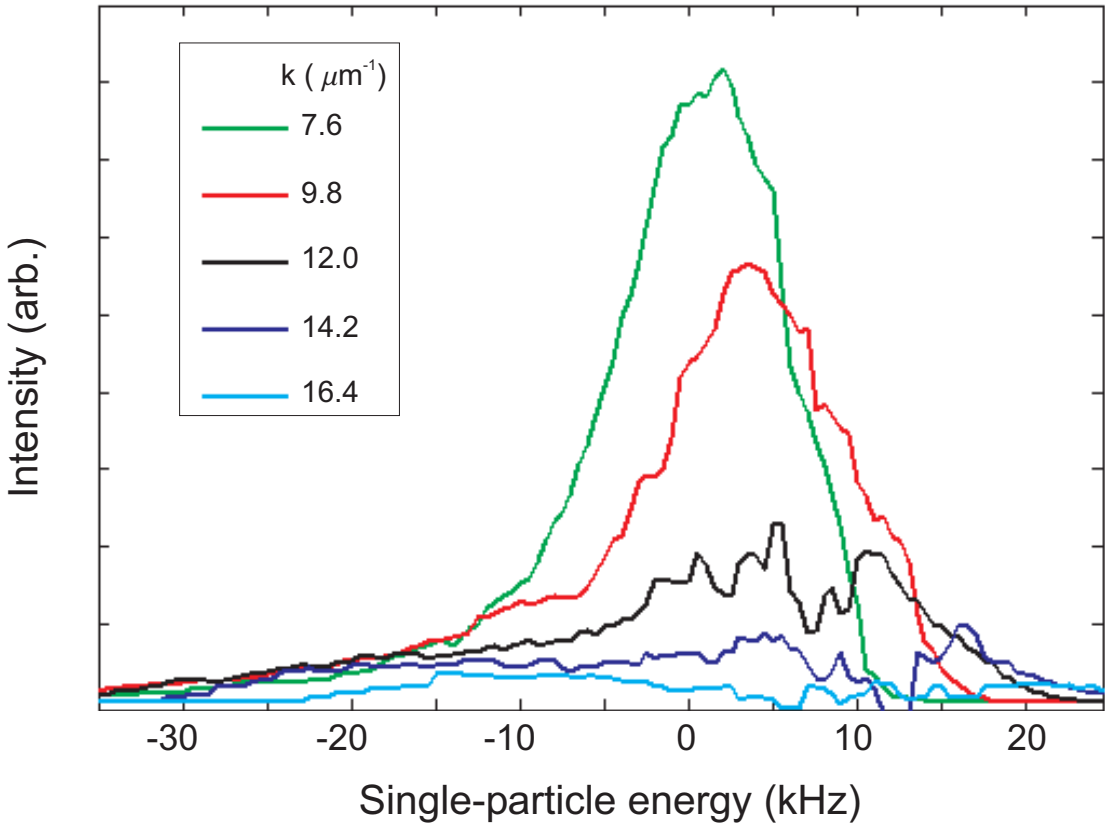

Figure 6.6: Energy distribution curves (EDCs) for a strongly interacting Fermi gas. We plot the intensity for selected values of k. Each curve is the average for seven neighboring values of k in Fig. 6.4b. The data have been smoothed with a 1.5-kHz-wide filter, and the energy is expressed in terms of frequency. The peak position of the EDCs approaches the Fermi energy for increasing k; however, the peak positions are eventually turned around by the pairing gap and tend to decrease for larger k.

the quadratic dispersion expected for free atoms (black line). We attribute this feature to unpaired atoms, which may be out of chemical equilibrium with the pairs. The second feature is very broad in energy, is shifted to lower energy and trends towards lower energy for increasing k. This feature we attribute to atoms in the paired state. An excitation gap separating the two features is evident in the data. We fit the centers of the molecule feature to a quadratic dispersion (white line) with the free parameters being the energy offset and an effective mass m^*, $E_s = \hbar^2 k^2/2m^* + E_B$. In the BEC limit, where the molecules are tightly bound, we would expect the energy offset to be the molecule binding energy, which equals 2Δ, and the effective mass to be $-m$. This negative effective mass reflects the fact that outcoupling an atom at high k leaves behind an excitation in the form of an unpaired atom. Or, in other words, as we discussed in the previous chapter, RF spectroscopy is a single-particle probe and therefore we observe the dispersion for only one of the constituent atoms. The best fit to the data gives an energy offset of $h \cdot (28\text{ kHz})$ and an effective mass of $m^* = -1.25m$.

The large energy width of the molecule feature seen in Fig. 6.4c is probably due to center-of-mass motion of the pairs. For comparison with the data, we performed a simple Monte Carlo simulation, assuming a thermal distribution for the center-of-mass motion and using the predicted distribution of relative kinetic energy for RF dissociation of weakly bound molecules [117]. We assume that the pairs are in thermal equilibrium with the unpaired atoms and use the measured temperature of the unpaired atoms in our simulation. Assuming a molecule binding energy of $h \cdot (25\text{ kHz})$, we calculate the intensity map shown in Fig. 6.7a. To easily compare the experimental data, we reproduce the white curve from Fig. 6.4c. The agreement is quite satisfactory.

We argued earlier that part of the appeal of studying the microscopics of a Fermi gas was that one can in turn determine its macroscopic quantities. For

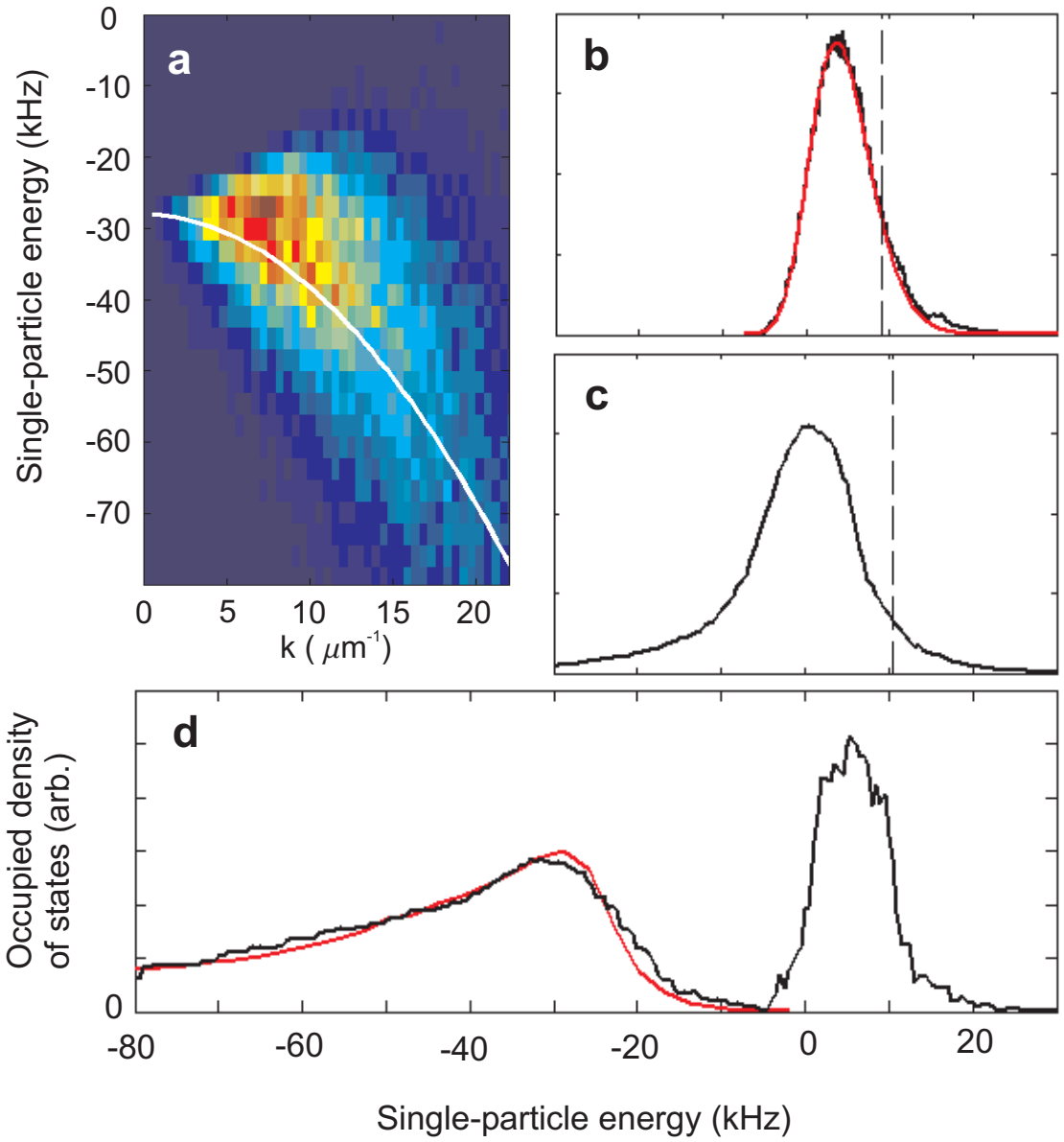

Figure 6.7: The occupied density of single-particle states. a) A calculated intensity map for a $T = 0.17$ μK thermal distribution of weakly bound molecules. The white line is the fit to the data shown in Fig. 6.4c. The agreement between theory and data is quite satisfactory. b) The density of states for a weakly interacting Fermi gas (black line) agrees well with a fit (red curve) for a Fermi gas in a harmonic trap. The fit, whose only free parameter is the amplitude, includes our measurement resolution. The dashed black vertical line shows E_F. c) The density of states taken at the peak of the Feshbach resonance is shifted to much lower energy and contains a high (negative) energy tail. d) The density of states on the BEC side of the resonance has two features: a peak due to unpaired atoms and a broader feature due to molecules. This time, the red curve is the expected density of states from the simulation shown in a). Energy is expressed in terms of frequency.

example, if we sum the photoemission spectra over all k, then we recover the number of atoms at each E_s, also referred to as the occupied density of states (DOS). We plot the DOS for our three spectra in Fig. 6.7b-d. For the nearly ideal Fermi gas 6.7b, we find good agreement with the expected DOS for a trapped Fermi gas at $T = 0.18\,T_F$ (red curve). The theory curve includes our measurement resolution and the only free parameter in the fit is the amplitude. For the strongly interacting gas (Fig. 6.7c), the occupied density of states becomes wider in energy and the position shifts towards lower energies. The shift we attribute to the strong attractive interactions in the system. We also observe a high (negative) energy tail, which indicates that strong interactions promote atoms into high energy states (as when two atoms are close together in pairing). On the BEC side of resonance (Fig. 6.7d), a pairing gap is readily apparent. This is because broken pairs are already available in the form of free atoms. The red curve is the expected density of states determined from the simulation of a thermal distribution of weakly bound molecules (Fig. 6.7a). The only free parameter in the simulation is an overall scaling factor for the amplitude.

Another macroscopic quantity easily obtained is the momentum distribution. This is obtained by summing the photoemission spectra over all E_s, giving the number of atoms as a function of k. The momentum distribution for an interacting Fermi gas was previously measured in Ref. [53] where an interacting Fermi gas was quickly jumped to the weakly interacting regime. In contrast, the momentum distribution as obtained from photoemission spectroscopy does not require this magnetic-field jump because the outcoupled atoms are already weakly interacting.

The momentum-integrated RF spectra we discussed last chapter, can also be recovered, generating a spectrum similar to that in Fig. 6.3a. At this point I would like to highlight, as we discovered last chapter, that while RF spectroscopy

is inherently a microscopic probe, in its momentum-integrated form it is inadequate for revealing the single-particle dispersion [89]. It is only when we resolve the momentum that we can observe the back-bending dispersion of the paired state. The MIT group has shown that if one is willing to make an assumption of the quasi-particle dispersion, then momentum-integrated RF spectroscopy can be used in a spin-imbalanced Fermi gas to determine the superfluid gap [82]. Unfortunately, this approach is not straightforward because it takes place at the interface between the superfluid and normal phase. Additionally, the work in Ref. [132] demonstrates that even in the best-case scenario for ^{6}Li, final-state effects may still be non-negligible.

From an ultracold atoms point of view, we are very excited about our new photoemission spectroscopy technique and its ability to directly probe the spectral function and determine many microscopic quantities such as the energy dispersion, energy gaps, and quasi-particle lifetimes. Much of this information was a first for the atomic physics community. In light of the importance of these importance of these concepts I would like to again acknowledge the work of Dao *et al.* [138] which we found to be the first proposal of ARPES for atomic systems. Additionally, I want to acknowledge previous experiments which probed microscopic qualities of a Fermi gas such as the Bragg spectroscopy experiments of Vale *et al.* [37] and the photoassociation experiments of Hulet *et al.* [140].

Thus far, photoemission spectroscopy has already proved to be very valuable for studying strongly interacting atomic Fermi gases. Currently we are already extending this technique to include spatially resolved momentum-resolved RF spectroscopy to study the effects of density inhomogeneity. We are also beginning to study these strongly interacting gases as a function of temperature and in particular probe the controversial pseudogap regime for temperatures above the superfluid transition temperature. In the future, it will be exciting to see

photoemission spectroscopy applied to other atomic systems as it is a general and conceptually simple probe of strongly correlated atom gases. As such, it could be applied to lattice systems to study band dispersions and the effect of interactions therein, as well as low dimensional systems. For example, photoemission spectroscopy has now been proposed as a possible tool for observing the FuldeFerrelLarkinOvchinnikov (FFLO) state in 1D Fermi gases [141]. Additionally, much like ARPES of electronic systems, our photoemission spectroscopy technique could be used for an atom system where the pairing is not isotropic as in higher partial-wave pairing [142, 143, 144].

Chapter 7

Conclusions and future directions

The work in this thesis aimed to answer the question of what can these new Fermi gas systems teach us about the general class of strongly interacting Fermi gases? We began by contributing to the broad demonstration that atomic Fermi gases are addressing universal physics. This demonstration of universality was imperative to be able to say that we are studying the relevant underlying physics found in nuclear and neutron matter, the quark-gluon plasma, and possibly even high temperature superconductors. Secure in the fact that we were addressing universal physics, we decided to answer the question head on by directly probing the microscopic physics.

Intimately connected with answering the above question is finding ways to make measurements that connect directly to many-body theories and ideas. In this way, with detailed enough measurements, we can use our relatively pure and simple system to constrain many-body theories and thereby modify our understanding of all strongly interacting Fermi gas systems. To do this, we created a new measurement technique (for the atomic physics community) using photoemission spectroscopy. Photoemission spectroscopy allowed us to directly probe the single-particle spectral function, which is in turn directly predicted by many-body theories. For the first time, we were able to probe the energy dispersion, the pairing gap, and the quasi-particle lifetimes of a strongly interacting atomic Fermi

gas. These measurements are now allowing for the most detailed microscopic comparisons between experiment and theory to date.

7.1 Future directions

In general, the future for atomic Fermi gases seems boundless. As these systems continue to address condensed matter and many-body ideas with greater accuracy, I think they will continue to make contributions relevant to the greater physics community. I think the photoemission spectroscopy technique developed here will continue to have an important role to play as well. In particular, as these gases are being introduced to lattices, higher partial-wave pairing, lower dimensions, impurities, etc., this measurement technique will become even more relevant for relating to condensed matter systems. Particular to these types of experiments, I would still like to see PES or IPES (inverse photoemission spectroscopy) used to observe the upper branch of the BCS-like dispersion (we tried for many months with little success).

7.2 The work not presented here

In addition to the work I have presented here, I also worked on a few other results. Before the work in this thesis, I took part in a study using atom shot noise to probe fermionic pairing [112]. All of the work I have discussed in this thesis was done in equal collaboration with John Gaebler and as such we divided up topics for our theses. Another topic we addressed, which John will likely cover in his thesis, was the first clear creation and observation of p-wave Feshbach molecules, found in Ref. [142]. In the near future, we hope to publish our recent work in which we have used photoemission spectroscopy to address the center of the cloud (a more homogeneous sample) by using holographic techniques to remove atoms at the edge of the sample. Also in the near future, we hope to publish our work in

which we have studied the dispersion of a strongly interacting Fermi gas above the superfluid temperature, relevant for pseudogap physics. Lastly, we have recently returned to this idea of universality in Fermi gases and hope to address this topic more broadly by studying the Tan relations [99, 145, 146]

Bibliography

[1] A. L. Fetter and J. D. Walecka, *Quantum Theory of Many-Particle Systems* (Dover Publications, Mineola, New York, 2003).

[2] C. Kittel, *Introduction to Solid State Physics* (John Wiley & Songs, Inc., Chichester, Brisbane, Toronto, 2003).

[3] G. A. Baker, Neutron matter model, *Phys. Rev. C* **60**, 054311 (1999).

[4] H. Heiselberg, C. J. Pethick, H. Smith, and L. Viverit, Influence of Induced Interactions on the Superfluid Transition in DiluteFermi Gases, *Phys. Rev. Lett.* **85**, 2418 (2000).

[5] H. Heiselberg, Fermi systems with long scattering lengths, *Phys. Rev. A* **63**, 043606 (2001).

[6] J. Carlson, S. Y. Chang, V. R. Pandharipande, and K. E. Schmidt, Superfluid Fermi Gases with Large Scattering Length, *Phys. Rev. Lett.* **91**, 050401 (2003).

[7] E. Shuryak, Strongly coupled quark-gluon plasma: the status report, *Prog. Part. Nucl. Phys.* **53**, 273 (2004).

[8] T.-L. Ho, Universal Thermodynamics of Degenerate Quantum Gases in the Unitarity Limit, *Phys. Rev. Lett.* **92**, 090402 (2004).

[9] A. Turlapov, J. Kinast, B. Clancy, L. Luo, J. Joseph, and J. Thomas, Is a Gas of Strongly Interacting Atomic Fermions a Nearly Perfect Fluid?, *J. Low. Temp. Phys.* **150**, 567 (2008).

[10] J. E. Thomas, Is an Ultra-Cold Strongly Interacting Fermi Gas a Perfect Fluid?, (2009), arXiv:0907.0140v1.

[11] L. N. Cooper, Bound electron pairs in a degenerate Fermi gas, *Phys. Rev.* **104**, 1189 (1956).

[12] J. Bardeen, L. N. Cooper, and J. R. Schrieffer, Microscopic theory of superconductivity, *Phys. Rev.* **106**, 162 (1957).

[13] J. Bardeen, L. N. Cooper, and J. R. Schrieffer, Theory of superconductivity, *Phys. Rev.* **108**, 1175 (1957).

[14] P. Noziéres and D. Pines, *The Theory of Quantum Liquids, Vol. II Superfluid Bose Liquids* (Addison-Wesley, Cambridge, Massachusetts, 1990).

[15] S. Giorgini, L. P. Pitaevskii, and S. Stringari, Theory of ultracold Fermi gases, *Rev. Mod. Phys.* **80**, 1215 (2008).

[16] M. Randeria, in *Bose-Einstein Condensation*, edited by A. Griffin, D. W. Snoke, and S. Stringari (Cambridge University Press, New York, 1995), pp. 355–392.

[17] Q. Chen, J. Stajic, S. Tan, and K. Levin, BCS-BEC crossover: From high temperature superconductors to ultracold superfluids., *Phys. Rep.* **412**, 1 (2005).

[18] I. Bloch, J. Dalibard, and W. Zwerger, Many-Body Physics with Ultracold Gases, *Rev. Mod. Phys.* **80**, 885 (2008).

[19] M. Greiner, O. Mandel, T. Esslinger, T. W. Hänsch, and I. Bloch, Quantum phase transition from a superfluid to a Mott insulator in a gas of ultracold atoms, *Nature* **415**, 39 (2002).

[20] S. Ospelkaus, C. Ospelkaus, O. Wille, M. Succo, P. Ernst, K. Sengstock, and K. Bongs, Localization of bosonic atoms by fermionic impurities in a 3d optical lattice, *Phys. Rev. Lett.* **96**, 180403 (2006).

[21] L. Fallani, C. Fort, and M. Inguscio, in *Advances in Atomic, Molecular, and Optical Physics*, edited by E. Arimondo, P. R. Berman, M. Phil, and C. C. Lin (Academic Press, Amsterdam, 2008), Chap. Bose-Einstein condensates in disordered potentials.

[22] M. White, M. Pasienski, D. McKay, S. Zhou, D. Ceperley, and B. DeMarco, Strongly interacting bonsons in a disordered optical lattice, (2009), arXiv:0708.3074.

[23] M. H. Anderson, J. R. Ensher, M. R. Matthews, and C. E. W. andE. A. Cornell, Observation of Bose-Einstein Condensation in a Dilute Atomic Vapor, *Science* **269**, 198 (1995).

[24] K. B. Davis, M.-O. Mewes, M. R. Andrews, N. J. van Druten, D. Durfee, D. M. Kurn, and W. Ketterle, Bose-Einstein Condensation in a Gas of Sodium Atoms, *Phys. Rev. Lett.* **75**, 3969 (1995).

[25] B. DeMarco, J. L. Bohn, J. P. Burke, Jr., M. Holland, and D. S.Jin, Measurement of p-Wave Threshold Law Using Evaporatively Cooled FermionicAtoms, *Phys. Rev. Lett.* **82**, 4208 (1999).

[26] B. DeMarco and D. S. Jin, Onset of Fermi Degeneracy in a Trapped Atomic Gas, *Science* **285**, 1703 (1999).

[27] M. Mackie, E. Timmermans, R. Cote, and J. Javanainen, Driving superlfuidity with photoassociation, *Optics Express* **8**, 118 (2000).

[28] M. Holland, S. J. J. M. F. Kokkelmans, M. L. Chiofalo, and R. Walser, Resonance Superfluidity in a Quantum Degenerate Fermi Gas, *Phys. Rev. Lett.* **87**, 120406 (2001).

[29] Y. Ohashi and A. Griffin, BCS-BEC crossover in a gas of Fermi atoms with a Feshbach resonance, *Phys. Rev. Lett.* **89**, 130402 (2002).

[30] C. A. Regal, M. Greiner, and D. S. Jin, Observation of Resonance Condensation of Fermionic Atom Pairs, *Phys. Rev. Lett.* **92**, 040403 (2004).

[31] C. A. Regal and D. S. Jin, Experimental realization of the BCS-BEC crossover with a Fermi gas of atoms, *Adv. Atom. Mol. Opt. Phys.* **54**, 1 (2006).

[32] H. Moritz, T. Stöferle, K. Günter, M. Köhl, and T. Esslinger, Confinement induced molecules in a 1D Fermi gas, *Phys. Rev. Lett.* **94**, 210401 (2004).

[33] M. Houbiers, H. T. C. Stoof, W. I. McAlexander, and R. G. Hulet, Elastic and inelastic collisions of Li-6 atoms in magnetic and optical traps, *Phys. Rev. A* **57**, R1497 (1998).

[34] K. M. O'Hara, M. E. Gehm, S. R. Granade, S. Bali, and J. E. Thomas, Stable, strongly attractive, two-state mixture of lithium fermions in anoptical trap, *Phys. Rev. Lett.* **85**, 2092 (2000).

[35] M. Bartenstein, A. Altmeyer, S. Riedl, S. Jochim, C. Chin, J. H. Denschlag, and R. Grimm, Crossover from a molecular Bose-Einstein condensate to a degenerate Fermi gas, *Phys. Rev. Lett.* **92**, 120401 (2004).

[36] W. Ketterle and M. W. Zwierlein, in *Proceedings of the International School of Physics "Enrico Fermi", Course CLXIV*, edited by M. Inguscio, W. Ketterle, and C. Salomon (OS Press, Amsterdam, 2008).

[37] G. Veeravalli, E. Kuhnle, P. Dyke, and C. J. Vale, Bragg spectroscopy of a strongly interacting Fermi gas, *Phys. Rev. Lett.* **101**, 250403 (2008).

[38] T. Fukuhara, S. Sugawa, Y. Takasu, and Y. Takahashi, All-Optical Formation of Quantum Degenerate Mixtures, *Phys. Rev. A* **79**, 021601 (2009).

[39] D. M. Eagles, Possible Pairing without Superconductivity at Low Carrier Concentrations in Bulk and Thin-Film Superconducting Semiconductors, *Phys. Rev.* **186**, 456 (1969).

[40] A. J. Leggett, Cooper pairing in spin-polarized Fermi systems., *J. Phys. C (Paris)* **41**, C7 (1980).

[41] P. Nozieres and S. Schmitt-Rink, Bose condensation in an attractive fermion gas: from weak to strong coupling superconductivity, *J. of Low Temp. Phys.* **59**, 195211 (1985).

[42] T. Loftus, C. A. Regal, C. Ticknor, J. L. Bohn, and D. S. Jin, Resonant Control of Elastic Collisions in an Optically Trapped Fermi Gas of Atoms, *Phys. Rev. Lett.* **88**, 173201 (2002).

[43] K. M. O'Hara, S. L. Hemmer, M. E. Gehm, S. R. Granade, and J. E.Thomas, Observation of a Strongly Interacting Degenerate Fermi Gas of Atoms, *Science* **298**, 2179 (2002).

[44] S. Gupta, Z. Hadzibabic, M. W. Zwierlein, C. A. Stan, K. Dieckmann, C. H. Schunck, E. G. M. van Kempen, B. J. Verhaar, and W. Ketterle, Radio-Frequency Spectroscopy of Ultracold Fermions, *Science* **300**, 1723 (2003).

[45] T. Bourdel, J. Cubizolles, L. Khaykovich, K. M. F. Magalhaes, S. J. J. M. F. Kokkelmans, G. V. Shlyapnikov, and C. Salomon, Measurement of the Interaction Energy near a Feshbach Resonance in a ^{6}LiFermi Gas, *Phys. Rev. Lett.* **91**, 020402 (2003).

[46] Q. Chen and K. Levin, Superconducting phase coherence in the presence of a pseudogap: Relation to specific heat, tunneling, and vortex core spectroscopies, *Phys. Rev. B* **63**, 184519 (2001).

[47] C. A. Regal, Experimental realization of BCS-BEC crossover physics with a Fermi gas of atoms, Ph.D. thesis, U. of Colorado, 2006.

[48] M. W. Zwierlein, High-Temperature Superuidity in an Ultracold Fermi Gas, Ph.D. thesis, Massachusetts Intitute of Technology, 2006.

[49] G. B. Partridge, Paring of Fermionic ^{6}Li Throughout the BEC-BCS Crossover, Ph.D. thesis, Rice University, 2007.

[50] B. DeMarco, Quantum Behavior of an Atomic Fermi Gas, Ph.D. thesis, University of Colorado, 2001.

[51] J. Kinast, S. L. Hemmer, M. E. Gehm, A. Turlapov, and J. E. Thomas, Evidence for Superfluidity in a Resonantly Interacting Fermi Gas, *Phys. Rev. Lett.* **92**, 150402 (2004).

[52] M. Bartenstein, A. Altmeyer, S. Riedl, S. Jochim, C. Chin, J. H. Denschlag, and R. Grimm, Collective Excitations of a Degenerate Gas at the BEC-BCS Crossover, *Phys. Rev. Lett* **92**, 203201 (2004).

[53] C. A. Regal, M. Greiner, S. Giorgini, M. Holland, and D. S. Jin, Momentum Distribution of a Fermi Gas of Atoms in the BCS-BEC Crossover, *Phys. Rev. Lett.* **95**, 250404 (2005).

[54] M. W. Zwierlein, J. R. Abo-Shaeer, A. Schirotzek, C. H. Schunck, and W. Ketterle, Vortices and superfluidity in a stronly interacting Fermi gas, *Nature* **435**, 1047 (2005).

[55] J. T. Stewart, J. P. Gaebler, C. A. Regal, and D. S. Jin, Potential Energy of a ^{40}K Fermi Gas in the BCS-BEC Crossover, *Phys. Rev. Lett.* **97**, 220406 (2006).

[56] M. E. Gehm, S. L. Hemmer, S. R. Granade, K. M. O'Hara, and J. E.Thomas, Mechanical stability of a strongly interacting Fermi gas of atoms, *Phys. Rev. A* **68**, 011401(R) (2003).

[57] T. Bourdel, L. Khaylovich, J. Cubizolles, J. Zhang, F. Chevy, M. Teichmann, L. Tarruell, S. J. J. M. F. Kokkelmans, and C. Salomon, Experimental Study of the BEC-BCS Crossover Region in Lithium 6, *Phys. Rev. Lett.* **93**, 050401 (2004).

[58] G. B. Partridge, W. Li, R. I. Kamar, Y. an Liao, and R. G. Hulet, Pairing and Phase Separation in a Polarized Fermi Gas, *Science* **311**, 503 (2005).

[59] J. Kinast, A. Turlapov, J. E. Thomas, Q. Chen, and J. S. andK. Levin, Heat Capacity of a Strongly Interacting Fermi Gas, *Science* **307**, 1296 (2005).

[60] J. Carlson and S. Reddy, Asymmetric Two-Component Fermion Systems in Strong Coupling, *Phys. Rev. Lett.* **95**, 060401 (2005).

[61] G. E. Astrakharchik, J. Boronat, J. Casulleras, and S. Giorgini, Equation of State of a Fermi Gas in the BEC-BCS Crossover: A Quantum MonteCarlo Study, *Phys. Rev. Lett.* **93**, 200404 (2004).

[62] G. E. Astrakharchik, J. Boronat, J. Casulleras, and S. Giorgini, Momentum Distribution and Condensation Fraction of a Fermion Gas in theBCS-BEC Crossover, *Phys. Rev. Lett.* **95**, 230405 (2005).

[63] E. Burovski, N. Prokof'ev, B. Svistunov, and M. Troyer, Critical Temperature and Thermodynamics of Attractive Fermions at Unitarity, *Phys. Rev. Lett.* **96**, 160402 (2006).

[64] A. Perali, P. Pieri, and G. C. Strinati, Quantiative Comparison between Theoretical Predictions and Experimetal Resultsfor the BCS-BEC Crossover, *Phys. Rev. Lett.* **93**, 100404 (2004).

[65] H. Hu, X.-J. Liu, and P. D. Drummond, Temperature of a trapped unitary Fermi gas at finit entropy, *Phys. Rev. A* **73**, 023617 (2006).

[66] H. Hu, X.-J. Liu, and P. D. Drummond, Equation of state of a superfluid Fermi gas in the BCS-BEC crossover, *Europhys. Lett.* **74**, 574 (2006).

[67] X.-J. Liu and H. Hu, Self-consistent theory of atomic Fermi gases with a Feshbach resonance atthe superfluid transition, *Phys. Rev. A* **72**, 063613 (2005).

[68] A. Damascelli, Probing the Electronic Structure of Complex Systems by ARPES, *Physica Scripta* **T109**, 61 (2004).

[69] J. T. Stewart, J. P. Gaebler, and D. S. Jin, Using photoemission spectroscopy to probe a strongly interacting Fermi gas, *Nature* **454**, 744 (2008).

[70] Q. Chen and K. Levin, Probing the Spectral Function Using Momentum Resolved Radio Frequency Spectroscopy in Trapped Fermi Gases, *Phys. Rev. Lett.* **102**, 190402 (2009).

[71] C. J. Myatt, N. R. Newbury, R. W. Ghrist, S. Loutzenhiser, and C. Wieman, Multiply loaded magneto-optical trap, *Opt. Lett.* **21**, 290 (1996).

[72] M. Greiner, Ultracold quantum gases in three-dimensional optical lattice potentials, Ph.D. thesis, Max-Planck-Institute for Quantum Optics, 2003.

[73] U. Fano, On the absorption spectrum of noble gases at the arc spectrum limit, *Nuovo Cimento* **12**, 154 (1935), a translation edited by Guido Pupillo, Alberto Zannoni, and Charles W. Clark. arXiv:cond-mat/0502210v1.

[74] U. Fano, Effects of configuration interaction on intensities and phase shifts, *Phys. Rev.* **124**, 1866 (1961).

[75] H. Feshbach, A Unified Theory of Nuclear Reactions. II, *Ann. Phys.* **19**, 287 (1962).

[76] J. P. Burke, Theoretical investigations of cold alkali atom collisions, Ph.D. thesis, University of Colorado, 1999.

[77] S. Simonucci, P. Pieri, and G. C. Strinati, Broad vs. narrow Fano-Feshbach resonances in the BCS-BEC crossover withtrapped Fermi atoms, *Europhys. Lett.* **69**, 713 (2005).

[78] B. Marcelis, B. Verhaar, and S. Kokkelmans, Total Control over Ultracold Interactions via Electric and Magnetic Fields, *Phys. Rev. Lett.* **100**, 153201 (2008).

[79] D. M. Bauer, M. Lettner, C. Vo, G. Rempe, and S. Durr, Controlling a magnetic Feshbach resonance with laser light, *Nature Physics* **5**, 339 (2009).

[80] A. M. Kaufman, R. P. Anderson, T. M. Hanna, E. E. Tiesinga, P. S. Julienne, and D. S. Hall, Radiofrequency Dressing of Multiple Feshbach Resonances, (2009), arXiv:0906.5587v2.

[81] J. Carlson and S. Reddy, Superfluid Pairing Gap in Strong Coupling, *Phys. Rev. Lett.* **100**, 150403 (2008).

[82] A. Schirotzek, Y. il Shin, C. H. Schunck, and W. Ketterle, Determination of the Superfluid Gap in Atomic Fermi Gases by Quasiparticle Spectroscopy, *Phys. Rev. Lett.* **101**, 140403 (2008).

[83] R. Haussman, Properties of a Fermi liquid at the superfluid transition in the crossover region between BCS superconductivity and Bose-Einstein condensation, *Phys. Rev. B* **49**, 12975 (1994).

[84] V. Gurarie and L. Radzihovsky, Resonantly-paired fermionic superfluids, *Annals of Physics* **322**, 2 (2007).

[85] B. Janko, J. Maly, and K. Levin, Pseudogap effects induced by resonant pair scattering, *Phys. Rev. B* **56**, R11407 (1997).

[86] Y. Yanase and K. Yamada, Theory of Pseudogap Penomena in High-Tc Cuprates Based on the Strong Coupling Superconductivity, *Journal of the Physical Society of Japan* **68**, 2999 (1999).

[87] A. Perali, P. Pieri, G. C. Strinati, and C. Castellani, Pseudogap and spectral function from superconducting fluctuations to the bosonic limit, *Phys. Rev. B* **66**, 024510 (2002).

[88] G. M. Bruun and G. Baym, Bragg spectroscopy of cold atomic Fermi gases, *Phys. Rev. A* **74**, 033623 (2006).

[89] P. Massignan, G. M. Bruun, and H. T. C. Stoof, Twin peaks in rf spectra of Fermi gases at unitarity, *Phys. Rev. A* **77**, 031601(R) (2008).

[90] N. Barnea, Superfluid to insulator phase transition in a unitary Fermi gas, *Phys. Rev. A* **78**, 053629 (2008).

[91] P. Magierski, G. Wlazlowski, A. Bulgac, and J. E. Drut, The Finite Temperature Pairing Gap of a Unitary Fermi Gas by Quantum Monte Carlo, (2009), arXiv:0801.1504v3.

[92] Q. Chen, Y. He, C. C. Chien, and K. Levin, Theory of Radio Frequency Spectroscopy Experiments in Ultracold Fermi Gases and Their Relation to Photoemission Experiments in the Cuprates, (2009), arXiv:0810.1940v1.

[93] S. Tsuchiya, R. Watanabe, and Y. Ohashi, Single-particle properties and pseudogap effects in the BCS-BEC crossover regime of an ultracold Fermi gas above Tc, (2009), arXiv:0907.4595v1.

[94] A. G. Truscott, K. E. Strecker, W. I. McAlexander, G. B. Partridge, and R. G. Hulet, Observation of Fermi Pressure in a Gas of Trapped Atoms, *Science* **291**, 2570 (2001).

[95] H. T. C. Stoof, M. Houbiers, C. A. Sackett, and R. G. Hulet, Superfluidity of Spin-Polarized ^{6}Li, *Phys. Rev. Lett.* **76**, 10 (1996).

[96] C. Menotti, P. Pedri, and S. Stringari, Expansion of an Interacting Fermi Gas, *Phys. Rev. Lett.* **89**, 250402 (2002).

[97] M. E. Gehm, S. L. Hemmer, K. M. O'Hara, and J. E. Thomas, Unitarity-limited elastic collision rate in a harmonically trapped Fermigas, *Phys. Rev. A* **68**, 011603 (2003).

[98] J. E. Thomas, J. Kinast, and A. Turlapov, Virial theorem and universality in a unitary Fermi gas, *Phys. Rev. Lett.* **95**, 120402 (2005).

[99] S. Tan, Generalized virial theorem and pressure relation for a strongly correlated Fermi gas, *Annals of Physics* **323**, 2987 (2008).

[100] R. B. Diener and T.-L. Ho, The Condition for Universality at Resonance and Direct Measurement of PairWavefunctions Using rf Spectroscopy, (2004), arXiv:cond-mat/0405174v2.

[101] R. B. Diener and T.-L. Ho, Projecting Fermion Pair Condensate into Molecular Condensates, , arXiv:cond-mat/0404517.

[102] M. H. Szymańska, K. Goral, T. Kohler, and K. Burnett, Conventional character of the BCS-BEC crossover in ultracold gases of 40K, *Phys. Rev. A* **72**, 013610 (2005).

[103] M. Mackie and J. Piilo, Feshbach-Resonant Interactions in 40K and 6Li Degenerate Fermi Gases, *Phys. Rev. Lett* **94**, 060403 (2005).

[104] J. Javanainen, M. Kostrun, M. Mackie, and A. Carmichael, Simple Mean-Field Theory for a Zero-Temperature Fermionic Gas at a FeshbachResonance, *Phys. Rev. Lett* **95**, 110408 (2005).

[105] L. Luo and J. E. Thomas, Thermodynamic Measurements in a Strongly Interacting Fermi Gas, *J. of Low Temp. Phys.* **154**, 1 (2009).

[106] A. Bulgac, J. E. Drut, and P. Magierski, Spin 1/2 Fermions in the Unitary Regime: A Superfluid of a New Type, *Phys. Rev. Lett.* **96**, 090404 (2006).

[107] M. Bartenstein, A. Altmeyer, S. Riedl, S. Jochim, R. Geursen, C. Chin, J. H. Denschlag, and R. Grimm, in *XIX International Conference on Atomic Physics* (American Institute of Physics, Melville, New York, 2004), p. 278.

[108] L. Luo, B. Clancy, J. Joseph, J. Kinast, and J. E. Thomas, Measurement of the Entropy and Critical Temperature of a Strongly Interacting Fermi Gas, *Phys. Rev. Lett.* **98**, 080402 (2007).

[109] G. M. Bruun, Two-component Fermi gas with a resonant interaction, *Phys. Rev. A* **70**, 053602 (2004).

[110] C. A. Regal, C. Ticknor, J. L. Bohn, and D. S. Jin, Creation of ultracold molecules from a Fermi gas of atoms, *Nature* **424**, 47 (2003).

[111] C. A. Regal and D. S. Jin, Measurement of Positive and Negative Scattering Lengths in a Fermi Gasof Atoms, *Phys. Rev. Lett.* **90**, 230404 (2003).

[112] M. Greiner, C. A. Regal, J. T. Stewart, and D. S. Jin, Probing pair-correlated Fermionic atoms through correlations in atom shot noise, *Phys. Rev. Lett.* **94**, 110401 (2005).

[113] Y. Shin, M. W. Zwierlein, C. H. Schunck, A. Schirotzek, and W. Ketterle, Observation of Phase Separation in a Strongly Interacting Imbalanced Fermi Gas, *Phys. Rev. Lett.* **97**, 030401 (2006).

[114] Y. Shin, C. H. Schunck, A. Schirotzek, and W. Ketterle, Tomographic rf spectroscopy of a trapped fermi gas at unitarity., *Phys. Rev. Lett.* **99**, 090403 (2007).

[115] C. H. Schunck, Y. i. Shin, A. Schirotzek, and W. Ketterle, Determination of the Fermion Pair Size in a Resonantly Interacting Superfluid, *Nature* **454**, 739 (2008).

[116] G. K. Campbell *et al.*, Probing Interactions Between Ultracold Fermions, *Science* **324**, 5925 (2009).

[117] C. Chin and P. S. Julienne, Radio-frequency transitions on weakly bound ultracold molecules., *Phys. Rev. A* **71**, 012713 (2005).

[118] C. Chin, M. Bartenstein, A. Altmeyer, S. Riedl, S. Jochim, J. H. Denschlag, and R. Grimm, Observation of the Pairing Gap in a Strongly Interacting Fermi Gas, *Science* **305**, 1128 (2004).

[119] J. Kinnunen, M. Rodriguez, and P. Torma, Pairing gap and in-gap excitations in trapped fermionic superfluids, *Science* **305**, 1131 (2004).

[120] C. H. Schunck, Y. Shin, A. Schirotzek, M. W. Zwierlein, and W. Ketterle, Pairing without superfluidity: The ground state of an imbalanced Fermi mixture, *Science* **316**, 867 (2007).

[121] Y. Ohashi and A. Griffin, Single-particle excitations in a trapped gas of Fermi atoms in the BCS-BEC crossover region, *Phys. Rev. A* **72**, 013601 (2005).

[122] Z. Yu and G. Baym, Spin-correlation functions in ultracold paired atomic-fermion systems: Sum rules, self-consistent approximations, and mean fields., *Phys. Rev. A* **73**, 063601 (2006).

[123] R. Combescot, S. Giorgini, and S. Stringari, Molecular signatures in the structure factor of an interacting Fermi gas, *Europhys. Lett.* **75**, 5 (2006).

[124] M. Punk and W. Zwerger, Theory of rf-spectrscopy of strongly interacting fermions., *Phys. Rev. Lett.* **99**, 170404 (2007).

[125] S. Basu and E. J. Mueller, Final-state effects in the radio frequency spectrum of strongly interacting fermions, *Phys. Rev. Lett.* **101**, 060405 (2008).

[126] F. Fumarola and E. J. Mueller, Single particle spectrum of resonant population imbalanced Fermi gases, (2007), arXiv:0706.1205v1.

[127] A. Perali, P. Pieri, and G. C. Strinati, Competition between final-state and pairing gap effects in the radio-frequency spectra of ultracold Fermi atoms., *Phys. Rev. Lett.* **100**, 010402 (2008).

[128] M. Veillette, E. G. Moon, A. Lamacraft, L. Radzihovsky, S. Sachdev, and D. E. Sheehy, Radio frequency spectroscopy of a strongly imbalanced Feshbach-resonant Fermi gas, *Phys. Rev. A* **78**, 033614 (2008), arXiv:0803.2517v1.

[129] Y. He, C. C. Chien, Q. Chen, and K. Levin, Radio Frequency Spectroscopy of Trapped Fermi Gases with Population Imbalance, *Phys. Rev. A* **77**, 011602 (2008).

[130] E. J. Mueller, Generic features of the spectrum of trapped polarized fermions, *Phys. Rev. A* **78**, 045601 (2008).

[131] Y. He, C. C. Chien, Q. Chen, and K. Levin, Temperature and final state effects in radio frequency spectroscopy experiments on atomic Fermi gases., *Phys. Rev. Lett.* **102**, 020402 (2009).

[132] P. Pieri, A. Perali, and G. C. Strinati, Enhanced paraconductivity-like fluctuations in the radiofrequency spectra of ultracold Fermi atoms, (2009), arXiv:0811.0770.

[133] W. Schneider, V. B. Shenoy, and M. Randeria, Theory of Radio Frequency Spectroscopy of Polarized Fermi Gases, (2009), arXiv:0903.3006v1.

[134] A. Damascelli, Z. Hussain, and Z.-X. Shen, Angle-resolved photoemission studies of the cuprate superconductors, *Rev. Mod. Phys.* **75**, 473 (2003).

[135] R. Clasessen, R. O. Anderson, J. W. Allen, C. G. Olson, C. Janowitz, W. P. Ellis, S. Harm, M. Kalning, R. Manzke, and M. Skibowski, Fermi-Liquid line shapes measured by angle-resolved photoemission spectroscopy on 1-T-TiTe2, *Phys. Rev. Lett.* **69**, 808 (1992).

[136] S. B. Kaplan, C. C. Chi, D. N. Landgenberg, J. J. Chang, S. Jafarey, and D. J. Scalapino, Quasiparticle and phonon lifetimes in superconductors, *Phys. Rev. B* **14**, 4854 (1976).

[137] R. C. Dynes, V. Narayanamurti, and J. P. Garno, Direct measurement of quasiparticle-lifetime broadening in a strong-coupled superconductor, *Phys. Rev. Lett.* **41**, 1509 (1978).

[138] T.-L. Dao, A. Georges, J. Dalibard, C. Salomon, and I. Carusotto, Measuring the One-Particle Excitations of Ultracold Fermionic Atoms by Stimulated Raman Spectroscopy, *Phys. Rev. Lett.* **98**, 240402 (2007).

[139] A. Bulgac, J. E. Drut, P. Magierski, and G. Wlazlowski, Gap and Pseudogap of a Unitary Fermi Gas by Quantum Monte Carlo, (2008).

[140] G. B. Partridge, K. E. Strecker, R. I. Kamar, M. W. Jack, and R. G. Hulet, Molecular Probe of Pairing in the BEC-BCS Crossover, *Phys. Rev. Lett.* **95**, 020404 (2005).

[141] M. R. Bakhtiari, M. J. Leskinen, and P. Torma, Spectral signatures of the Fulde-Ferrell-Larkin-Ovchinnikov order parameter in one-dimensional optical lattices, *Phys. Rev. Lett.* **101**, 120404 (2008).

[142] J. P. Gaebler, J. T. Stewart, J. L. Bohn, and D. S. Jin, p-wave Feshbach molecules, *Phys. Rev. Lett.* **98**, 200403 (2007).

[143] Y. Inada, M. Horikoshi, S. Nakajima, M. Kuwata-Gonokami, M. Ueda, and T. Mukaiyama, Collisional Properties of p-Wave Feshbach Molecules, *Phys. Rev. Lett.* **101**, 100401 (2008).

[144] J. Fuchs, C. Ticknor, P. Dyke, G. Veeravalli, E. Kuhnle, W. Rowlands, P. Hannaford, and C. J. Vale, Binding Energies of 6Li p-wave Feshbach Molecules, *Phys. Rev. A* **77**, 053616 (2008).

[145] S. Tan, Large momentum part of a strongly interacting Fermi gas, *Annals of Physics* **323**, 2971 (2008).

[146] S. Tan, Energetics of a strongly correlated Fermi gas, *Annals of Physics* **323**, 2952 (2008).

[147] C. A. Regal, M. Greiner, and D. S. Jin, Lifetime of molecule-atom mixtures near a Feshbach resonance in 40K, *Phys. Rev. Lett.* **92**, 083201 (2004).

[148] K. Xu, T. Mukaiyama, J. R. Abo-Shaeer, J. K. Chin, D. E. Miller, and W. Ketterle, Formation of quantum-degenerate sodium molecules, *Phys. Rev. Lett.* **91**, 210402 (2003).

[149] Y. Shin, C. H. Schunck, A. Schirotzek, and W. Ketterle, Phase diagram of a two-component Fermi gas with resonant interactions, *Nature* **451**, 689 (2008).

Appendix A

Fermi gas thermometry

In this Appendix I will describe an experiment we pursued regarding Fermi gas thermometry. The goal of these experiments was to use a novel technique to determine the temperature of a strongly interacting Fermi gas. As we will shortly see, the temperature of a very cold trapped Fermi gas is a tricky thing to measure, and strong interactions make the problem worse. In this appendix, I will motivate why measuring temperature is important in these systems, why it is hard, and why, unfortunately, our new technique was of limited value. I am including this material because I find it interesting and with the hope that it may be of value to anyone else who decides to develop a new thermometer for these gases.

Temperature is an important parameter when describing a Fermi gas. The temperature relative to the Fermi temperature (T/T_F) separates a classical gas from a quantum gas. When interactions are present, the temperature relative to the transition temperature separates a superfluid from the normal state. Throughout the BCS-BEC crossover, the temperature and the transition temperature are again important parameters, and of current theoretical interest. Unfortunately, this regime of cold temperatures and strong interactions is particularly difficult for two reasons. First, we determine temperature from time-of-flight expansion. For a trapped ideal Fermi gas, as we will see, it is already difficult to measure the temperature of a gas much below $0.1\,T_F$ [47]. Second, as interactions are

turned on, the interaction energy becomes convoluted with the release energy in time-of-flight expansion. To extract the temperature in this way would require a model of the release energy. Thus, it would be nice to have a model independent thermometer that would work for low temperatures and strong interactions.

A.1 Ideal Fermi gas thermometry

To measure the temperature of a weakly interacting Fermi gas, we release the gas from its confining potential and use time-of-flight imaging. For sufficiently long expansion times, the momentum distribution is captured on the CCD. Recall from Chapter 4, we fit the 2D image using an appropriate Fermi-Dirac function

$$OD(y,z) = pk\, g_2\Big(-\xi\, e^{-\frac{y^2}{2\sigma_y^2}-\frac{z^2}{2\sigma_z^2}}\Big)/g_2(-\xi) \tag{A.1}$$

where ξ, σ_y, σ_z, and pk are independent fitting parameters and $g_n(x) = \sum_{k=1}^{\infty} \frac{x^k}{k^n}$. Recall the fugacity, ξ, appears in the Fermi-Dirac distribution function

$$\mathcal{F}_{FD}(\epsilon) = (\xi^{-1} e^{\epsilon/k_B T} + 1)^{-1} \tag{A.2}$$

as $\xi = e^{\mu/k_b T}$, where μ is the chemical potential. In this way, the fugacity only depends on the relative temperature

$$\frac{T}{T_F} = -\left(\frac{6}{g_3(-\xi)}\right)^{1/3}, \tag{A.3}$$

and therefore we can extract T/T_F directly from our fit.

This procedure for determining the temperature works very well for a range of temperatures, namely from $0.1\,T_F < T < 0.5\,T_F$ [47]. For temperatures above $0.5\,T_F$, subtle differences between the Fermi-Dirac distribution and a classical distribution cannot be picked out by the fit (but of course in this limit we can rely on the classical distribution to determine temperature). For temperatures much below $0.1\,T_F$, the finite temperature distribution approaches the zero temperature

distribution and it is dominated by the Fermi energy. In this limit, our fitting routine cannot differentiate between the two, at least within our signal-to-noise, and we are in need of a new thermometer.

To better understand the challenge in fitting a low temperature gas, let us first consider the simplest case (Eqn. A.2), the distribution function for an ideal Fermi gas. In Fig. A.1 a), I show the distribution function as a function of k for a zero temperature gas (black line) and a finite but small temperature (red line). The temperature of the red line distribution can be determined by counting the excitations above k_F (and correspondingly the holes below k_F). Generally, one would say the width of the broadening of the distribution is proportional to $k_B T$. In Fig. A.1 b), I show a similar calculation assuming this time a spherical square-well potential, and integrate through one direction similar to imaging an atom gas in time-of-flight imaging. The red curve represents the same finite temperature as in Fig. A.1 a), but now the differences in the two distributions are much more subtle. As this example shows, integrating through one of the directions of an atom cloud (projecting a 3D object onto 2D) already masks much of the signal.

As it turns out, real potentials are not even spherical square wells and this further complicates matters. Because, in a real trap, the density decreases as a function of the gas radius and the local Fermi temperature T_F decreases, the relative temperature T/T_F increases. In Fig. A.2, I reproduce the expected momentum distributions after integrating through one dimension of a gas expanded from a harmonic trap as found in Ref. [47]. The distributions are shown for various temperatures. The distribution at $T/T_F = 0.1$ is very similar to the zero temperature distribution. With our current signal-to-noise, the coldest relative temperature we can accurately measure is $T/T_F = 0.1$. However, the distribution at $T/T_F = 0.2$ is still clearly differentiated from the zero temperature distribution and we can fit it quite accurately. Mapping a temperature at or be-

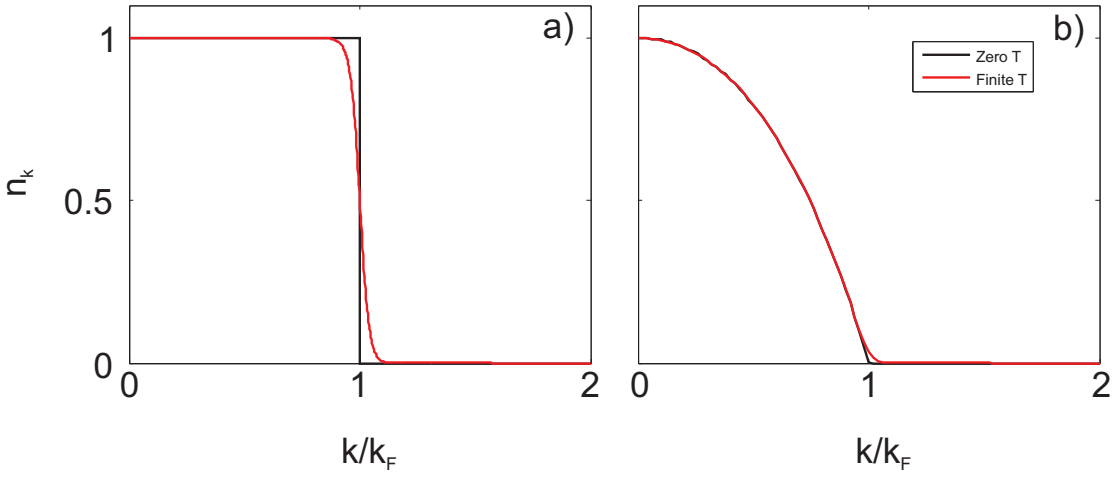

Figure A.1: Momentum distributions at zero temperature (black line) and a finite but small temperature (red line). a) Fermi distribution function for a homogeneous system. The temperature can be determined from the difference in the finite and zero temperature distributions. b) Here, I have integrated through one dimension (similar to imaging an atom cloud) of a 3D spherical square well potential. For the same finite temperature, the distributions are much more similar. Determining the temperature from such a distribution is much more difficult.

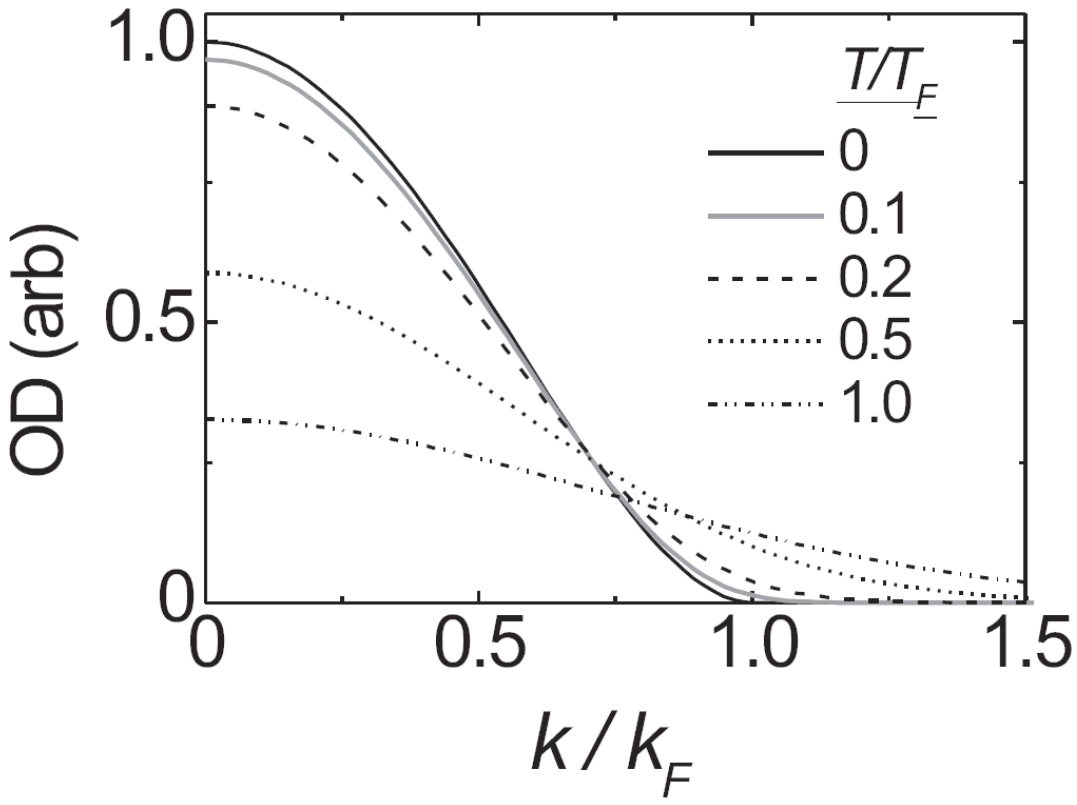

Figure A.2: Momentum distributions after integrating through one dimension of a gas expanded from a harmonic trap as found in Ref. [47]. There is very little difference between the distributions at $T/T_F = 0$ and 0.1.

low $T/T_F = 0.1$ on to a $T/T_F = 0.2$ distribution was at the heart of our attempt at a new thermometer.

A.2 Third spin-state thermometry

The ability to measure temperatures accurately below $0.1\,T_F$ would be useful for a couple reasons. Firstly, to create a gas below $0.1\,T_F$ it helps to be able to measure those low temperatures. For example, how does one modify an evaporation trajectory to make a colder gas if the thermometer is stuck at $0.1\,T_F$? Secondly, a colder gas would allow us to access a larger portion of the superfluid phase diagram, particularly on the BCS side. A thermometer that could determine low temperatures and also worked for a strongly interacting gas would be doubly beneficial for BCS-BEC crossover studies.

The idea behind using a third spin state as a thermometer is as follows: place a small population of atoms in a third spin state in thermal contact with the Fermi gas. Because the atoms in the third spin state are in thermal contact with the other atoms, they have the same temperature T. However, the number of atoms in the third spin state is chosen to be substantially smaller than the states we wish to study, so that the third spin state has a smaller Fermi temperature T_F. In this way, we can map the absolute temperature of the states we are interested in (but have difficulty measuring) onto a state with a higher relative temperature T/T_F, that we can accurately measure.

For example, let us assume we begin with our typical conditions of 10^5 atoms per spin state ($|9/2, -9/2\rangle$ and $|9/2, -7/2\rangle$ states) with a degeneracy of $T/T_F = 0.1$. Notice this temperature is at the limit we can accurately measure. Imagine now that we place this cloud into thermal contact with $2 * 10^4$ atoms in a third spin state ($|9/2, -5/2\rangle$). Recall that the Fermi temperature goes as $T_F = \hbar\omega(6N)^{1/3}/k_B$, so that our 5% population in the third spin state now has

a relative temperature of $T/T_F \approx 0.27$, a value we can again accurately measure. This technique was introduced as an impurity thermometer in Cindy Regal's thesis and was shown, at low magnetic field where the spin states are stable, to be able to duplicate temperature as well as the 2D surface fit explained above.

Practically, impurity thermometry has a couple of challenges. First, because we tend to study the Fano-Feshbach resonance between the $|9/2, -9/2\rangle$ and $|9/2, -7/2\rangle$ states, our impurity spin state is the $|9/2, -5/2\rangle$ state. Because this state has does not have a closed cycling transition for imaging and the number of atoms is chosen to be small, signal-to-noise tends to be quite low. Additionally, for this probe to be useful it should be applicable for magnetic fields near the Fano-Feshbach resonance (around 200 G). However, we find that these spin-state combinations are not stable at high fields. In particular, we find rather counter-intuitively that while the $|9/2, -5/2\rangle$ and $|9/2, -7/2\rangle$ states are stable, the $|9/2, -5/2\rangle$ and $|9/2, -9/2\rangle$ states are not (they are stable on the order of one second). Presumably, spin-exchanging collisions are due to the instability, but rather puzzling is that likely exchange culprit for the $|9/2, -5/2\rangle + |9/2, -9/2\rangle$ collision would be that both states leave as $|9/2, -7/2\rangle$, which would mean entering in a s-wave channel and leaving on a p-wave channel, which should be suppressed for our ultra cold temperatures. Regardless, the spin mixture is sufficiently stable for the third spin state to come into thermal equilibrium the sample and we measure good agreement between impurity thermometry and the 2D surface fits, even at high magnetic fields.

A.3 Three spin states near a Fano-Feshbach resonance

Although we would like to have a good thermometer for a weakly-interacting gas, the real potential with impurity thermometry is the possibility to probe the temperature of a strongly interacting Fermi gas. As we mentioned earlier, it is

difficult to extract the temperature of a strongly interacting Fermi gas from typical time-of-flight expansion experiments. This is because the interaction energy can become convolved with the expansion energy, and extracting the temperature becomes model dependent. Our current method is to measure the temperature of a weakly interacting Fermi gas and then adiabatically turn on the interactions. In this way, various theoretical models can predict the temperature of the gas in the strongly interacting regime.

Impurity thermometry, however, has the possibility to bypass the problem of the release energy effecting the time-of-flight expansion. This is because while there may exist strong interactions between the $|9/2, -9/2\rangle$ and $|9/2, -7/2\rangle$ states near their Fano-Feshbach resonance, they each still interact fairly weakly with the impurity state $|9/2, -5/2\rangle$. Thus, if we use the $|9/2, -5/2\rangle$ state as our impurity state, we can measure its temperature in the traditional way. This could be very helpful for, say, measuring the temperature (and transition temperature) of the strongly interacting gas throughout the BCS-BEC crossover.

This idea of impurity thermometry on a strongly interacting gas seemed very promising. In particular, the time required for thermalization between the impurity spin state was almost an order of magnitude smaller then the lifetime of the $|9/2, -9/2\rangle$ and $|9/2, -7/2\rangle$ states near their Fano-Feshbach resonance (a stringent requirement if the impurity state was to be used as a thermometer). Unfortunately, as we tried these experiments for the very first time on an ultracold sample, we found out that the entire sample became extremely unstable as the spin mixture approached the Fano-Feshbach resonance. We understand this now as the third (distinguishable) spin state de-stabilizing the fragile fermion pairs.

To understand why impurity spin state thermometry fails to work near the Fano-Feshbach resonance we return to the case of the strongly interacting gas without a third spin state. A key property of these strongly interacting Fermi

gases is that they have a relatively long lifetime (with respect to collision time scales, trap periods, etc.) [147]. In ^{40}K, the lifetime of fermionic pairs at the Fano-Feshbach resonance is 100s of milliseconds, and can be even larger in ^{6}Li. What is surprising, however, is that the sample is so stable (consider our discussion in Chapter 2 in which we found these are very large, fragile pairs). Similar conditions for a Bose gas will result in orders of magnitude smaller lifetimes [148]. So, where does the increased lifetime of fermionic pairs originate? The answer lies in the fermionic nature of the constituent atoms. Namely, because the entire gas is made up of spin-up and spin-down fermions, and a fermionic pair is made up of the same, a collision to de-stabilize the pair is suppressed because no two identical fermions approach each other (due to the Pauli exclusion principle). This is explained in detail in Ref. [47].

We can now see why adding a third (distinguishable) spin state causes a problem. While the fragile fermionic pairs are still Pauli protected from atoms in the identical spin states, they are not Pauli protected from the newly introduced third spin state. Atoms in this third distinguishable spin state are able to collide with the fermionic pairs and carry away their excess energy as the pairs decay into deeper bound states. This process is sufficiently detrimental to the Fermi gas that we could not even observe a fermionic condensate in the presence of the impurity spin state. One might argue that impurity thermometry may still be applicable for temperatures above the pairing temperature, but our typical thermometry techniques are already sufficiently accurate in that regime. Alternatively, it may also be useful for spin-imbalanced studies as found in Ref. [149].